IMST2007
EDEN DISH HOTEL
ENSCHEDE
THE NETHERLANDS
JUNE 18, 19, 20

Innovative Mass Storage Technologies
2007

Emerging and Future Technologies

Magnetic Memories

Solid State Memories

Optical Memories

Architecture System Software

Program Book

IMST (Innovative Mass Storage Techniques)

IMST began in 2001 to provide a unique forum in Europe to gather specialists from all areas of mass storage technologies and emerging nonvolatile solid state memories. A strong interaction of industrial and academic specialists is encouraged in IMST activities, providing valuable opportunities for experts with different backgrounds to gain a deeper and broader understanding of the field.
IMST activities include international workshops, roadmap definition, strategy discussions, and collaborative EU projects. A key feature of the IMST workshops is the industrial review that opens every conference where leading researchers in the field of memory and data storage technology give a worldwide view on the latest developments and the hottest topics. Past industrial speakers have come from Sony, Samsung, Thomson, Infineon, Philips, Motorola, Seagate, Nanomagnetics, TuiOptics, Plasmon, STMicroelectronics, IBM. The IMST Committee has also played a major role in developing a 'community' for EU-based data storage research, and has generated an EU Roadmap for data storage technologies, the so-called IMST White Book 2006, which aims to put forward a European view on the future of data storage. The White Book is downloadable at www.imst.org.

IMST and WIND

The IMST activities are now supported directly as part of an EU FP6 SSA (Specific Support Action) project called WIND - **W** ide **IN** tegrated Technologies **D** iffusion.

WIND

Memory is at the heart of most everyday electronic products used in a host of different application areas - health, avionics, telecommunication, automotive, computing, home systems - and a wide array of mixed technologies and competencies is needed to design and fabricate such memories. Furthermore, our technologically-oriented society is moving steadily towards a new era of 'ambient intelligence', where distributed intelligent systems help to process, understand and utilize the plethora of digital information that pervades our everyday life. Since intelligence cannot exist without memory, it is clear that the memories of the future have a key role to play.
The development of a future generation of 'intelligent memories' is thus a strategic issue for Europe, since it is in just such advanced technology areas that Europe can and should develop a competitive advantage. It is therefore essential to provide for Europe an overall vision of the future possibilities in the area of memory technology - a clear 'road map' that should be disseminated to all interested parties - leading industrial and research laboratories, leading European user companies, as well as the important SME community. It has often been pointed out that the productivity gap currently observed between the USA and Europe is largely due to the difference in usage of information technologies (IT) possibilities. WIND will help to plug this productivity gap for memory and related technologies and their numerous applications.

Organization Committee

Co-chair: Bernard Bechevet	CEA, Grenoble, France
Local chair: Leon Abelmann	University of Twente, The Netherlands
Organisation: Karen Wannyn	University of Twente, The Netherlands
Infrastructure: Thijs Bolhuis	University of Twente, The Netherlands
Finance: Hans Groenland	University of Twente, The Netherlands
Communication: Martin Siekman	University of Twente, The Netherlands

Technical Committee

Chair: Manfred Albrecht	University of Konstanz, Germany
Co-chair: Yves Samson	CEA, Grenoble, France

Members

Claude Chappert	Université Paris Sud, France
David Wright	University of Exeter, United Kingdom
Matthias Wuttig	RWTH Aachen, Germany
Hartmut Richter	Thomson, France
Roberto Bez	ST Microelectronics, Italy
Doris Keitel-Schulz	Qimonda, Germany

Monday 18th of June

17:00 – 19:00 **Tutorial Session on System Aspects (sponsored by ProTeM*)**

Abu Sebastian, IBM Zurich, CH (invited):
Tutorial on positioning

Oleg Zaboronski, Arithmatica, UK (invited):
Tutorial on coding

Sape Mullender, Bell Labs, USA (invited):
Tutorial on filesystems

*ProTeM is the Probe-based Terabit Memory project. More information is available on the web. http://www.ctit.utwente.nl/research/projects/international/ip/protem.doc

Tuesday 19th of June

8:15 – 8:30 **Welcome**

9:00 – 10:30 **Emerging and Future Technologies**

H. Richter, Thomson Villingen, D (invited)
Application & Technology Trends in Optical Storage

S. Parkin, IBM Almaden RC, USA (invited)
The Magnetic Racetrack Memory: a novel spintronic device based on current induced precessional motion of domain walls

Haris Pozidis, IBM Research Laboratory Rüschlikon, CH (invited)
Scanning-probe-based Data Storage

Coffee Break

11:00 – 12:00 **Future and Emerging Technologies / Magnetic Recording**

Dorothea Wiesmann, IBM (invited)
Ultra-high storage densities with thermo-mechanical probes and polymer media

L. Abelmann et al., University of Twente, NL
Scanning probe array memory research at the University of Twente

J.B.C. Engelen et al., University of Twente, NL
Anomalous hall effect measurements on a nanosized CoPt dot array

M. C. Hickey et al., University of Leeds, UK
Domain walls compressed by shape anisotropy in magnetic nanoconstrictions

Lunch

14:00 – 15:30 **Magnetic Recording**

T. Schrefl ,University of Sheffield, UK (invited)
Micromagnetic simulations on magnetic recording

M. Asbahi, et al., SPINTEC, F
Recording performances onto nano-imprinted pre-patterned perpendicular magnetic media

R. Luttge et al., University of Twente, NL
Nanolithography for patterned magnetic data storage media

T.C. Ulbrich et al., University of Konstanz, D
Magnetic films on nanospheres: Realization of tilted media

Coffee Break

16:00 – 18:00 Poster Session

18:30 – … Conference Dinner

Wednesday 20th of June

8:30 – 10:15 Optical Storage / Future and Emerging Technologies

M. Mansuripur ,Univ. Tucson, USA (invited)
Information Storage and Retrieval using Macro-molecules as Storage Media

J. Om, Hynix Semiconductor Inc, Korea (invited)
Scaling Issues in NAND FLASH Memory

K. Curtis, InPhase Technologies, USA (invited)
Holographic drive and media developments at InPhase

A.S. Matharu et al., University of York, GB
Novel azothiophene polyesters for holographic storage

Coffee Break

10:45 – 12:15 Phase Change / Solid State Memories

D. Keitel-Schulz, Qimonda, D (invited)
Data security in memory systems and solutions

R. Pandian et al., University of Groningen, NL
Phase-change and electrolytic switching in chalcogenide thin films

J. Gutwirth et al., University of Pardubice, CZ
RF magnetron sputtered Ge2Sb2Te5 thin film characterization

F. Merget et al, RWTH Aachen, D
Conduction mechanisms of amorphous and crystalline Ge2Sb2Te5 at low temperatures

C.D. Wright et al., University of Exeter, GB
Understanding multi-state phase-change memories and processors

Lunch

14:00 – 16:00 **Phase Change /Solid State Memories / Others**

Wellnic RWTH Aachen University, D (invited)
The role of vacancies in phase change materials – controlling material properties from first principles

Dae-Hwang Kim et al., RWTH Aachen, D
3d-simulation based analysis of cell design concepts for phase change random access memory

M. Armand et al., CEA-LETI MINATEC, F
Random approach for crystallization modelling in phase-change memory

H. Gatzen et al., University of Hannover, D
A Slider with an Integrated Microactuator (SLIM) for Second Stage Actuation in Hard Disc Drives

V.L. Safonov, Mag & Bio Dynamics Inc., USA
Hard Disk Drive as a logic device

16:15 **Goodbye from local chair**

Application & Technology Trends in Optical Storage

Hartmut Richter

Deutsche Thomson oHG,
Hermann-Schwer-Str. 3, D-78048 Villingen-Schwenningen, Germany,
Phone: +49-7721-85-2007, Fax: +49-7721-85-2241,
E-mail: hartmut.richter@thomson.net

In today's world data storage is ubiquitous. In 2006 more than 10 exabytes of new data were created. The year 2007 will be the first time the volume of information created will surpass available storage capacity (source: IDC Storage Report). Higher resolution commercial and personal content, personal content sharing, social networking and professional archiving needs will fuel the demand for larger storage capacities even further. In particular the personal digital content creation is growing fast and the total data volume is expected to exceed commercial content in the next years. According IDC, the content creation worldwide will increase 10-fold by the middle of the next decade.

Cost-effective hardware and storage has enabled this digital revolution so far. However, existing technologies do not cope with the above-mentioned future application trends. There is a huge incentive for either improving existing technologies or developing new technological approaches towards e.g. terabytes capacities, Gbit/s data transfer rates and long-term archival (to store our "digital lives" or "digital legacy"). Other important technical challenges associated with storage devices and systems are content security, digital right management and efficient usage of vast data files, i.e. strategies for organizing, finding and interpreting content (these aspects will not be subject of the presentation).

Optical disc storage technologies are robust against environmental impact, versatile, future-proof and inexpensive. Today's major applications are content distribution and personal content archival. Optical storage systems for practical application in 3+ years from today with hundreds of gigabytes per data carrier will likely be provided by a mixture of today's evolving and future technologies:

- Super-resolution either by optical near-field and/or by thermal masking layers on the disc
- Multi-layer based e.g. on 2-photon absorption or micro-holograms
- Page-oriented holographic data storage.

On the conference the following subjects will be addressed in more detail:

- consumer expectations and preferences (removable media, download-to-own, grid_storage@www., etc.)
- future applications for optical storage and major technological competitors
- optical storage technology trends
- Specific interests and R&D activities @ THOMSON.

Invited Talk

The Magnetic Racetrack Memory: a novel spintronic device based on current induced precessional motion of domain walls

Stuart Parkin

IBM Almaden Research Center, San Jose, California, USA
parkin@almaden.ibm.com

The current induced motion of magnetic domain walls confined to nanostructures is of interest for applications in magnetoelectronic devices in which the domain wall serves as the logic gate or memory element. A proposal for a novel storage-class memory is described in which magnetic domains are used to store information in a "magnetic race-track" [1]. The magnetic race-track promises a solid state memory with storage capacities and cost rivaling that of magnetic disk drives but with much improved performance and reliability: a "hard disk on a chip". The magnetic race track is comprised of tall columns of magnetic material arranged perpendicularly to the surface of a silicon wafer. The domains are shifted up and down the race-track by nanosecond long pulses of spin polarized current using the phenomenon of spin momentum transfer. We discuss the current induced resonant excitation and motion of domain walls in permalloy nanowires [2,3]. The injection of spin polarized current below a threshold value through a domain wall confined to a pinning potential results in its precessional motion within the potential well [4]. We show that, by using a short train of current pulses, whose length and spacing are tuned to this precession frequency, the domain wall's oscillations can be resonantly amplified [5]. This makes possible the motion of domain walls with much reduced spin polarized currents, more than five times smaller than in the absence of resonant amplification.

[1] S. S. P. Parkin, US Patent # 6,834,005 (2004)
[2] M. Hayashi, L. Thomas, C. Rettner, R. Moriya, and S. S. P. Parkin, Nat. Phys. **3**, 21 (2007).
[3] M. Hayashi, L. Thomas, C. Rettner, R. Moriya, Y. B. Bazaliy, & S. S. P. Parkin, Phys. Rev. Lett. **98**, 037204 (2007).
[4] L. Thomas, M. Hayashi, X. Jiang, C. Rettner and S.S.P. Parkin, Nature **443**, 197 (2006)
[5] L. Thomas, M. Hayashi, X. Jiang, R. Moriya, C. Rettner, and S. Parkin, Science **315**, 1553 (2007).

Invited Talk

Scanning-probe-based Data Storage

M. Lantz[1], P. Bächtold, H. Bhaskaran, J. Bonan, R. Cannara, G. Cherubini, M. Despont, U. Drechsler, U. Duerig, E. Eleftheriou, R. Guerre, B. Gotsmann, W. Häberle, C. Hagleitner, D. Jubin, A. Knoll, A. Pantazi, D. Pires, H. Pozidis, H. Rothuizen, D. R. Sahoo, A. Sebastian, R. Stutz, M. Varsamou, and D. Wiesmann

[1]IBM Research Laboratory, CH-8803 Rüschlikon, Switzerland

Ultrahigh storage densities of up to 1 Tb/in^2 or more can be achieved by using atomic force microscopy (AFM) techniques to write, read back, and erase data in very thin polymer films. The thermomechanical scanning-probe-based data-storage concept combines ultrahigh density, small form factor, and high data rates. Thermal and mechanical robustness, long-term bit retention, and repeated erasability of written indents are the essential criteria for a polymer storage medium. Based on extensive research, we can reconcile these criteria in terms of generic physical material properties, namely, the glass transition temperature, cross link density, and yield activation energy. We have shown that all basic requirements for a storage medium, viz. fast bit writing, repeated erase/overwriting of the same bit, and a bit-retention time greater than 10 years, can be achieved with suitably engineered polymers.

High data rates are achieved by parallel operation of large 2D arrays having thousands of micronanomechanical cantilevers/tips that can be batch-fabricated by silicon-surface micromachining techniques. The very high precision required to navigate the AFM probes over the storage medium is achieved by MEMS-based x/y actuators that position the large arrays of probe tips for the parallel write/read/erase operations. In this presentation the fundamental elements of a probe-storage system will be discussed, and various system aspects, including the navigation of the probe array over the storage medium, will be addressed. Finally, results of the first small-scale prototype storage system with servo navigation and parallel read/write/erase capability using our scanning-probe thermomechanical recording technology are presented. This is the first time a scanning-probe recording technology has reached this level of technical maturity, demonstrating the joint operation of all building blocks of a storage device.

ULTRA-HIGH STORAGE DENSITIES WITH THERMO-MECHANICAL PROBES AND POLYMER MEDIA

D. Wiesmann, U. Duerig, B. Gotsmann, A. Knoll, H. Pozidis, F. Porro*, and R. Vecchione*

IBM Research GmbH, Saeumerstrasse 4, 8803 Rueschlikon, Switzerland, dor@zurich.ibm.com

** STMicroelectronics, P.le Enrico Fermi 1, Porto del Granatello, 80055 Portici (NA), Italy*

The scalability of data density is an important attribute of any viable storage technology. In this paper, we show that multi-Tb/in2 densities can be achieved using thermo-mechanical writing and thermo-resistive read back of data encoded as nanometer-scale indentations in a highly cross-linked polymer. Empirically, we have found that the depth of an indentation depends both on its lateral extension as well as the apex radius of the indenter. Experimentally verified scaling laws predict that a maximum indentation depth on the order of 5 nm at 1 Tb/in^2 can be achieved with a 5 nm radius indenter, dropping to about 1 nm depth at 4 Tb/in^2. The ability to sense such shallow indentations is limited by sensor noise and surface roughness of the media. The optimization of these sources of interference is therefore critical to the quest for ever higher data densities.

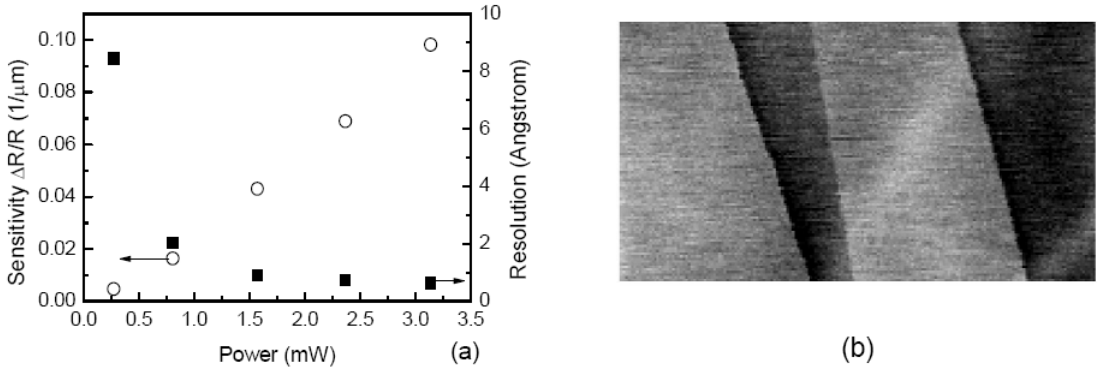

Figure 1: (a) Sensitivity and resolution of thermal sensor for 10 kHz bandwidth. (b) Image of 4-Å-high terraces in HOPG measured with thermo-resistive sensor.

The read sensor is one of two low-doped areas of the silicon cantilever over which electrical power can be dropped selectively. Distance-dependent cooling as well as temperature-dependent resistivity are exploited for sensing. Upon encountering an indentation, the distance and in turn the thermal resistance between read sensor and polymer substrate are reduced. This leads to a decrease in temperature and thus resistance of the sensor that is detected. Figure 1(a) shows the measured sensitivities to vertical displacement as well as the resolution as determined from sensor noise. The appropriate choice of sensor geometry and doping levels reduces the 1/*f* excess noise such that sub-Angstrom resolution can be achieved. Figure 1(b) shows an image of 4-Åhigh terraces on highly-oriented pyrolytic graphite (HOPG) measured with the read sensor.

The polymer media usually consists of a 100-nm-thick film spin-coated on a Si wafer from a diluted solution. Subsequent thermal curing initiates the formation of permanent cross-linksbetween the polymer molecules needed for the mechanical stability of the polymer medium. Regardless of details of the preparation procedure and the cross-link density in the film, we always observe a residual media roughness with an rms value of 0.5 nm measured over spatial frequencies ranging from 1/100 to 1/1 nm. This residual roughness arises from thermally excited surface waves during the curing process.

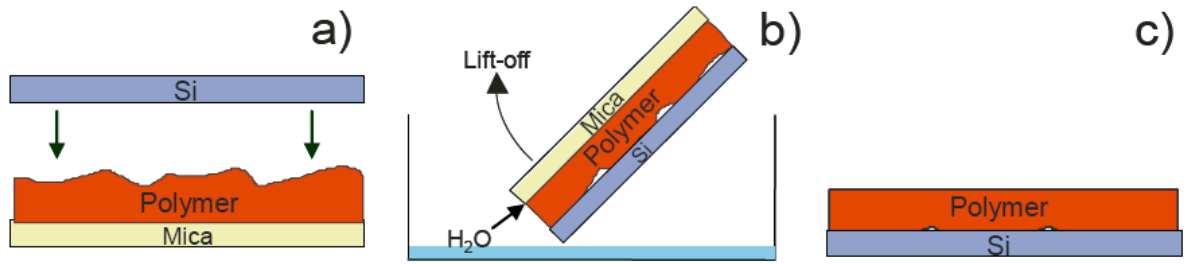

Figure 2: Schematic of the media transfer process.

This problem can be overcome by a transfer process shown in Fig. 2. First, Fig. 2a, the media is spin-coated and cured on a freshly cleaved mica surface, which acts as a template surface. Then, a HF-treated Si wafer is put in contact with the free polymer surface. Then the sandwich is submerged in water, Fig. 2b. As the mica surface is highly hydrophilic, water creeps between the polymer and mica surfaces, thereby releasing the polymer film from the mica surface. Conversely, water is expelled from the hydrophobic polymer-Si interface, allowing the polymer film to become firmly attached to the substrate. As a result, Fig. 2c, the mica surface is replicated on the polymer surface, resulting in a reduced surface roughness of <0.1 nm rms.

A media sample prepared by means of the transfer process was used for the feasibility study of thermo-mechanical writing and thermo-resistive reading at a density of 4 Tb/in^2 (Fig. 3). The minimum distance between adjacent indentations in both directions is 14.7 nm. The data in each row are encoded with a (d,k) code with d=1, which places at least one 0 between adjacent 1's and increases the effective storage density by 4/3 over an uncoded system with the same minimum indentation pitch. The mean depth of the indentations is 1.1 nm, and the height distributions for logical 0's and 1's are clearly separated, allowing for potentially low error rates in the detection of the data.

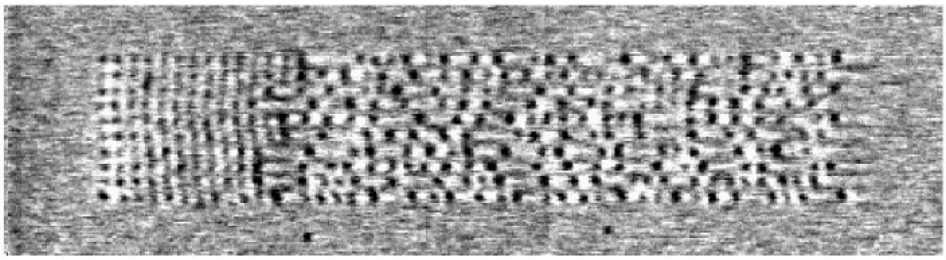

Figure 3: Topographic image of a thermo-mechanically recorded data pattern at a density of 4 Tb/in^2.

The authors gratefully acknowledge fruitful discussions with and vital technical support provided by the probe storage team at IBM. They also thank James Hedrick and Russell Pratt of the IBM Almaden Research Center for fabrication of the polymer samples.

SCANNING PROBE ARRAY MEMORY RESEARCH AT THE UNIVERSITY OF TWENTE

Leon Abelmann, Mink Hoexum, Alexander Le Febre, Johan Engelen, Wabe Koelmans, Regina Luttge, Martin Siekman, Thijs Bolhuis, Hans Groenland, Cock Lodder, Henk van Wolferen, Edin Sarajic, Gijs Krijnen, Mohammed Khatib, Berend-Jan van der Zwaag, Hylke van Dijk, Gerard Smit, Pieter Hartel, Mihai Patrascu, Stefano Stramigioli

University of Twente, The Netherlands
www.uspam.nl
L.Abelmann@utwente.nl

Introduction

Since the invention of the hard disk we have seen a gradual decrease of its size and power consumption, going down from the 24" IBM 350 to the .85" Toshiba microdrives of today. Further miniaturisation will inevitably lead to using microsystem technology. One architecture investigated today is based on a huge array of read/write probes, derived from the cantilevers used in scanning probe microscopy [Knoll06]. The use of scanning probe techniques opens up a road which might lead to molecular or even atomic storage. The road towards this goal will at least need the transition from continuous media to patterned media, of which magnetic patterned media will be the first step.

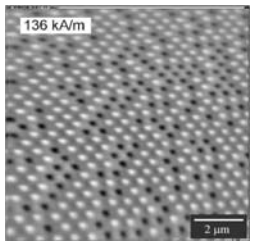

Figure 1 MFM image of magnetic patterned medium produced by LIL

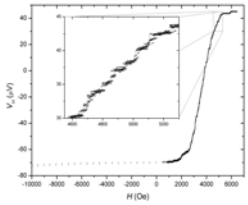

Figure 2 Anomalous Hall Effect revealing individual switching of dots

Media

A relatively simple way to realise arrays of single domain magnetic dots is Laser Interference Lithography (Figure 1., [Luttge07]). Periodicities down to 150 nm can be obtained, and magnetic dots of 70 nm have been realised. By using the ultra-sensitive Anomalous Hall Effect, the switching behaviour and thermal stability of the dots was investigated (Figure 2, [Engelen07]).

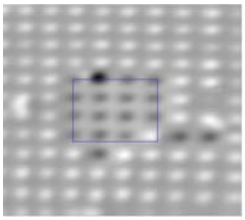

Figure 3 Write experiment with MFM

Probes

By using a vacuum, in-field Magnetic Force Microscope with fiber inteferometric detection, dots in the array could be individually written and erased (Figure 3, [Siekman07, Bolhuis07]). Of course interferometry would be difficult to implement for an array of probes. As alternative, using field-emission currents to sense the tip/sample distance is being investigated. This method has been shown to have a sensitivity of better than 0.3 V/nm and can in princple be used to detect magnetic stray fields (Figure 4, [LeFebre07]).

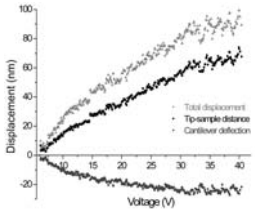

Figure 4 Tip/sample distance as a function of tip/sample voltage

Positioning

Most probe recording systems suggested today use one single XY scanner to position the probes with respect to the data. However when using electrostatic stepper micro actuators, tens of scanners can be used simultaneously. This has advantages with respect to power consumption and concurrency (Figure 5, [Patrascu07]). Still the probe array is limited by the size of the array. For very high capacity, the array can be split up into independent parts, where Image Charge Stepping Actuators are integrated with the array (Figure 6, [Hoexum07a]). These StoBots can be produced in large quantities on a MEMS wafer, and subsequently be transferred to a cheap data storage substrate (Figure 6, [Hoexum07b]).

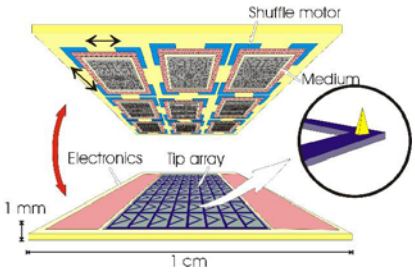

Figure 5 Architecture using multiple scanners

Systems

The thousands of probes, and tens to hundreds of scanners give these new architectures a large degree of parallelism, which can be exploited in the total system to increase performance, or tune the quality of service (data rate, access time) for instance relative to the available power [Zwaag07]. The physical location of the data significantly affects the achieved data rates, energy consumption, and reliability of the system. Therefore new striping policies are required (Figure 7 [Khatib07]).

Also the fact that future recording systems will use patterned media has serious implications for the system architecture. We will need to deal with issues like write synchronisation. Another important aspect of patterned media is that the data between tracks has a phase-relation. Unlike continuous media, like hard disks or phase change, we know exactly where the adjacent bits are positioned. This opens the possibility to extend our data detection and coding strategies from one dimension (along the track), to two dimensions (Figure 8, [Groenland07]).

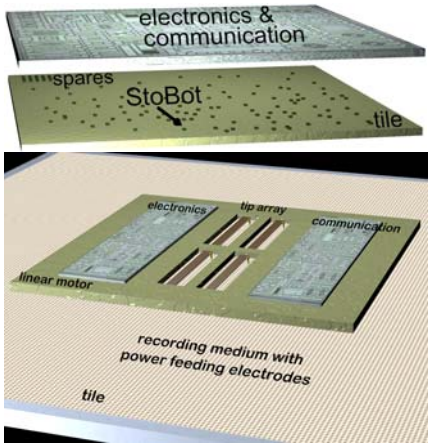

Figure 6 Architecture using Stobots

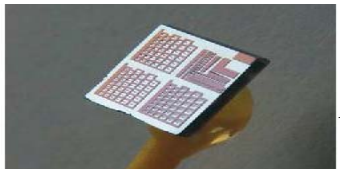

Figure 7 StoBots Transfer technique

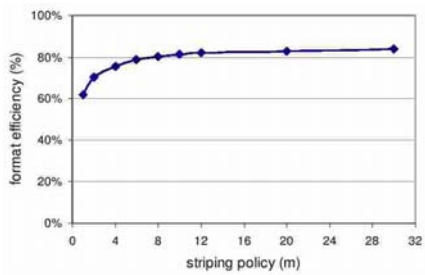

Figure 8 Efficiency increases as data is striped over more probes

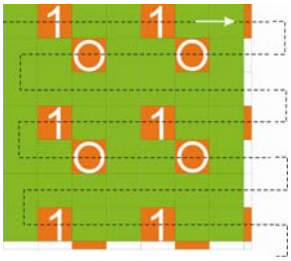

Figure 9 2D coding can be succesfully applied in patterned media.

[Knoll2006] Microelectronic Engineering 83 p1692-7 (2006)
[Luttge2007] This conference
[Engelen2007] This conference
[Siekman2007] This conference
[Bolhuis 2007] This conference
[Le Febre 2007] This conference
[Patrascu07] This conference
[Hoexum07a/b] This conference
[Khatib07] This conference
[Zwaag07] This conference
[Groenland07] This conference

ANOMALOUS HALL EFFECT MEASUREMENTS ON A NANOSIZED CoPt DOT ARRAY

Johan B.C. Engelen, Thijs Bolhuis, Leon Abelmann and J.C. Lodder

MESA+ Research Insitute for Nanotechnology, University of Twente, The Netherlands
j.b.c.engelen@utwente.nl, www.uspam.nl

Introduction

The increase in magnetic data storage density is currently being limited by the thermal stablity of the magnetisation in the grains. A further decrease in grain size can only be achieved if higher anisotropy materials are used. Apart from the writing problem, the maximum achievable anisotropy is material limited. Next to improving the material, also the number of grains used to define a bit has to be decreases. Ultimately we will arrive at the single-bit-per-grain situation, in which the grains have to be positioned on well known locations. We than speak about patterned media. One main issue in patterned media is that not all grains switch at the same field [1]. The difference between switching fields of these 'weak' and 'strong' dots makes writing data difficult. The described research was done to obtain understanding of this difference, so that the difference might be decreased. The very sensitive anomalous Hall effect (AHE) was used to measure the magnetisation of the dots. This method enabled relatively quick (and therefore a large quantity of) measurements of the switching field of the first and last switching dots, and statistical analysis of the switching field distribution is possible.

Experimental procedure

An array of 180nm wide $Co_{80}Pt_{20}$ dots on Ru(20nm)/Pt(10nm)/Ta(5nm) buffer layers on a oxidized Si substrate [2] was created by ion beam etching through a mask created by laser interference lithography [3]; etching was stopped halfway the Ru layer. A Hall cross (4 x 4 µm) was etched into the conductive buffer layers by ion beam etching. A microscope image

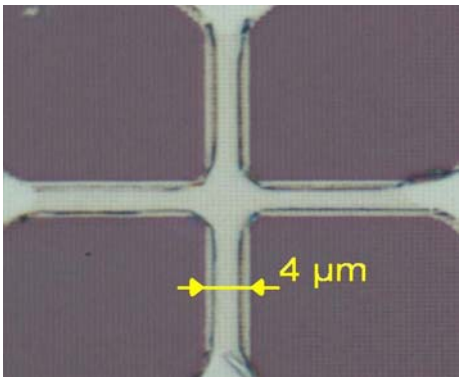

Figure 1 A close-up image of the Hall cross (w=l= 4 µm). The center has about 80 dots.

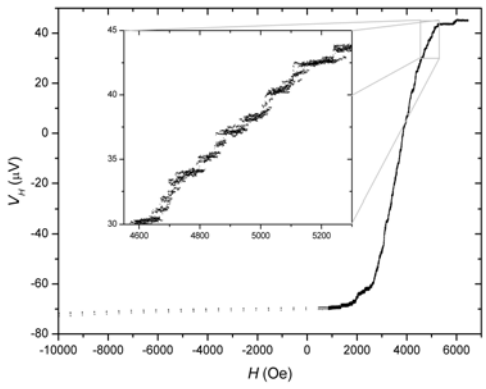

Figure 2 Six overlying AHE measurement curves

of the Hall cross is given in Figure 1. The measured Hall voltage depends linearly on the magnetisation of the dots. All measurements were performed at room temperature with the applied magnetic field perpendicular to the surface.

Results

Figure 2 shows six Hall measurements on top of each other, with magnetic field sweep rate R = $^1/_3$ $^{Oe}/_s$. The close-up shows the switching of individual dots. As can be seen, for every pass the dots switch at slightly different fields. This is caused by thermal fluctations. The switching fields of the first and last switching dots were measured more than 140 times; histograms of the thermal fluctuation of the switching field are shown in Figures 3 and 4. The deformation of the histogram for the first dot is caused by the measurement noise; deformation is minimal for the last dot because of the wider distribution. The lines in the figures are fits to two extreme statistical models of switching field distributions, one for domain wall induced reversal (n=1) and one for coherent reversal (n=2). The shapes of the models' distributions are equal and therefore it is not possible to determine which model applies. From mathematical fits to the histograms, the anisotropy constant and switching volume of the dots are calculated (Table 1). The switching volumes can be compared to the mean volume of crystals in the dot, which is $(13\text{nm})^3$; the anisotropy constants differ more from the expected $K_u = 1.27\ 10^6\ \text{Jm}^{-3}$ [7]. For the last ('strong') dot, $n = 1$ gives an unlikely large anisotropy constant, and therefore n must be 2 (or between 2 than 1) and the dot seems to reverse more coherently. For the first ('weak') dot, n is more likely to be 1, which would imply domain wall motion.

[1] M. Siekman, this conference
[2] T. Shimatsu et alii, IEEE Trans. Magn. 40 p2483–5 (2004)
[3] R. Luttge, this conference

		First switching dot	Last switching dot
K_u	$n = 1$	$0.73 \cdot 10^6\ \text{J/m}^3$	$3.1 \cdot 10^6\ \text{J/m}^3$
	$n = 2$	$0.099 \cdot 10^6\ \text{J/m}^3$	$0.42 \cdot 10^6\ \text{J/m}^3$
V	$n = 1$	$(11\,\text{nm})^3$	$(6.9\,\text{nm})^3$
	$n = 2$	$(29\,\text{nm})^3$	$(19\,\text{nm})^3$

Table 1 Calculated anisotropy constant and switching volume from fits to the measurement data.

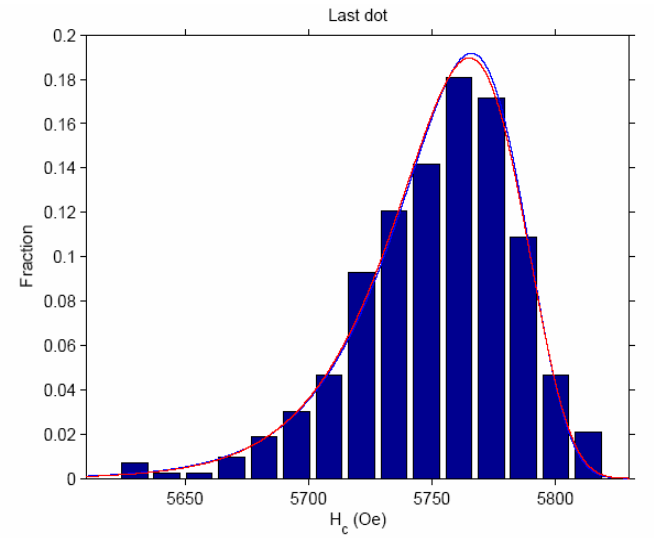

Figure 3 Switching field distribution of last switching dot.

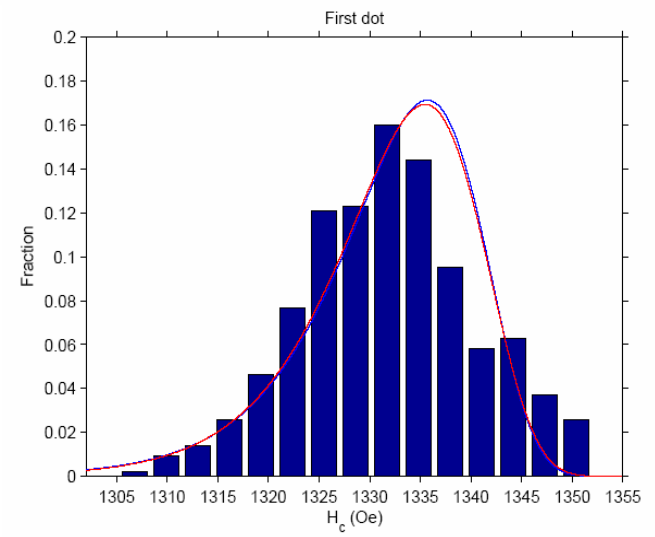

Figure 4 Switching field distribution of first switching dot.

Domain walls compressed by shape anisotropy in magnetic nanoconstrictions

M. C. Hickey, C. H. Marrows& B. J. Hickey

E.C. Stoner Laboratory,University of Leeds, Leeds, LS2 9JT
Phone : ++44(0)113 3433818, Fax : +44 (0)113 343 3846
m.c.hickey@leeds.ac.uk

D. A. Atkinson

Durham University, Durham , DH1 3LE, UK
Phone : +44 (0) 191 33 43592, Fax : +44 (0)191 334 5823
d.a.atkinson@durham.ac.uk

Introduction

Magnetic domain walls in soft magnetic materials such as $Ni_{81}Fe_{19}$ and $Co_{60}Fe_{20}B_{20}$ are of growing importance in the device physics of magnetic logic [1] and magnetic memory elements. The absence of intrinsic magnetic anisotropy in these materials means that domain walls can be controlled by the shape anisotropy of a nanostructure - a geometrical effect. Apart from the powerful technological applications, these domain walls are manifest examples of topological solitons. We have developed nanostructure devices based on $Ni_{81}Fe_{19}$ which show domain wall formation controlled by shape anisotropy. These structures are used as a platform to study the influence of magnetic shape anisotropy on domain wall configurations and the domain wall magnetoresistance which arises in constrictions varying in size from 50nm to 400nm.

Experiment

The magnetic structures of interest comprise two $Ni_{81}Fe_{19}$ pads of differing coercive field separated by a nanoconstriction. In this way, a domain state is configured in the field region between the coercivities of the two pads. This has been shown via simulation[2] and micron-scale MOKE measurements (see Figure 1) to be localized to the dimensions of the nanoconstriction and below.

This type structure, as part of an electrical device can be used to extract the diffusive current spin polarization[3] via the domain wall resistance. Further, affects associated with reduction of dimensionality of the structure and the domain wall structure under non-equilibrium conditions (i.e. with a high applied current density J ~ 10^{11} A cm^{-2}) can be explored at a length scale within the critical device dimensions (50-400nm).

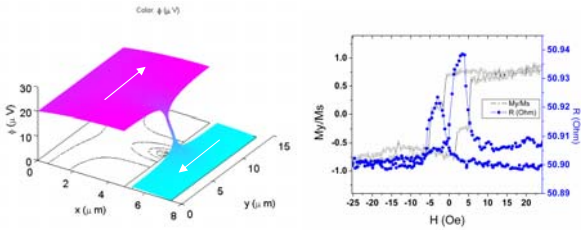

Figure 1: Simulation of the electrostatic potential across the nanoconstriction under applied voltage bias (left). MOKE loops showing the domain wall formation across the nanoconstriction at H = 3 Oe. (right). The domain wall is electrically detected by magnetoresistance.

References

[1] D. A. Allwood *et al.*, Science **309**, 1688 (2005).
[2] M.J.Donahue and D.G. Porter, *Object Orientated Micromagnetic Framework*, http://math.nist.gov/oommf.
[3] C. H. Marrows and B. C. Dalton, Phys. Rev. Lett. **92**, 097206 (2004).

Oral Presentation

Simulation of extremely high density magnetic storage systems

A Goncharov[1], T Schrefl[1], G Hrkac[1], S Bance[1], D Suess[2], TC Ulbrich[3], M Albrecht[3]

[1]University of Sheffield, Department of Engineering Materials,
Mappin Street, Sir Robert Hadfield Building, Sheffield S1 3JD, UK
phone: +44 114 222 5965, fax: +44 114 222 5943, email: t.schrefl@sheffield.ac.uk,
[2]Vienna University of Technology, Solid State Physics,
Wiedner Hauptstr. 8-10/138, A-1040 Vienna Austria
[3]University of Konstanz, Department of Physics, D-78457 Konstanz, Germany Introduction

Introduction

Multiscale simulation is a useful tool for prototyping new storage systems. Novel concepts for recording media and recording head design can be testing virtually and guidelines for systems development can be drawn from the simulations results. Hard disk storage at high densities has to overcome a fundamental limit. With decreasing bit size thermal stability can only be achieved in recording media with highly coercive small structural units such as grains, particles or patterned elements. However, such highly coercive recording media cannot be written using conventional write heads. Means to overcome this problem are assisted writing and/or continuous bit patterned media. In assisted writing the coercive field of the media is reduced during writing by pumping energy into the system. Well known concepts that are currently explored to reduce the write field are laser heating (thermally assisted writing) or magnetic coupling of different materials (domain wall assisted writing). The effective volume of a structural unit in bit patterned media is much larger than the grain volume in thin film granular media. Thus thermal stability can be achieved at moderate coercivities.

In this work we explore three different storage systems for magnetic storage at densities of one Tbit/in^2 and beyond: (1) Multilayer exchange spring media that combines magnetically soft and hard layers to achieve high thermal stability and sufficiently small coercive fields, (2) bit patterned media with small head to soft-underlayer spacing, and (3) magnetic storage on magnetic nano-caps on top of self-assembled spherical particles.

Method

Recording simulation software is required to take into account the detailed microstructure of a magnet and the interactions between the different magnetic parts of magnetic device. In addition to the calculation of magnetization reversal processes and the simulation of domain images, the software developed during the project enables the fully integrated simulation of entire magnetic devices. For example in magnetic recording simulations, the input for the simulations are the detailed microstructure of the recording media, the geometry of the write head, the layer stack and shield geometry of the read head, the intrinsic magnetic properties and the current wave form of the write current. Macropscopic properties like current wave form, read back voltage, transition jitter are input/output of a multiscale simulation that treats the functional behavior of a recording system while taking into account the microscopic magnetization processes during recording and read back. The multiscale simulation process is illustrated in figure 1.

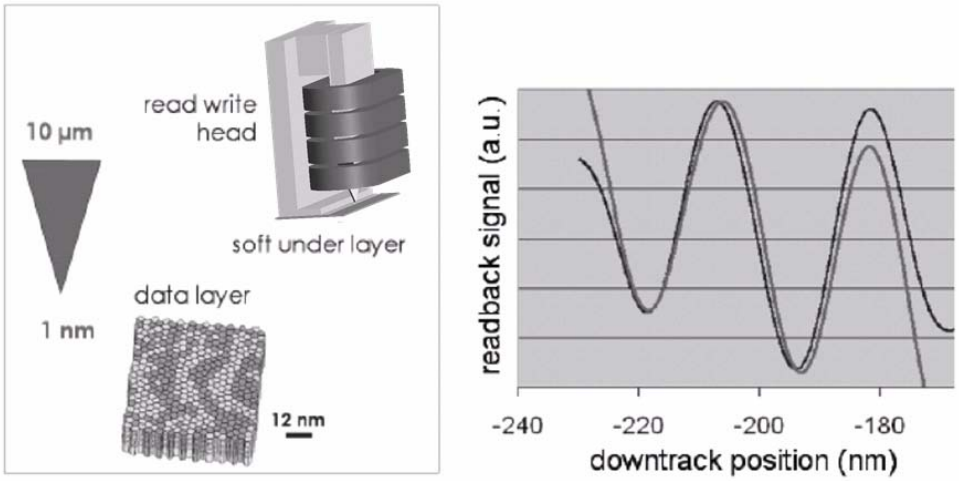

Figure 1. Multiscale simulation of high density magnetic recording systems. Left: Magnetic system used in recording simulations, Right: Computed read back signals for bits recorded at densities of 1.2 Tbit/in^2 on multilayer recording media.

Results

In exchange spring media, magnetically hard and magnetically soft layers are combined, so that the soft magnetic layer reduces the switching field and the hard magnetic layer provides a high energy barrier [1,2]. By increasing the magnetic hardness gradually from a soft magnetic nucleation layer to a hard magnetic storage layer a storage density of 1.2 Tbit/in^2 was demonstrated in the simulations. The computed jitter values are in the range from 0.53 nm to 0.72 nm depending of the strength of the intergrain exchange interactions.

In bit patterned media [3,4], a recording density of 2 Tbit/in^2 was achieved by writing on arrays on 7.5 nm times 30 nm sized islands of elliptical shape. As opposed to continuous media, bit patterned media requires the synchronization of the write current with the pre-patterned bit locations. The computed write margins are 1.75 ± 0.25 nm.

Magnetic multilayers deposited on self-assembled nano-spheres [5] have promising properties for high density magnetic recording by combining the merits of patterned and exchange spring media. The magnetic caps on each sphere are magnetically isolated and the intrinsic properties change gradually within one cap. We will discuss writing on magnetic nano-caps with conventional write heads and explore magnetic probe recording with MFM tips.

Acknowledgements

This research is support by the INSIC-EHDR programme and the EC FP6 project MAFIN (026513).

[1] RH Victora, X Shen, IEEE Trans Magn 41 (2005) 2828.
[2] D Suess, T Schrefl, S Fähler, M. Kirschner, G. Hrkac, F. Dorfbauer, J. Fidler, Appl Phys Lett 87 (2005) 012504.
[3] HJ Richter, AY Dobin, RT Lynch, D Weller, RM Brockie, O Heinonen, KZ Gao, J Xue, RJM v d Veerdonk, P Asselin, MF Erden, Appl. Phys. Lett. 88 (2006) 222512.
[4] T Thomson,G Hu, BD Terris, PRL 96 (2006) 257204.
[5] TC Ulbrich, D Makarov, G Hu, IL Guhr, D Suess, T Schrefl, M Albrecht, PRL 96 (2006) 077202.

Recording performances onto nano-imprinted pre-patterned perpendicular magnetic media

M. Asbahi, J. Moritz, B. Dieny and J.P. Nozières

SPINTEC, Unité de Recherche Associée CEA/CNRS
CEA/Grenoble - 17 rue des Martyrs, 38054 Grenoble Cedex 9, France
mohamed.asbahi@.cea.fr

R.J.M. van de Veerdonk

Seagate Research, 1251 Waterfront Place, Pittsburgh, PA 15222

C. Gourgon, C. Perret

LTM -CNRS, 17 rue des Martyrs, 38054 Grenoble Cedex 9, France

Patterned magnetic media, where magnetic bits are recorded on predefined single domain dots, are potential candidates for future ultra-high-density magnetic recording. They have been proposed as a way to circumvent the issue of superparamagnetic limit of excessively small grains in conventional magnetic media. This limit is expected to be reached at areal densities of the order of 300 Gbit/in².

Implementation of patterned media requires the fabrication of sub-50nm features over large areas at high-throughput manufacturing and low cost. A number of techniques have been developed to produce patterned media. In our approach, called pre-patterned media [1], perpendicular magnetic isolated tracks of sub-100nm square dots have been prepared using nano-imprint lithography (NIL) and plasma etching, followed by sputter deposition of a Co/Pt storage multilayer. NIL is a promising technique for a wide range of applications, since it allows fast replication of nanostructures on large size wafers [2] with high resolution and low-cost for mass production. NIL has the capability of patterning sub-10nm features [3] with a relatively simple equipment.

Pre-patterned silicon dot arrays of 80x80nm² spaced by 65nm and 160x80nm² spaced by 80nm were prepared over 8-in silicon wafers using nanoimprint technology (Figure.1). The arrays were fabricated by applying an imprinting force of 15kN over an 8-in silicon mould pressed in a NEB22 resist film at 130°C during 5min. The pattern was then transferred into the silicon by RIE: the residual resist in the compressed area was removed by a short oxygen-based plasma prior to pattern transfer into the Si.

(a) ***(b)***

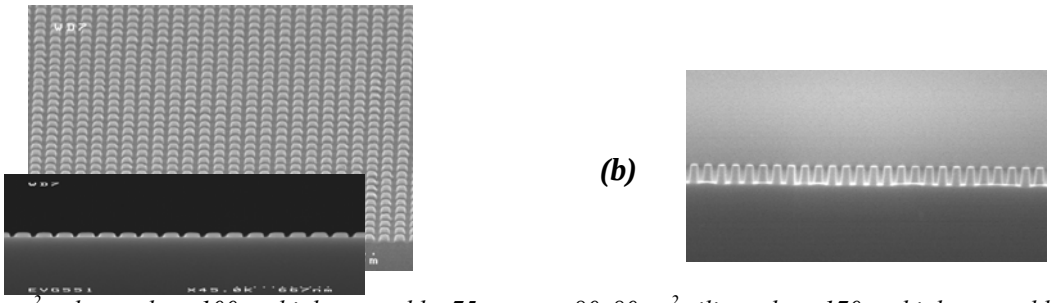

100x100nm² polymer dots, 100nm high, spaced by 75nm *80x80nm² silicon dots, 170nm high, spaced by 75nm*

Figure.1: SEM micrograph of replicated resist dots (a) and silicon dots (b).

The recording performances on the pre-patterned magnetic structures were studied with a contact tester using a high-resolution (~1nm) piezoelectric positioning stage and commercial giant magnetoresistive write/read heads. Bits with different lengths (BL), *i.e.* including a varying number of dots, were written on the pattern. The synchronization requirements needed for writing bits in patterned media were investigated along tracks of dots revealing a significant ‘‘write window,’’ where islands can be written correctly, of about half the dot period (figure.2). Moreover, the signal to noise ratio (SNR) has been calculated, by evaluating the correlation coefficients of the readback voltages of periodically written pseudo random bit sequences (PRBS) (figure.2). We concluded that the major sources of medium noise are the bit size fluctuations, stiction of the head on the medium and bit amplitude.

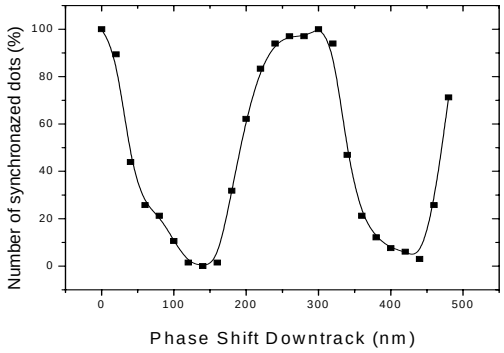

Figure.2: Bit synchronization percentage as a function of phase shift in the downtrack direction measured on a medium with 150nm dot period.

References:

[1] S.Landis, B.Rodmacq, B.Dieny, B.Dal’Zotto, S.Tedesco, M.Heitzmann, Applied Physics Letters 75, 2473 (1999); S. Landis, B.Rodmacq, B.Dieny; Physical Review B, 62, 12271 (2000); J. Moritz, B. Dieny, J.P. Nozières, S. Landis, A. Lebib, and Y. Chen. *J. Appl. Phys.* ***91****, 7314 (2002).* Landis,-S.; Rodmacq,-B.; Bayle-Guillemaud,-P.; Baltz,-V.; Dieny,-B, Japanese-Journal-of-Applied-Physics,-Part-1-Regular-Papers,-Short-Notes-&-Review-Papers. June 2004; 43(6B): 3790-5

[2] C. Gourgon, C. Perret, J. Tallal, F. Lazarino, S. Landis, O. Joubert, and R. Pelzer. *J. Phys. D: Appl. Phys.* ***38*** *(2005) 70.*

[3] S. Y. Chou, P. R. Krauss, W. Zhang, L. Guo and L. Zhuang, *J. Vac. Sci. Tachnol.* ***B 15****, 2897 (1997).*

NANOLITHOGRAPHY FOR PATTERNED MAGNETIC DATA STORAGE MEDIA

R. Luttge, H.A.G.M. van Wolferen, and L. Abelmann

Transducer Science and Technology Group, Division of Systems and Materials for Information storage (SMI), MESA+ Institute for Nanotechnology, University of Twente, PO Box 217, 7500AE Enschede, The Netherlands, phone: +31534891032, fax: +31 534893343 l.abelmann@utwente.nl

Introduction

We report on nanolithography for magnetic data storage employing CAR and LIL. Propylene glycol monoethyl ether ester as a chemical amplification positive tone resist (p-CAR) allowed us to fabricate a 18Gbit/in2 dot pattern for the first time. Using 266nm-DUV interferometric lithography, a Lloyd's mirror laser set-up is a simple and useful tool for the fabrication of high-density test samples for patterned magnetic media research [1].

Nanolithographic experiments

We characterized the new tri-layer resist that consists of a stack of BARC (Brewer Science), photosensitive p-CAR (Sumitomo Chemical) and TAR-coating (Brewer Science) at 54µW/cm2 laser intensity. Samples were prepared by spin-coating p-CAR on BARC/silicon, softbaking on a hotplate for 90s at 110°C, and performing exposure at a variable angle of incident (Θ). After postexposure bake of 90s on a hotplate at 105°C the resist is developed in OPD4262 for 60s, rinsed, spin-dried, and inspected by SEM at fixed magnification. Figure 1 shows the results in a 140nm-thick p-CAR layer at Θ=30° (P=266nm) as a function of BARC thickness. Line width in the p-CAR can be tuned achieving Critical Dimensions (CD) of 39nm. Reducing p-CAR thickness to 100nm and increasing the exposure time to 70s, successful sub- 50nm lithography was carried out at Θ=72° (P=140nm). Figure 2 shows lines/spaces pattern transfer with CD 37nm into silicon by established dry etching. Figure 3 depicts approximately 100nm-diameter dots produced by orthogonal double exposure of 21s each at Θ=45° (P=188nm) on surfaces of different reflectivity using the original resist thickness of 140nm. The standard development time of 60s was not sufficient to open the structure. Increasing the time to 90s, the dots on silicon are overdeveloped (Fig. 3B) while they are still underdeveloped (Fig. 3C) on 30nm sputtered platinum (Pt).

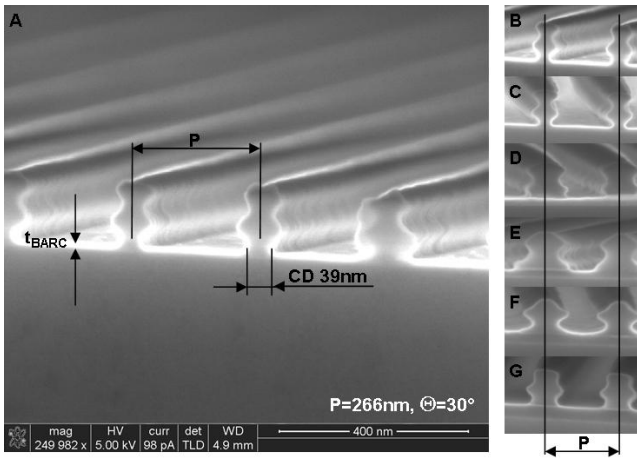

Figure 1 Optimization of p-CAR nanolithography, P=266nm: (A) SEM micrograph of p-CAR lines/spaces at CD 39nm, (B-G) shows the lithographic performance as a function of the BARC layer thickness, tBARC equals 6, 13, 21, 29, 39, and 47nm from top to bottom, respectively, at the same SEM magnification as (A).

Etch transfer and optimization

To characterize p-CAR/BARC pattern transfer we carried out exposure on a stack of TAR/p-CAR/BARC on silicon using the lithographic settings equivalent to figure 1D. TAR removes during the development process, while Figure 2A shows the cosssectional view of the p-CAR imaging layer after development. This layer acts as an etch barrier in O2 plasma using a PlasmaTherm 790 RIE tool. A standardized halogen etch is used to transfer the pattern into silicon at 37nm critical dimensions (figure 2B,C). To fabricate patterned magnetic media, however, we have to optimize lithographic performance on a magnetic film or a seed layer suitable for magnetic layer deposition, e.g. Pt. Here, nanolithography of dots on Pt was achieved by developing for 120s (figure 3A, inset D) using a BARC thickness of 21nm. The optimization of p-CAR interferometric nanolithography on Pt according to the findings in figure 1 allows for patterned magnetic media by lift-off processing using BARC as a sacrificial layer or as a transfer layer into magnetic films by ion-beam etching.

Acknowledgements

We thank J.G.M. Sanderink for the SEM micrographs, ASML for providing the resist system, and STW for financial support.

[1] R. Murillo et al., Microelectronic Engineering 78-79 (2005) 260-265

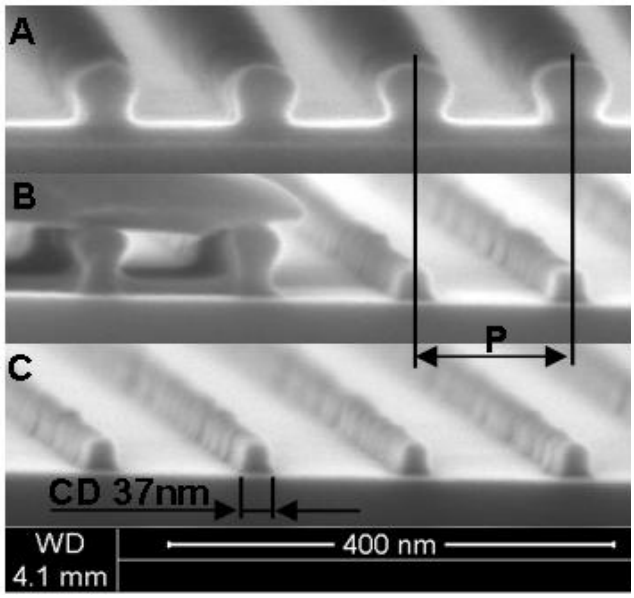

Figure 2 Cross-sectional view showing the pattern transfer, P=140nm: (A) sub-50nm p-CAR lines on 23nm BARC/silicon, (B) particle (left-hand of image) protecting resist during etching, (C) lines etched in silicon with dimensions.

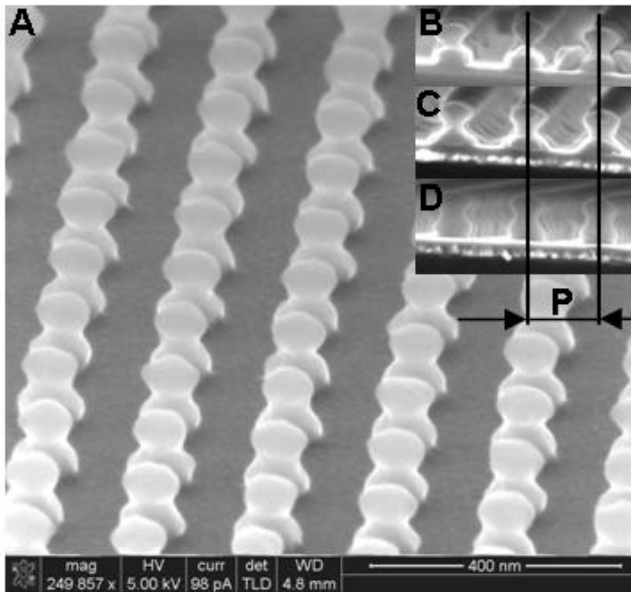

Figure 3 18Gbit/in2-dot array in p-CAR on 21nm BARC, P=188nm: (A) Overview of optimized dots on Pt/silicon, inset shows cross-sections (B) on silicon, (C) on Pt/silicon, and (D) optimized on Pt/silicon.

Magnetic Films on self-assembled nanosperes: Realization of tilted media

T. Ulbrich[1], I. Guhr[1], and M. Albrecht[1]

[1]University of Konstanz, Department of Physics, 78457 Konstanz, Germany, Phone: +49 7531 883886, Fax: +49 7531 883090, email: till.ulbrich@uni-konstanz.de

Introduction

Since its invention, the sorage density in magnetic recording has increased dramatically. But further increase might soon be slowed down by physical limitations. The structure size of the magnetic grains composing a magnetic bit is reduced to sizes, where superparamagnetic effects start to play a role. The energy barrier of the grain comes close enough to the thermal energy and the thermal stability of the grain is reduced. To delay this problem, materials with very high magnetic anisotropy have to be used. Now, maitaining writability by the limited field of the magnetic recording head becomes a problem. Several concepts like thermally assisted recording, patterned media and tilted media have been proposed as possible solutions. All methods imply major technological challenges. In a recent work we propose a combination of self-assembled nanospheres with magnetic film evaporation opening up the possibility of generating tilted media. The deposition of Co/Pt multilayer films onto self-assembled spherical particle arrays with particle sizes down to 50 nm leads to pronounced curvature-induced physical properties [1]. The so formed nanostructures on top of a sphere are monodisperse, reveal a uniform magnetic anisotropy and are magnetically exchange isolated. The film is extended over a wide region of the sphere and thus shows substantial curvature.

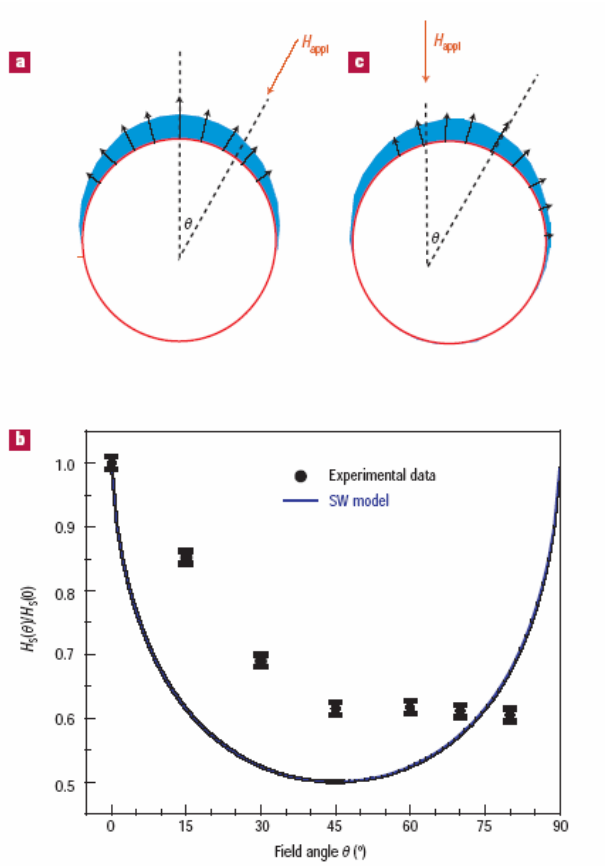

Figure 1 ***(a)*** *Schematic of a magnetic fi lm deposited on a nanosphere showing the anisotropy distribution indicated by arrows. (b) By changing the deposition direction, the anisotropy distribution is tilted by the angle of the evaporation direction. (c) Switching fi eld as a function of applied fi eld angle for an array with 50-nm particles (black dots). The angular dependence based on the Stoner–Wohlfarth (SW) model is shown as a blue line for comparison. The error bars are the standard deviation of the measurement.*

.

The film thickness varies and so do the intrinsic magnetic properties most notable the magneto-crystalline anisotropy, which is a key factor affecting the fundamental nature of the reversal process [2]. For Co/Pt multilayer film deposition, the magnitude and direction of the anisotropy depend critically on the Co layer thickness and are mainly given by the interface anisotropy between Co and Pd layers. Its direction points perpendicular to the interface layer. Therefore, film deposition on a spherical surface will in general result in a spread of the anisotropy axis across the surface with the average anisotropy axis pointing along the deposition direction. A model of the anisotropy distribution for perpendicular and tilted evaporation direction si shown in fig. 1 (a) and (b). Thus a simple change of the deposition direction results in a tilted media with user-defined tilt.

Experimental

In our studies, [Co(3Å)/Pd(8Å)]x8 multilayers were evaporated in a molecular beam epitaxy chamber operating at a base pressure of 2×10^{-10} mbar on arrays of self-assembled spherical particles with a diameter of 270 nm. The evaporation direction was tilted by 45° with respect to the sample normal. The angle dependence of the switching field was measured by magneto-optical Kerr effect (MOKE). As seen in fig. 2 the loop measured parallel to the evaproation direction (θ=0°) shows the typical behaviour of an easy axis loop while an off axis loop was measured parallel to the sample normal.

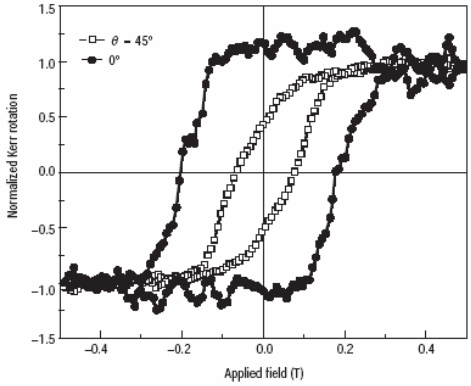

Figure 2 MOKE hysteresis loops taken under different field angles for an array of particles with a diameter of 270 nm where the deposition angle was tilted by 45° with respect to the substrate normal resulting in a tilt of the average anisotropy axis by 45°. Note that θ = 0° indicates that the applied magnetic field and the average anisotropy axis are pointing in the same direction, however, both are tilted by 45° with respect to the substrate normal.

Acknowledgements

Financial support was provided by the Deutsche Forschungsgemeinschaft through the Emmy-Noether program and the EU-Strep project MAFIN.

[1] M. Albrecht et al., Nature Material 4, (2005) 203.
[2] T. Ulbrich et al., Phys. Rev. Lett. 96, (2006) 077202.

Information Storage and Retrieval using Macro-molecules as Storage Media

Masud Mansuripur

Professor and Chair of Optical Data Storage
College of Optical Sciences
The University of Arizona
Tucson, AZ 85721
Phone: (520) 621-4879
Fax: (520) 621-4358
E-mail: masud@optics.arizona.edu
Website: www.optics.arizona.edu/masud/

Digital information can be encoded in the building block sequence of macromolecules such as RNA and single-stranded DNA. In principle, the four DNA nucleotides can be used to represent a 2-bit sequence (e.g., A = 00, C = 01, G = 10, T = 11), although practical considerations may impose certain restrictions on the specific sequences that can be used. A data storage device built around this concept must have the ability to (i) create macromolecules with any desired sequence of building blocks, i.e., write or encode the digital information into macromolecular strands; (ii) analyze and decode the sequence of a previously created macromolecule, i.e., read the recorded information; (iii) provide an automated and reliable mechanism for transferring the macromolecules between the read station, the write station, and designated locations (parking spots) for storing each such macromolecule. Although methods of writing and reading macromolecular strands are currently available, these methods require large machines and are slow and expensive. In an ideal molecular data storage system, routine operations such as write, read, erase, store, and transfer must be carried out within an integrated chip, reliably and at high speed. As a possible alternative to present-day magnetic and optical disks and tapes, we envision a system in which data blocks are encoded into macromolecules constructed from two or more distinct bases, say, *x* and *y*; the bases can be strung together in arbitrary sequence such as *xxyxyyxy*… *xyx* to represent binary sequences of user-data (e.g., *x* = 0, *y* = 1). The macromolecular data blocks are created in a *write station*, transferred to *parking spots* for temporary storage, and brought to a *read station* for decoding and readout. The "erase" operation is as simple as discarding a data block and allocating its parking spot to another macromolecule. The capacity of the proposed molecular storage system can easily exceed 10^{15} bytes/cm^3. For a comparison with a current state-of-the-art technology, note that storing 10^{15} bytes on DVDs requires a 128 meter-tall stack of these 12cm-diameter platters.

SCALING ISSUES IN NAND FLASH MEMORY

Jaechul Om

Hynix Semiconductor Inc.
San 136-1,Icheon –si, Kyoungki-do, 467-701, Korea
031-639-9079; fax: 031-630-4545; e-mail: jcom@hynix.com

Introduction

Recently, various mobile appliances such as hand-held phone, digital still camera, USB driver, MP3 player drive a new demand for non-volatile memory which is small, light, with high density, high speed ,low cost and low power. Solid-State-Disk (SSD) application will open another new market to non-volatile memories. But, the development of Flash memory, mainly floating gate cell structure, which has been continued for last two decades, faces a few technical challenges for further scaling. This paper listed typical technical issues for floating gate cells and suggested candidate cells to avoid or reduce them for the design rule beyond 40 nm.

Density Migration and Design Rule Shrink Trend

Due to dramatic demand for mass storage memory for mobile appliances, the density of NAND flash memory has doubled every year since early 2000's (See figure 1). In early 2000's, the density doubling was mainly made by lithographic tool development for higher resolution, that means ~$4F^2$ cell size, where F means minimum design rule. But, the density doubling was made by both lithographic tool development and 2 bit MLC (Multi-Level-Cell) in the middle 2000's that means ~$2F^2$ cell size. If we want to continue this trend to late 2000's, it requires innovative lithographic tool development which could shrink cell size down to ~F^2 or 4bit MLC. The prospect for late 2000's is very unclear considering this shrink trend.

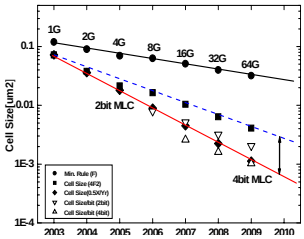

Figure 1 Tech. vs. Cell Size Trend.

Scaling Limits of Floating Gate Cell

a) Program Speed

As technology is shrunk to meet density doubling trend every year, cells are get closer to increase capacitive coupling between adjacent cells(see figure 2). This interference widens Vt distribution of cells to induce failures especially for MLC operation. To reduce this, cross-sectional area of floating gate is reduced lowering coupling ratio between floating and control gate which causes slow program speed. To maintain program speed, it is required to reduce the thickness of IPD (Inter-Poly-Dielectric) which is typically composed of ONO(Oxide-Nitride-Oxide)stack. But scaling of ONO thickness is limited to guarantee non-volatile storage. It is expected that ONO stack will be replaced by high-K material like Al2O3, HfO2, ZrO2 under 40nm technology.

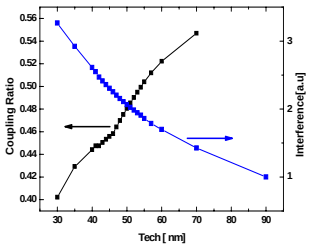

Figure2 Tech. vs C.R & Interference

b) Interference

Interference between cells makes wide vt distribution and makes MLC operation difficult when scaled down to under 40nm technology. To avoid this interference fundamentally and to secure MLC operation, cells which store charges at traps in a dielectric layer is suggested. One type of charge trap cell is NROM[4] cell which is initially suggested for NOR application, can operate in 2 bit/cell or 4bit/cell mode. The other type is TANOS[5] cell which is suggested for NAND operation, can operate up to 2bit/cell.

c) Reliability

As cell size is scaled down, the number of charge in floating gate is reduced drastically, so a few electron losses may result in a fatal failure. It is suggested to develop a robust tunnel oxide which has less SILC effect. Another solution may be to increase effective cell area by using 3-dimensional cell structure like finFET. Nitride trap memory which is immune to leakage may provide fundamental solution to this issue.

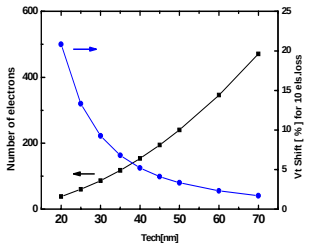

Figure 3 Tech. vs # of charges in a Cell

How to Extend the Life of Floating Gate Cell

a) Increase Coupling Capacitance using High-K IPD

As technology is shrunk down to under 40nm, the space between adjacent floating gate is so small that control gate can not wrap around (see figure 4) the floating gate which results in small coupling ratio. So, it is mandatory to adopt high-k IPD to maintain same program speed as technology is shrunk.

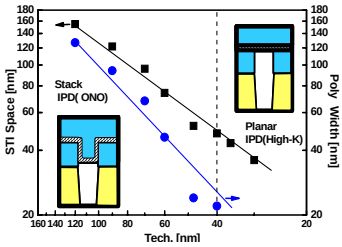

Figure4 Tech. vs. Cell Size Trend.

b) High Tunneling Current with Low Leakage

To increase program speed , it is also required to enhance tunneling current through tunnel oxide. But, the scaling of tunnel oxide thickness induce retention failure because the SILC (Stress-Induced-Leakage-Current) is closely depends on the tunnel oxide thickness. New concepts like VARIOT[6] or BE-tunnel oxide[7] will be solution to this issue.

Nitride Memory as an Alternative

Recently, CTF(Charge-Trap-Flash) with TANOS structure has been considered to be one of candidate cells for next generation beyond 40nm technology. But CTF technology still has problems to be solved in terms of program speed and retention characteristics. The former is due to the finite number of traps in nitride compared to floating gate. So, the program speed of CTF is always slower than floating gate cell. The latter is related to erase mechanism of CTF compared to floating gate. In CTF deeper traps in the band-gap shows slower erase speed and longer retention characteristics (see figure 5). To secure long retention, the erase speed may be slower than floating gate cell. For CTF, these technical barriers are lying in the road to the next generation cell.

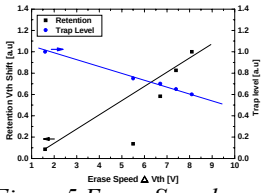

Figure5 Erase Speed vs. Nitride Trap Level

Reference

[1] F.Masuoka et al , IEEE Tech. Dig. IEDM 1987, pp. 552-555.

[2] Y.Shin ,"NVM Technologies for Beyond 2010 " , Symp. on VLSI Circuits Dig. 2005, pp.156-159.

[3] C.H.Lee et al," Multi-Level NAND Flash Memory with 63 nm node TANOS cell structure ", SOVT. Dig. 2006.

[4] A. Shappir et al ," NROM window sensing for 2 and 4-bits cell products ", NVSMW 2006.

[5] J.D.Lee et al,"Effects of floating gate interference on NAND flash memory cell operation "EDL,pp. 264 2002.

[6] J.V.Houdt et al ,"High-K materials for nonvolatile memory application," IRPS. Tech Dig.2005, pp. 234-239.

[7] H.T. Lue et al IEEE Tech. Dig IEDM. 2005, pp. 555-558.

Holographic drive and media developments at InPhase

Kevin Curtis

InPhase Technologies, Inc., 2000 Pike Road, Longmont, Colorado 80501 USA
kevincurtis@inphase-tech.com

Abstract

InPhase Technologies is developing a holographic recordable optical drive and media for professional archive applications. The user capacity for the first product is 300GB with sustained write/read user transfer rates of 20MByte/s. The architecture, design and implementation of this holographic drive and media are described. In addition, a holographic consumer ROM product is under development and will briefly be described.

About the speaker

Kevin Curtis is Chief Technology Officer and founder of InPhase Technologies in Longmont, Colorado. In this role, Kevin manages and provides the technical direction for the advanced research and development of InPhase's holography-based technologies for storage.

Prior to founding InPhase, Kevin was a member of the technical staff at Bell Laboratories where he directed the efforts of the holographic storage program upon which InPhase was founded. This included business development and raising the Series A investments to start InPhase. Kevin has worked at Caltech, Northrop and Bell Labs on holographic optical systems for over 16 years.

Dr. Kevin Curtis received his B.S., M.S., and Ph.D. degrees in electrical engineering in 1990, 1992 and 1994, respectively, all from the California Institute of Technology, Pasadena, California. He has authored > 70 publications and has more than 50 U.S. Patents awarded on holographic storage.

NOVEL AZOTHIOPHENE POLYESTERS FOR HOLOGRAPHIC STORAGE

Avtar S Matharu[a*], Shehzad Jeeva[a] and PS Ramanujam[b]

a. Department of Chemistry, University of York, York YO10 5DD. England. Tel: +44 1904 434187. Fax: +44 1904 432516. Email: am537@york.ac.uk.

b. Optics and Plasma Research Department, Risoe National Laboratory, PO Box 49, Frederiksborgvej 399, DK-4000, Denmark. Tel: +45 4677 4507; E-mail: p.s.ramanujam@risoe.dk.

Introduction

The need for new optical storage media is ever evolving as we are overburdened with a modern-day society that craves for ever-increasing amounts of information. For example, satellite images, X-ray images, movies, music etc utilise mega- to giga-bytes of information requiring both regular retrieval and archiving. BluRay DVD is already upon us, which effortlessly stores 27 GB [1], whereas InPhase Technologies' boast their holographic Tapestry™ media which offers in excess of a staggering 100 GB of storage capacity [2]. Holographic data storage continues to interest us and to this effect we have developed novel azothiophene polyester **1** capable of storing data. Azothiophenes are known in the literature but primarily for their use as disperse dyes, non-linear optical materials and potential materials for solar cell applications [3]. To the best of knowledge they have yet to be investigated for their data storage properties, the results of which are summarized below.

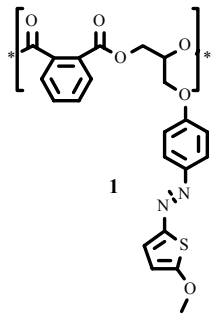

1

*Figure 1 Structure of azothiophene polyester **1***

Results and Discussion

Our novel polyester (figure 1) is synthesized via *in vacuo* high temperature melt transesterification to yield a light yellow powder. Figures 1 and 2 show its UV-Vis steady state characteristics of the azodiol precursor when probed at 410 nm (π-π* *trans*-isomer, λmax 406 nm, *trans-cis*-photoreversion) and at 314 nm (π-π* *cis*-isomer, λmax 346 nm, *cis-trans*-photo-reversion). The isosbestic point is clearly detected at 357 nm.

An investigation of the optical data storage characteristics of a solution cast film of azopolyester **1** with a thickness of 65 μm is summarised in Figures 3-6. Preliminary measurements are presented for a wavelength of 532 nm, as the large film thickness together with maximum absorption at 410 nm, precluded measurements at 405 nm. The first order diffraction efficiency at a wavelength of 633 nm

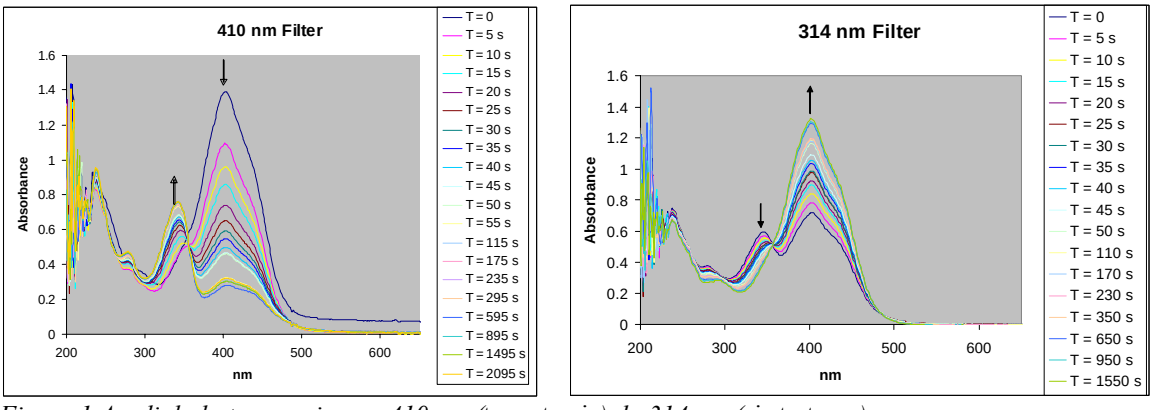

*Figure 1 Azodiol photoreversion a. 410 nm (*trans to cis*), b. 314 nm (*cis to trans*)*

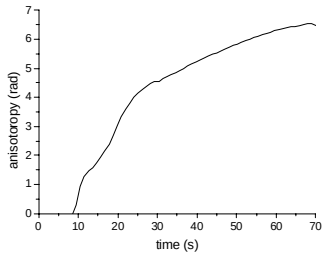

Figure 3 Anisotropy induced at 532 nm as a function of time, probed at 633 nm

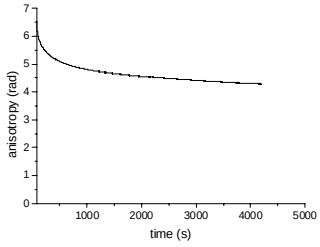

Figure 4 Room temperature stability of the anisotropy

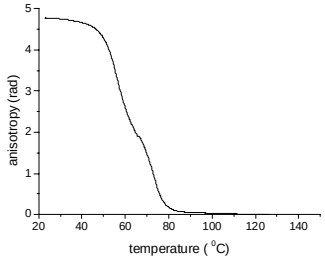

Figure 5 Thermal stability of the induced anisotropy

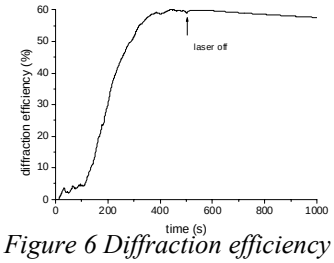

Figure 6 Diffraction efficiency measurement at 633nm

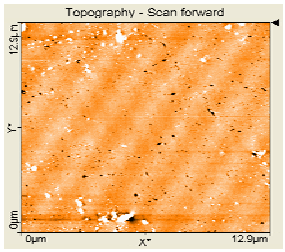

Figure 7 AFM scan of the diffraction grating

when a polarisation holographic recording is made in the film, with two orthogonally circularly polarised beams is shown in Figure 6. The read-out beam was circularly polarised. The grating was recorded at an intensity of 30 mW/cm^2. High diffraction efficiency is achieved, which is also stable at room temperature.

Previously, recording with two orthogonally circularly polarised beams has resulted in a very large surface relief pattern [4], which is detrimental for multiplexing due to increased scattered noise. However, in the present case, an AFM scan of the grating shows very little surface relief (Figure 7). The maximum surface relief obtained is found to be less than 5 nm. This is also confirmed by the fact that only one order of diffraction is present, when the grating is read-out with a circularly polarised beam [5]. Thus this material is ideally suited for polarisation holographic multiplexing.

[1] For full account of the development of Blu Ray technology see http://www.blu-ray.com.
[2] For full account of Tapestry Media see http://www.inphase-tech.com.
[3] J. O. Morley, O.J. Guy and M. H. Charlton, *J. Phys. Chem. A*., 2004, **108**, 10542; M. Maggini, G. Possamai, E. Menna, G. Scorrano, N. Camaioni, G. Ridolfi, G. Casalbore-Miceli, L. Franco, M. Ruzzi and C. Corvaja, *Chem. Commun*., 2002, 2028; S. Beckmann, K. H. Etzbach, R. Sens, United States Patent, 1998, US 5 783 649.
[4] N. C. R. Holme, L. Nikolova, S. Hvilsted, P. H. Rasmussen, R. H. Berg and P. S. Ramanujam, *Appl. Phys. Lett.* 1999, **74**, 519.
[5] L. Nikolova and T. Todorov, *Opt. Acta*, 1984, **31**, 579.

Data security in memory systems and solutions

Doris Keitel-Schulz

Quimonda AG, Munich, Germany

PHASE-CHANGE AND ELECTROLYTIC SWITCHING IN CHALCOGENIDE THIN FILMS

Ramanathaswamy Pandian[1], Bart J. Kooi[1*], George Palasantzas[1], Jeff Th. M. De Hosson[1] and Andrew Pauza[2]

[1]Department of Applied Physics, Zernike Institute for Advanced materials, University of Groningen, Nijenborgh 4, 9747 AG Groningen, The Netherlands.
*[2]Plasmon Data Systems Ltd., Whiting Way, Melbourn Royston Hertsfordshire, SG8 6EN, U. K., *e-mail: b.j.kooi@rug.nl*

Abstract

We are presenting our important finding that certain chalcogenide materials, well-known from rewritable optical recording, allow resistive memory states which are a combination of two electrically-induced (reversible) switching processes i.e., an actual amorphous-crystalline phase transformation and a (electrolytic) polarity-dependent resistance change. Nanocrystalline marks were written electrically in amorphous $Ge_2Sb_{2+x}Te_5$ films using atomic force microscopy, and their resistance was found to depend on the polarity of the applied voltage with a resistance difference greater than 3 orders of magnitude. However, no contrast in current has been detected between the crystalline higher-resistance state and surrounding amorphous phase. This resistance switching is reversible for bias voltages well-below the threshold voltage required to induce the phase transformation. The switching mechanism is attributed to the solid-state electrolytic behaviour due to the presence of excess Sb in the films. Our results render exciting technological opportunities for data storage and encryption by combining both switching concepts.

Introduction

In recent years, the main focus of phase-change data-storage research is returned to *resistance switching* that is based on the structural switching between the amorphous and crystalline phase of the chalcogenide material. Apart from this, certain chalcogenides containing Ag show a special phenomenon of *polarity-dependent resistance switching*, which is related to the solid-state electrolytic character and high ionic conductivities of the chalcogenides, and is also called ionic or electrolytic switching. For one polarity, the chalcogenide medium becomes electrically conductive by forming conducting filamentary pathways between the electrodes, whereas for the reverse polarity it becomes relatively insulating or at least low-conducting by breaking the previously formed conducting filaments.

Although the two abovementioned resistance switching mechanisms (phase- and polarity-dependent) were up to now treated separately, it was recently conjectured that they were '*different faces of a chameleon*' that should be brought together and studied in a unified approach. In this study, we exploit these two mechanisms simultaneously at the nanoscale using an atomic force microscope (AFM). In $Ge_2Sb_{2+x}Te_5$ (GST) film, we demonstrate that the *contrast* between crystalline marks and the amorphous background can be written and erased for a significant number of cycles using AFM only.

Highlighting results

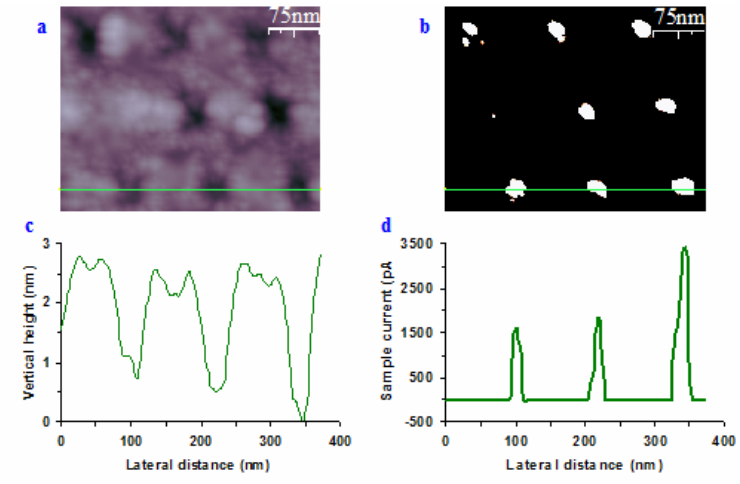

1. Electro-thermal data writing. a: A contact mode AFM topograph showing a written crystalline bit pattern in a 40 nm amorphous GST film. **b:** Current image that is simultaneously recorded with image **a**. **c:** A line profile drawn in the topography image (**a**) over a row of crystalline bits. In the profile, the bits are visible as small nano-valleys. **d:** A line profile drawn in the current image (**b**) on a row of highly conducting spots. The conductive spots are well distinguishable from the background with about 3 orders of magnitude contrast even though the current flowing through them is only a few nano-Amperes.

2. Polarity-dependent resistive switching at the nanoscale. a, An AFM topograph showing a crystalline bit pattern in a 40 nm amorphous GST film. **b**, **c** and **d** are the height images (topographs) of a bit during the SET, RESET and SET operations, respectively, with ±1.5 V. **e**, **f** and **g** are the current images showing the ON, OFF and ON states, respectively, of the bit. **h**, **i** and **j** are the current profiles showing the ON, OFF and ON state current, respectively. The height images **b**, **c** and **d** indicate that there is no detectable topographical change due to SET/RESET operations. ON state current profiles **h** and **j** show more than 3 orders current contrast between the high-conductive bit and the amorphous background. The current image **f** and current profile **i** of the bit at OFF state indicate that the conductivity of the bit in the OFF state is as low as the background amorphous phase (i.e. < 5 pA).

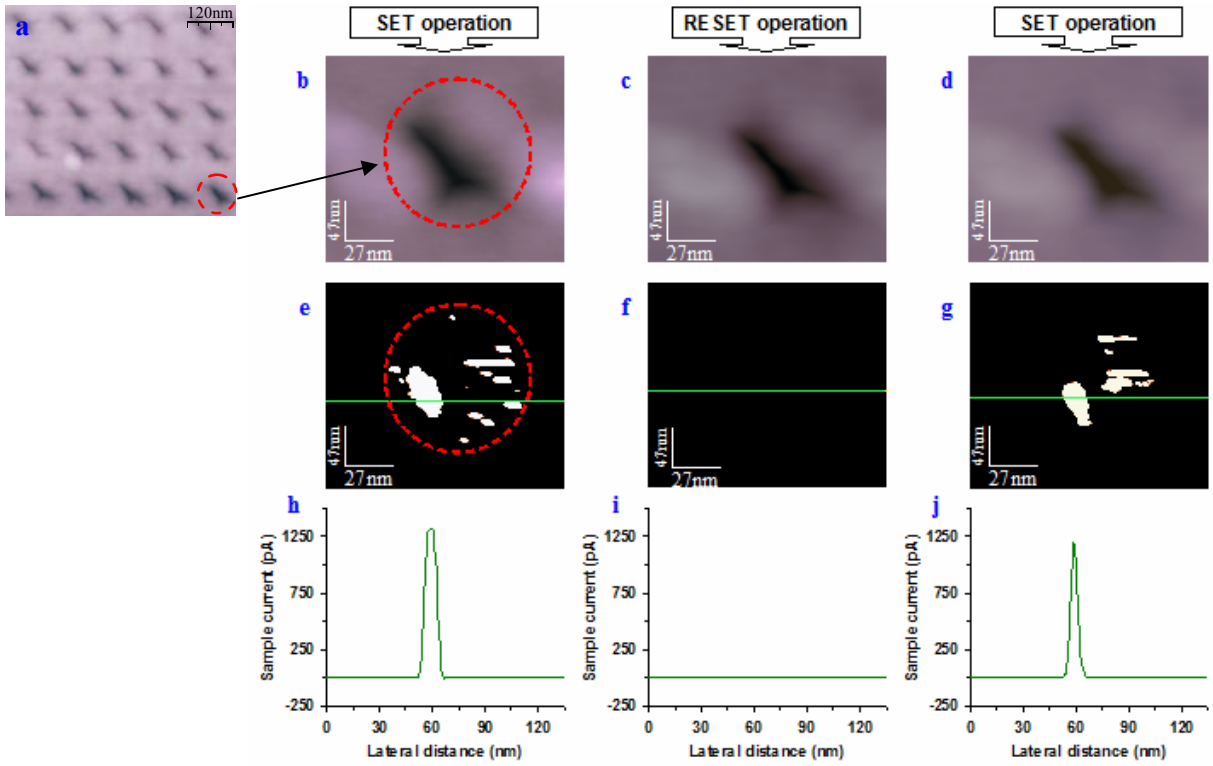

RF magnetron sputtered $Ge_2Sb_2Te_5$ thin films characterization

J. Gutwirth[1], T. Wagner[1], M. Hrdlicka[1], J. Prikryl[1], P. Bezdicka[2], Mil. Vlcek[3], M. Frumar[1]

[1] University of Pardubice, Research Centre LC 523 and Department of General and Inorganic chemistry, Legions' sq. 565, 53210 Pardubice, Czech Republic E-mail: Tomas.Wagner@upce.cz, tel: +420 466 037 144, fax: +420 466 037 311
[2] Institute of Inorganic Chemistry of AS CR, 25068 Husinec-Rez, Czech Republic
[3] Joint Laboratory of Solid State Chemistry of University of Pardubice and IMC of AS CR, Studentska 84, 53210 Pardubice, Czech Republic

Introduction

Currently, chalcogenide materials were used massively for rewritable non-volatile data storage. They are widely applied as active layers of rewritable optical discs as well as they are under intensive research targeted to development for alternative memories (called Phase-Change RAM (PC-RAM) or Chalcogenide RAM (C-RAM)) to commercially successful semiconductor FLASH memories [1]. Both optical and electrical recording is based on reversible phase transformation between amorphous and crystalline phase [2] caused by laser/electrical pulses. Detection is based on contrast in reflectivity/resistance between amorphous and crystalline state. Dominant compositions included doped Sb-Te system, usually Ge-Sb-Te (GST) or Ag-In-Sb-Te (AIST).

Results

Thin amorphous GST films were prepared by RF (f = 13.56 MHz) magnetron sputtering in argon plasma. 1 inch target of composition $Ge_2Sb_2Te_5$ and geometry with rotated planparallel angle resolved substrate holders (A - D) was used. Silicon, silica glass and microscope slides were used as a substrates. Depositions were carried out under different conditions; i.e. different RF power and Ar pressure (Table 1.).

Sample	Ar pr. [Pa]	RF pow. [W]	Dep. Time [min]	Dep. Rate [nm*min^{-1}]	E_g^{opt} [eV]	Film Thick. [nm]	Film Rough. [nm]	n ($\lambda\rightarrow\infty$)
1 A	2.0	20	60	3.78	0.75	226.6	7.4	2.97
2 A	2.0	10	60	1.57	0.81	94.2	7.6	2.89
3 A	1.0	20	60	7.67	0.74	460.1	6.4	2.83
4 A	4.0	10	60	0.77	0.80	46.2	7.8	2.94

Table 1. Deposition conditions together with some properties obtained by VASE.

Thin films were characterized by SEM-EDX (composition (Tab. 2., 3.), surface morphology), XRD (crystallinity) and by Vis-NIR spectroscopy and VASE (thin film thickness/roughness, spectral dependence of refractive index n and extinction index k, optical band gap energy Egopt (some of these properties are summarized in Tab. 1. and Fig. 1.)) .

Sample	Composition			Composition Ratio		
	Ge	Sb	Te	Ge:Te [0.4]	Sb:Te [0.4]	Ge:Sb [1.0]
1 A	2.17	1.97	4.87	0.446	0.404	1.103
2 A	1.98	1.99	5.04	0.393	0.394	0.995
3 A	2.37	2.01	4.61	0.514	0.437	1.178
4 A	2.31	1.68	5.02	0.459	0.334	1.376

Table 2. Composition and composition ratio (together with ideal values of $Ge_2Sb_2Te_5$ in brackets) of samples deposited on Si substrates.

Temperature dependence of sheet resistance was measured by Van der Pauw method [3] at average heating rate v = 5s°C*min-1 as seen at Fig. 2. This way thermally treated films were characterized by SEM-EDX and by XRD.

Sample	Substrate	Composition			Composition Ratio		
		Ge	Sb	Te	Ge:Te [0.4]	Sb:Te [0.4]	Ge:Sb [1.0]
3 A	Si	2.37	2.01	4.61	0.514	0.437	1.178
	SiO_2	2.07	2.01	4.92	0.420	0.409	1.027
3 B	Si	2.16	1.91	4.92	0.439	0.388	1.132
	SiO_2	2.21	1.98	4.82	0.459	0.410	1.118
3 C	Si	2.42	1.88	4.69	0.517	0.402	1.286
	SiO_2	2.39	1.91	4.71	0.507	0.405	1.251
3 D	Si	2.31	1.92	4.77	0.484	0.402	1.203
	SiO_2	2.09	2.02	4.89	0.428	0.413	1.037

Table 3. Composition and composition ratio (together with ideal values of $Ge_2Sb_2Te_5$ in brackets) of different angle resolved sputtering positions of sample 3.

Several $Ge_2Sb_2Te_5$ thin films were prepared by RF magnetron sputtering. Influence of deposition conditions (RF power and Ar pressure) and substrate characteristics (substrate holder angle deviation from normal direction and substrate material) to stoichiometry, crystallinity, surface morphology and some optical properties (as written above) important for optical data storage were established. Influence of conditions (summarized above) to sheet resistance thermal dependence of prepared samples was also studied due to potential application for multilevel PC-RAM memories.

Acknowledgements
Authors thank to Ministry of Education, Youth and Sports of Czech Republic (Research Centre grant LC 523, grant MSM 0021627501), to EC (project CAMELS) and to Czech Science Foundation (grant GA 203/06/1368) for financial support.

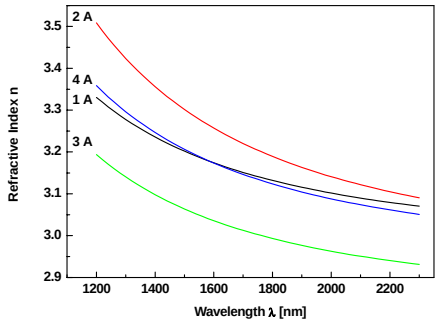

Figure 1. Refractive index spectral dependence of prepared thin films.

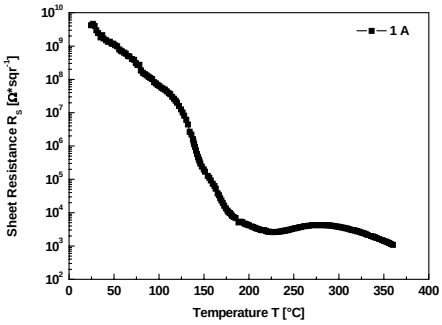

Figure 2. Typical sheet resistance temperature dependence (sample 1 A).

[1] S. J. Hudgens, *Mat. Res. Soc. Symp. Proc. Vol*. 918 0918-H05-01-G06-01 (2006).
[2] S. R. Ovshinski, *Phys. Rev. Lett* 21, 1450 (1968).
[3] P. M. Hemenger, *Rev. Sci. Instrum.* 44, **6** (1973).

CONDUCTION MECHANISMS OF AMORPHOUS AND CRYSTALLINE $Ge_2Sb_2Te_5$ AT LOW TEMPERATURES

F. Merget[1], B. Berghoff[1], D. H. Kim[1], H. Kölpin[2], M. Först[1], H. Kurz[1]

[1] *Institute of Semiconductor Electronics, RWTH Aachen University, Sommerfeldstrasse 24, D-52074 Aachen, Germany*
**E-mail: merget@iht.rwth-aachen.de*

[2] *Materials Chemistry – RWTH Aachen University, Kopernikusstr. 16, 52074 Aachen, Germany*

Introduction

The conduction mechanisms of $Ge_2Sb_2Te_5$ (GST) and other chalcogenide phase change materials have been studied extensively in the amorphous and crystalline phase state at room temperature and elevated temperatures. Kim et al. have reported an Arrhenius-like temperature dependence of the electrical low-field conductivity for the amorphous and crystalline phase. i.e.:

$$\sigma_\alpha(T) = \sigma_{\alpha,0} \cdot \exp\left\{-\frac{E_{A,\alpha}}{k_B \cdot T}\right\} \quad and \quad \sigma_\chi(T) = \sigma_{\chi,0} \cdot \exp\left\{-\frac{E_{A,\chi}}{k_B \cdot T}\right\} \qquad (1)$$

Activation energies of $E_{A,\alpha}$ = 120 meV and $E_{A,\chi}$ = 20-70 meV have been determined [1].

Here, we present electrical low-field resistance measurements of amorphous, micro-crystalline and crystalline $Ge_2Sb_2Te_5$ at low temperatures down to 8 K. The temperature dependences of the electrical conductivity of amorphous and crystalline $Ge_2Sb_2Te_5$ films clearly deviate from single Arhenius-type behaviours in this cryogenic temperature regime. In the crystalline phase the conductivity is reduced by the freeze-out of thermally activated carriers, so that carrier mobility is primarily determined by grain boundaries. In the amorphous state the carrier transport is dominated by carrier-hopping from localized states and variable-range-hopping at very low temperatures.

Sample Preparation

Figure 1 shows a shematic cross-sectional view of the samples fabricated for the low-temperature measurements. The sputter-deposited GST-layer is embedded in a layer stack of SiO_2 on a silicon substrate. Ti/Au-contacts with various distances are fabricated on top of the GST-layer to provide electrical access. The fabrication process for the metal contacts includes low-resolution contact lithography, CHF_3-RIE etching of the SiO_2 capping layer, electron-beam metal deposition and lift-off.

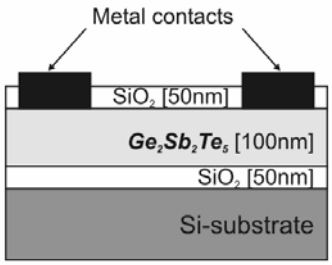

Fig. 1: Schematic cross-sectional view of the dedicated two-point resistance measurement samples for low-temperature measurements.

Low-temperature measurements are performed in an evacuated *He*-cooled cryo-chamber with semi-automated Au-plated Tungsten needle-probes.

The amorphous sample (α-sample) is in the as-deposited state, the micro-crystalline sample (μχ-sample) has been annealed for 20 min at 160 °C, and the crystalline sample (χ-sample) has been annealed for 3 h at the same temperature.

Results & Discussion

Figure 2 shows the temperature dependent electrical conductivities σ of amorphous, µ-crystalline and crystalline GST. Obviously, the conductivities of all three phase states cannot be described by single activation energies over the investigated temperature range, in contrast to observations at elevated temperatures above 300 K [1].

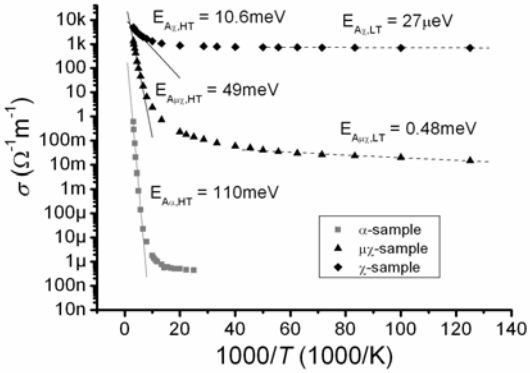

Fig. 2: Temperature dependence of electrical conductivity of amorphous, µ-cristalline, and crystalline $Ge_2Sb_2Te_5$.

For χ-GST and µχ-GST Arrhenius-type activation energies of $E_{A\chi,HT}$ = 10.6 meV, $E_{A\mu\chi,HT}$ = 49 meV, respectively, can be identified for temperatures down to 150 K. If the temperature is further decreased, a large amount of thermally activated carriers are "frozen out". Consequently, the transport is primarily limited by grain boundarys which decrease the carrier mobility [2]. The corresponding activation energies decrease drastically by more than two orders of magnitude to values of $E_{A\chi,LT}$ = 27 µeV and $E_{A\mu\chi,LT}$ = 0.48 meV, respectively.

In contrast, the amorphous phase exhibits three conduction regimes (see Fig. 3). Again, down to temperatures of about 150 K an Arrhenius-type activation energy of $E_{A\alpha,HT}$ = 110 meV can be identified. At lower temperatures (150 to 60 K) the carrier transport is dominated by carrier hopping from localized states following an ~exp ($(E_{A\alpha,HT} - \Phi_T)/k_BT$) dependence with Φ_T the energy offset of trap levels to the mobility edge [3]. At very low temperatures the electrical conductivity diverges from the Arrhenius-type temperature dependence and can be described by a ~exp ($E_{A\alpha,LT}$ / k_BT $^{1/4}$) dependence [4]. This is attributed to variable-range-hopping.

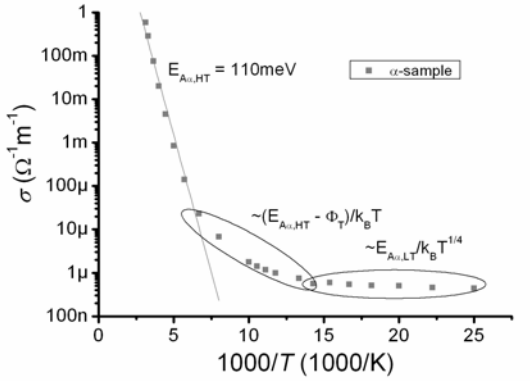

Fig. 3: Temperature dependence of electrical conductivity of amorphous $Ge_2Sb_2Te_5$.

Acknowledgement

This work has been supported by the *Deutsche Forschungsgemeinschaft (DFG)* under contract KU540/48-1.

References

[1] D.H. Kim et al., submitted to APL, 2006
[2] P. Sheng et. al., Phys. Rev. Lett., Vol. 31, 44, 1973
[3] N. F. Mott, Electronic Processes in Non-crystalline materials, Oxford (1979)
[4] A. J. Grant et. al., Solid State Comm., Vol.15, p. 563, 1974

UNDERSTANDING MULTI-STATE PHASE-CHANGE MEMORIES AND PROCESSORS

C D Wright, K Blyuss and P Ashwin

School of Engineering, Computer Science and Mathematics, University of Exeter
Exeter EX4 4QF, UK e-mail: David.Wright@exeter.ac.uk

Introduction

Electrical memory devices based on the reversible transition between amorphous and crystalline phases in chalcogenide alloys, such as GeSbTe, are attracting much interest, in particular as possible replacements for silicon 'Flash' memory. The development of binary memories currently predominates, but multi-state memories will be of much interest in future since they offer greater storage capacity. More remarkable and far-reaching potential applications of phase-change technology, recently discussed by S.R. Ovshinsky and coworkers [1,2], include the provision of non-Von-Neumann (micro) processing devices capable of both general-purpose computation and 'cognitive' function. The origins of such possibilities lie in the detail of the phase-transformation event itself. In conventional phasechange memories crystallization relies on both electronic and thermal effects; applying a voltage above a certain value induces a conducting on-state in the previously high-resistance amorphous material, allowing current to flow which in turn generates heat to drive crystallization. The electrical resistance during switching changes abruptly at the 'percolation threshold', where growing (nano)cystallites merge to form the first conducting pathways between device electrodes. It is the pre-threshold region that offers the potential to perform general-purpose computation and provide artificial neuron-like capabilities. This may be explained by considering pre-percolation behaviour to involve energy-accumulation; energy is accumulated and crystal clusters grow as each input pulse is applied and when enough energy has been accumulated to reach the percolation threshold the cell resistance changes abruptly. This energy accumulation property has the potential to implement basic mathematical operations such as addition, subtraction, multiplication and division, as well as more complex functions such as factoring, encryption and logic [1,2]. The accumulation property, the presence of a distinct threshold, and a non-linear (output) transition (between resistance states) mimic the basic action of a biological neuron. Furthermore, the (synaptic) weighting of inputs might be provided by another phase-change cell operating in the multilevel storage regime. Thus, an artificial neuron might be achieved using only phase-change cells. Some of these novel concepts for the use of phase-change materials are studied here using a theoretical approach based on rate-equation models [3].

Theory

The basis of the rate-equation approach is determination of the distribution function, $Z(n, t)$, representing the density of crystal clusters of size n (monomers) at moment t. Changes in the crystal cluster sizes occur when 'monomers' are attached to or detached from existing clusters. In all the simulations presented here a discrete version of the rate-equation has been used for which the temporal evolution of the cluster density Z is given by [3]

$$\frac{\partial Z(n,t)}{\partial t} = f(n-1,t,T)Z(n-1,t) + d(n+1,t,T)Z(n+1,t) - f(n,t,T)Z(n,t) - d(n,t,T)Z(n,t)$$

where f(n, t,T) and d(n, t,T) are, respectively, the rates of attachment to and detachment from a crystal cluster of size n units (monomers). We have used this model to investigate the use of a phase-change cell as both a processor and a multi-state memory.

Results

Figure 1 shows the case for an initially amorphous cell (all monomers) subject to successive heat pulses (each pulse set the temperature in the cell to 3500C for 50 ns with pulses 1μs apart). The cell was reset by the tenth pulse into the amorphous state. Figure 1 reveals a monotonically increasing crystallized fraction with increasing number of pulses. The number of monomers (not shown) decreases monotonically while the number of dimers (n=2) and multimers (n = nmax) increases monotonically. The phase-change cell is effectively accumulating energy with each pulse and crystal clusters grow in size and number as the anneal progresses. Each particular crystallized fraction in the annealing cycle corresponds to a particular cell resistance in a real device and so by monitoring the cell resistance a decimal counter/adder, or more general purpose processor, could easily be obtained.

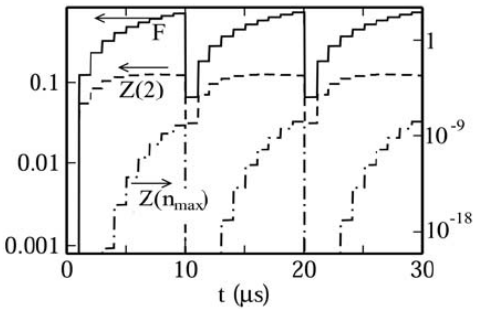

Figure 1: Crystallized fraction F (i.e. sum of Z(n) from n = 2 to n = nmax) (solid), density of dimers Z(2) (dashed) and density of multimers Z(nmax) (dash-dot) for an anneal cycle comprising successive 350 0C, 50ns pulses at 1μs intervals, followed by a reset pulse.

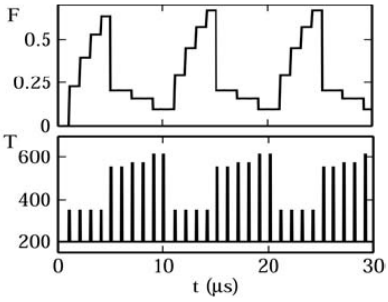

Figure 2: The crystalline fraction (top) as a function of time during an anneal comprising 100 ns pulses at 3500C (4 pulses), 5500C (2 pulses), 5700C (2 pulses) and 6100C (2 pulses).

Next, we explore the so-called 'direct overwrite' or 'multi-state' storage regime. Figure 2 shows the results of simulations together with details of temperature variation during the anneal. For relatively low temperature anneals the crystalline fraction is 'remembered' from the previous step and we are in the energy accumulation regime, while for higher temperatures the crystalline fraction moves repeatably within the space of one pulse directly to a given state. In this latter so-called multi-state or direct-overwrite regime, the final crystallized fraction is independent of the initial state and depends only on the annealing pulse duration and amplitude (temperature), yielding a controllable multi-state memory.

Acknowledgements

The Leverhulme Trust via its Fellowship scheme (for C D Wright) is acknowledged, as is the EPSRC via grant GR/S31662/01.

[1] S.R. Ovshinsky and B. Pashmakov, MRS Proceedings, 803, 49 (2004).
[2] S.R. Ovshinsky, Jpn J Appl Phys, 43, 7B, 4695 (2004).
[3] S. Senkader and C.D.Wright, J. Appl. Phys. 95, 504 (2004).

The role of vacancies in phase change materials – controlling material properties from first principles

Matthias Wuttig[1], Daniel Lüsebrink[1], Daniel Wamwangi[1], Wojciech Welnic[1]*, Michael Gilleßen[2], Richard Dronskowski[2]

[1] Physikalisches Institut IA, RWTH Aachen, 52056 Aachen, German
[2] Institut für anorganische Chemie der RWTH Aachen, 52056 Aachen, Germany
**current address: Laboratoire des Solides Irradiés, École Polytechnique, Palaiseau, France, European Theoretical Spectroscopy Facility (ETSF),*
tel: +33 (0)169 334747, fax: +33 (0)169 333022, email: welnic@theory.polytechnique.fr

Introduction

In recent years, nonvolatile solid state memories have in many applications replaced magnetic hard disk drives. A promising contender for the most popular nonvolatile memory - the FLASH random access memoryis the phase change random access memory (PRAM). The PRAM utilizes phase change materials (PCM) already successfully employed in rewritable optical data storage. The storage concept of these materials is based on a unique combination of properties: On one side they show a rapid phase transition (~10100ns) from a metastable crystalline to the amorphous phase upon heating. On the other side this phase transition is accompanied by a fundamental change in the electronic and optical properties between the two phases unknown from common semiconductors such as Si, Ge or GaAs. However, many fundamental properties of PCM's, such as the role of vacancies, remain poorly understood. PCM's based on the ternary composition GeSbTe contain vacancy concentrations of around 10% in their metastable crystalline structure. In this work we use densityfunctional theory (DFT), to reveal the origin of these high vacancy concentrations.

Calculations & experiments

We investigate the role of composition for GeSbTe alloys by investigating systems with varying amounts of vacancies in the metastable crystalline phase using DFT [1]. As Ge1Sb2Te4 and Ge2Sb2Te5 have considerable vacancy concentrations on the Ge/Sb sublattice, we investigated the role of vacancies on this particular sublattice. In Fig. 1 defect formation energies are shown for both structurally unrelaxed (i.e. an exact rocksalt lattice) and relaxed (locally distorted rocksalt) structures. The energy of the crystal decreases on removing Ge atoms from the Ge2Sb2Te4 crystal, in striking contrast to the behaviour in Si or GaAs where vacancy formation energies are large and positive. Fig. 1 also shows that it is even favourable to remove several Ge atoms from Ge2Sb2Te4 yielding a composition of Ge1.5Sb2Te4 most favourable. Finally the local distortions of the rocksalt lattice lead to a further lowering of the total energy. A Crystal Orbital Hamilton Population (COHP) analysis of the electronic

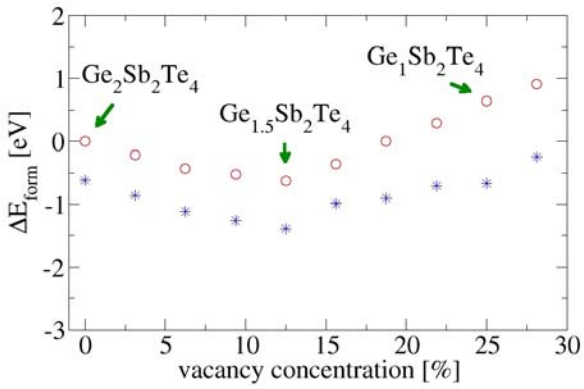

Figure 1 Formation energies for Ge vacancies for different concentrations. The distortions lead to a further reduction.

structure shows that Gerich compositions such as Ge2Sb2Te4 exhibit a high concentration of antibonding valence states. Thus, the energetic gain by emptying antibonding states favours the Gepoor composition Ge1Sb2Te4, whereas maintaining a maximum number of strong Ge–Te bonds strives for the Gerich Ge2Sb2Te4; the energetic compromise arrives at Ge1.5Sb2Te4. For expelling Sb atoms (instead of Ge atoms), analogous arguments apply. Moreover the energy minimization upon structural relaxation can be explained by the Peierls mechanism. It occurs to optimize the local necessity of the Te electronic structure, just as expected for the Peierlsunstable Te atom..

The compositions predicted by the calculations have then been synthesized by magnetron sputtering and analyzed for their phasechange properties. A striking result is found for the optical contrast between the amorphous and metastable crystalline state. Fig. 2 shows the absorption spectra for Ge1Sb2Te4, Ge1.5Sb2Te4, Ge2Sb2Te4 and Ge2Sb1Te4. The optical contrast—which is of great importance for the optical data-storage application of phasechange materials—in the novel compositions Ge1.5Sb2Te4, Ge2Sb1Te4 and in particular Ge2Sb2Te4 is significantly more pronounced than in the wellknown PCM Ge1Sb2Te4. To our knowledge, this is the first time that a PCM with superior properties for optical data storage has been first developed by advanced calculations and subsequently produced and tested experimentally. Once a microscopic model for electric switching has been established, such a method could possibly also be applied to develop new materials for electronic data storage.

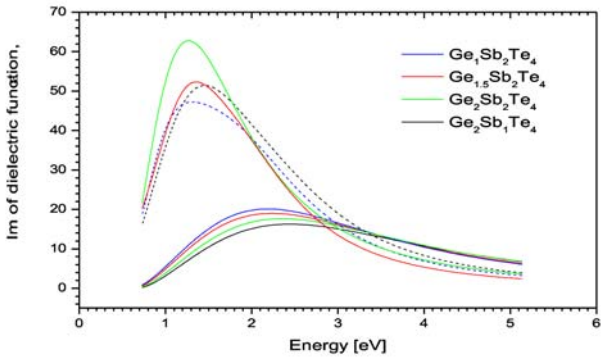

Figure 2 The imaginary part of the dielectric function for the amorphous (solid lines) and crystalline (dashed lines) phases of the Ge1Sb2Te4−Ge2Sb2Te4 alloys and of Ge2Sb1Te4 showing the effect of vacancies and distortions on the optical contrast. It can be seen that there is a systematic increase in absorption with decreasing Ge and Sb vacancy concentration.

[1] M. Wuttig, D. Lüsebrink, D. Wamwangi, W. Wełnic, M. Gilleßen and R. Dronskowski, Nature Materials 6, 122 (2007)

3D-SIMULATION BASED ANALYSIS OF CELL DESIGN CONCEPTS FOR PHASE CHANGE RANDOM ACCESS MEMORY

Dae-Hwang Kim, Florian Merget, Michael Först*, and Heinrich Kurz

Institute of Semiconductor Electronics, RWTH Aachen University,
Sommerfeldstrasse 24, D-52074 Aachen, Germany
**E-mail: foerst@iht.rwth-aachen.de*

Introduction

Phase change random access memory (PCRAM) technology has become the most attractive solution for future memory applications by potentially unifying high speed (like DRAM) and non-volatility (like Flash). Until lately, high RESET currents have hindered high density integration of PCRAM. Only recent industrial efforts to reduce these currents have enabled the commercialization of this technology [1-2]. The key to this success was the optimization of cell-design concepts with advanced thermal and electrical properties.

In this contribution, three different design concepts are quantitatively evaluated in terms of their geometrical and thermal features. To this end, we developed a three-dimensional (3D) phase change simulation model based on the finite difference discrete time method [3]. This simulation tool is capable of specifying guidelines for the design of cell architectures with the goal of reduced RESET currents.

Modeling of Device Operations

The simulation tool consists of four individual sets of sub-models: electrical model, thermal model, phase change model and percolation model. In the first time step of RESET operation modelling, the distribution of the electrical potential within the PCRAM cell is computed. Once this distribution is determined, the resulting electrical field, current density and heat source are calculated for each grid point of the simulation volume. The heat source is then fed into the thermal simulation to calculate the temperature distribution throughout the device. This temperature is used to simulate the phase state at each grid point on the basis of the classical theory of nucleation. Finally, changes in the thermal and electrical conductivity induced by phase transformation for each grid point are updated based on the classical percolation theories of Bruggeman and Wiener. They subsequently enter into the electrical and thermal models for the next time step.

Results and Discussion

First, we consider the vertical cell with minimum feature size F_{min}=80 nm. Figure 1(a) and (b) show the calculated temperature and phase distributions at the end of the RESET pulse (U_0=3 V, t_{pulse}=20 ns) and RESET operation (t=40 ns), respectively. The maximum current at the end of the pulse is 1.31 mA, which is significantly larger than current drivability of CMOS transistors at the same F_{min}.Hence, a high density integration of these cell select transistors is limited. In such a cell, the reduction of the RESET current can be practically achieved only by scaling down the GST-BEC contact size. However, it is severely limited by the lithographic resolution.

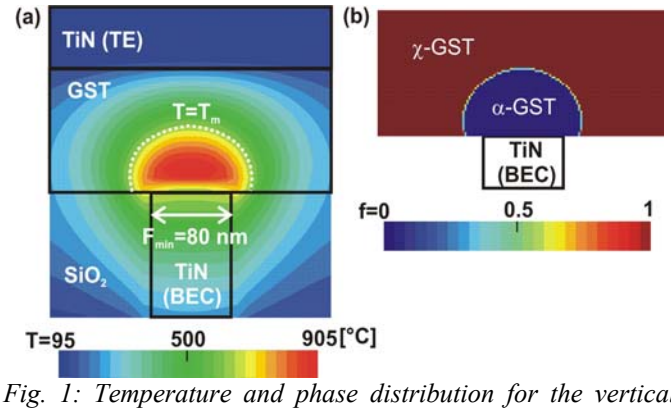

Fig. 1: Temperature and phase distribution for the vertical PCRAM cell.

To overcome this problem at a given technology node, Pirovano et al. introduced the confined cell design [4]. Compared to the vertical cell, the confined cell features an improved thermal management, leading to a reduction of the RESET current. Our simulation model can well explore this feature. Figure 2(a) and (b) show the calculated temperature and phase distribution within the confined cell with F_{min}=80 nm at the end of the RESET pulse (U_0=3 V, t_{pulse}=20 ns) and RESET operation (t=40 ns). The maximum current at the end of the pulse is 0.64 mA, which is significantly lower than that of the vertical cell with the same F_{min}. As shown in Fig. 2(b), one can see that the switching zone is thermally isolated from the heat sink (BEC) by the thermally poor conducting GST material itself. The correspon-ding reduced heat dissipation is the reason for the lower RESET current of the confined cell compared to the vertical cell, in which the switching zone is in direct contact with the BEC.

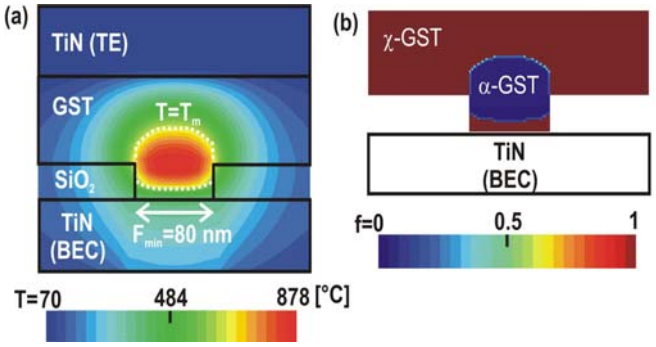

Fig. 2: Temperature and phase distribution for the confined PCRAM cell.

Another drastic current reduction can be achieved in the lateral cell design [5]. Figure 3(a) and (b) show the calculated temperature and phase distribution within the lateral cell with F_{min}=80 nm at the end of the RESET pulse (U_0=3 V, t_{pulse}=20 ns) and RESET operation (t=40 ns), respectively. The maximum current at the end of the pulse is 0.23 mA. This value is significantly lower compared to that of vertical and confined cell with the same F_{min}. Two reasons can be identified. One is the minimized current cross section defined by F_{min}×t (thickness of GST layer), as t is smaller than F_{min}. A second reason is the improved thermal isolation of the switching zone. As shown in Fig. 3(b), the switching zone is decoupled from two metal electrodes and isolated by the poor conducting ZnS-SiO2 layer from the Si substrate (heat sink). In addition to the current reduction, the thermal properties allow improvement of the long-term reliability and relaxed design constraints for metal electrodes.

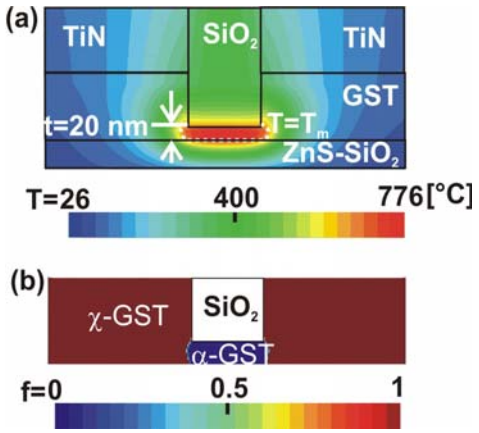

Fig. 3: Temperature and phase distribution for the lateral PCRAM cell.

This work is financially supported by the Deutsche Forschungsgemeinschaft.

References:

[1] S. Lai et al., Techn. Dig.-Int. Electron Devices Meet., p. 36.5.1, 2001
[2] G. H. Koh et al., Symposium on Circuits, Digest of Technical Papers, p. 98, 2005
[3] D.H. Kim et al., J. Nanosci. Nanotechnol., Vol. 7, pp. 298, 2007.
[4] A. Pirovano et al., Techn. Dig.-Int. Electron Devices Meet., p. 29.6.1, 2003
[5] Proceedings of Nonvolatile Memory Semiconductor Workshop, 2004

RANDOM APPROACH FOR CRYSTALLIZATION MODELLING IN PHASE-CHANGE MEMORY

M. Armand, J. Hazart, L. Poupinet, B. Hyot

CEA-LETI MINATEC, 17 rue des Martyrs, 38054 Grenoble Cedex 9
Tel: +33(0)4 38 78 20 33, Fax: +33(0)4 38 78 50 46
marilyn.armand@cea.fr

Introduction

Recent improvements in phase-change memory (PCM) technology related in the literature mainly address the reduction of the reset current by adjusting the cell design and/or the phase-change material composition. A comprehensive understanding of the involved physical and phase-change processes becomes essential for further development. In particular, analysis at the nanostructure level through modeling is required when reliability and scalability issues are to be considered. We extended our existing model developed for optical recording to simulate the phase-change processes in PCM, i.e. implementing the nucleation and growth processes in the electro-thermal mechanism and evaluating the nanostructure evolution during the programming steps.

The model

Writing and erasing in PCM are based on an electro-thermal process which is modeled by the system of coupled equations consisting of Laplace and Heat equations. To model the amorphous to crystalline transition, the non-linearity of the electrical properties of chalcogenide glasses has been introduced. This effect relies on the transition of the amorphous phase from a highly resistive state to a conductive one when submitted to an elevated temperature and/or a relatively high electric field. This behavior has shown to be consistent with a temperature and electric field dependent conductivity expressed by [1,2]:

$$\sigma_{am}(T,E)=\sigma_0 \exp\left(-E_a/kT\right)\exp(E/E_0) \qquad [1]$$

where Ea is the activation energy, E the electric field and E0 the critical electric field. Nucleation and growth processes are based on the model previously developed [3] from classical theory. Due to the very high heating and cooling rates (of the order of 10°C/ns) that take place during writing and erasing in PCM as in optical recording, transient nucleation rate, given by Eq. 2, was introduced. The random number of nucleation events was then calculated during each time step, for each isothermal zone by considering the local transient nucleation rate.

$$I_{transient}(T,t)=I_{stat}\exp\left(\frac{-\tau}{t(T)}\right) \qquad [2]$$

where I_{stat} is the steady state nucleation rate, t the time necessary for a population of nuclei to reach a steady-state and t the isothermal holding time, considering a 5K temperature increment.

The Simulation results

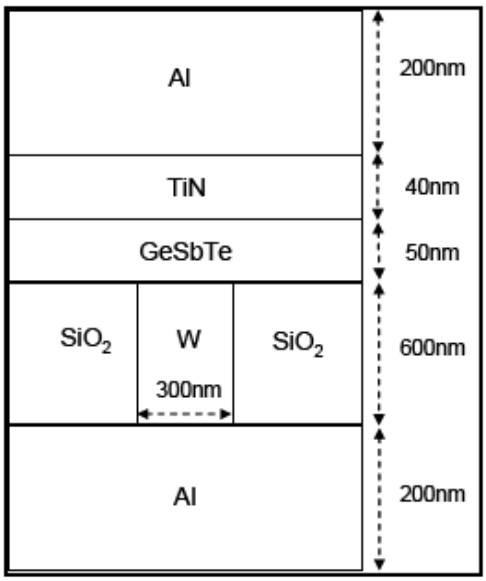

Figure 1: 2D geometry

The model was entirely developed in a Matlab code and applied to the 2D geometry depicted in Figure 1. A voltage ramp up to 8V was applied between the top and the bottom Al electrodes for 100ns. Figure 2 shows the temperature distribution in the PC layer and the corresponding nucleation rate when the first nucleus appears. The nucleation rate being temperature dependent and centered around 400°C, it does not occur in the middle of the structure but slightly shifted aside (Cf. Figure 3a). This crystalline grain starts to grow, modifying the electric field and thus the temperature distributions and subsequent grains are formed, as shown in Figure 3 which represents the crystalline structure at different times of the calculation.

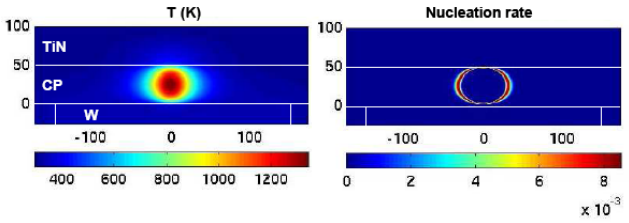

Figure 2: Temperature distribution and nucleation rate

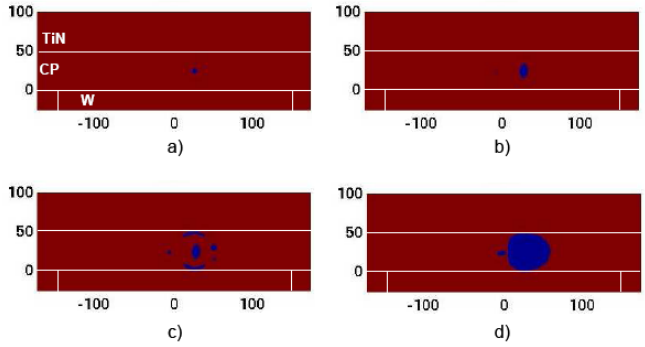

Figure 3: Evolution of the crystallization process representing the nucleation and growth of crystalline grains at different times of the calculation (from a to d)

The present model is still being developed since particular attention must be paid when dealing with physical processes at the nanometer scale and such high and extremely fast thermal and electrical transitions. Other reported models are often based on a macroscopic and continuous approach of the PC processes, in which phase transition is triggered by a temperature increase or modeled by the JMA equation. The model we propose, in which we follow the crystalline grains distribution, will enable an accurate analysis of cyclability, retention and statistics of the PCM cells. Several simulation results will be presented, comparing different writing conditions, the objective being to correlate them to the experimental data.

[1] M.H. El-Fouly, J.T. Edmond, Phys. Stat. Soli. A, 48(2) (2006) 395-405
[2] C.D. Wright, M. Armand, M.M. Aziz, IEEE Trans. Nanotech., 5(1) (2006) 50-61
[3] B. Hyot, L. Poupinet, V. Gehanno, P.J. Desre, J. Magn. Magn. Mat., 249 (2002) 504-508

A Slider with an Integrated Microactuator (SLIM) for Second Stage Actuation in Hard Disc Drives

Hans H. Gatzen[1], Paulo J. P. de Freitas[2], Ernst Obermeier[3], John Robertson[4]

[1]Leibniz Universitaet Hannover , Center for Production Technology, Institute for Microtechnology
An der Universitaet 2, 30823 Garbsen, Germany
Phone: +495117625104, FAX: +495117622867, gatzen@imt.uni-hannover.de

[2]INESC MN Microsystems & Nanotechnologies
Rua Alves Redol 9, 1000-029 Lisboa, Portugal
Phone: +351213100348, FAX: +351213145843, pfreitas@inesc-mn.pt

[3]Berlin University of Technology, Microsensor & Actuator Technology
Gustav-Meyer-Allee 25, 13355 Berlin, Germany
Phone: +493031472769, FAX: +493031472603, ernst.obermeier@mat.ee.tu-berlin.de

[4]University of Cambridge, Department of Engineering
Trumpington Street, Cambridge CB2 1PZ, United Kingdom
Phone: +441223332689, FAX: +441223332662, jr@eng.cam.ac.uk

Introduction

With increasing recording density of Hard Disc Drives (HDD), the distances between flux reversals as well as the width of the magnetic data track decrease. To increase the first one, a dynamic reduction of the head-to-disc spacing during writing and/or reading is desirable and has been implemented into latest generation recording heads. Track following is accomplished by rotary voice coil actuators positioning the recording heads on the required data track. The head itself consists of a suspension mounted to the actuator on one side and carrying a slider, which "flies" over the disc and contains the read/write element, on the other side. These actuator systems run into limitations in regard to track following, posing a handicap for further increasing the radial (track) density. To resolve this issue, a second stage actuator may be integrated in the read/write head to accomplish more accurate and higher frequency track following than possible with existing actuators [1, 2]. Concepts for the design of such actuators are known. However, since the HDD industry is extremely price sensitive, it could not convince itself to accept additional cost even for the sake of a performance increase.

Second Stage Actuation Concept

For coming up with a cost competitive solution for second stage micro actuation, the following approach is taken. A slider with an integrated microactuator (SLIM) allows both vertical (for head-to-disc spacing adjustment) and lateral (for fine tracking) motion of the read/write element. The read/write element is part of a chiplet, which requires only a fraction of the wafer real estate required for fabricating a present slider containing the read/write element. Therefore, SLIM is a solution that not only provides the required actuation capabilities, it also allows its fabrication at lower costs than a present slider [3].

SLIM Design

Figure 1 depicts the SLIM design. SLIM is a two-part design and is fabricated on two separate wafers. The actuator magnetics are located in the bottom part of the device and consist of a pair of active parts. The actuator mechanics are situated in the upper part. A mounting platform suspended by a pair of leaf springs carries a chiplet containing the read-write element. Figure 2 depicts the simulation results for magnetic forces of a single actuator system. A simultaneous excitation of both active parts lowers the chiplet to its flying height position, while an alternative excitation of the two active parts causes a minute rotation of the chiplet and thus a lateral displacement of the read/write element, allowing a micro positioning for track following. A desired lateral displacement of ±625 nm results in a rotation of 0.18°. For the micro actuation to function, both the slider body and the chiplet are equipped with air bearing surfaces (ABS), which are coated with a thin DLC (diamond like carbon) layer.

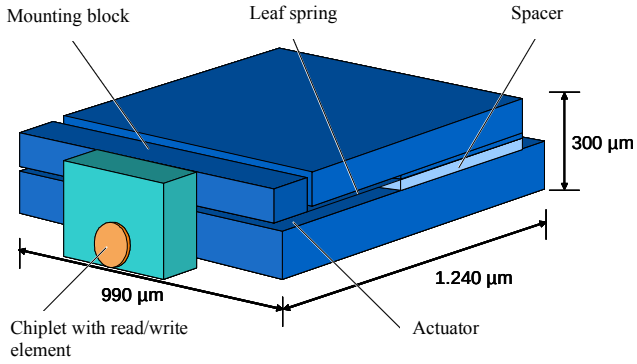

Figure 1 Slider with Integrated Microactuator (SLIM).

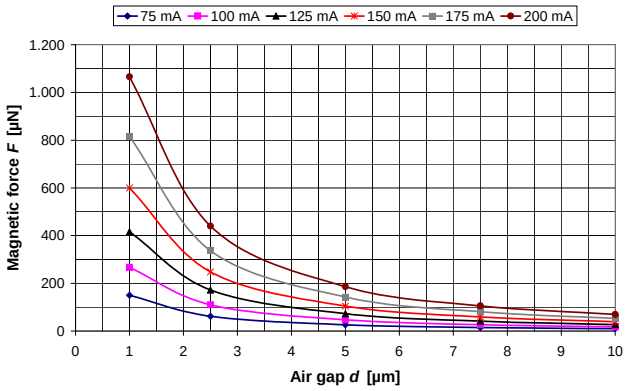

Figure 2 Simulation results for microactuator forces

For fabricating SLIM, a thin-film batch fabrication approach is taken, fabricating the actuator magnetics and mechanics on two separate silicon wafers. Since the energy a microactuator is able to transduce is proportional to its volume, high aspect ratio micro system technologies (HARMST) are applied. Actuator mechanics are fabricated using MEMS processes and as a base material utilize single crystalline silicon. The suspended platform which carries the read/write element is realized by sacrificial layer technology and DSE (deep silicon etch). The two cantilevers of the platform consist of polysilicon that is deposited by LPCVD and doped in a following process. System integration of the SLIM device is accomplished by bonding the top wafer to the bottom wafer. The two main challenges are developing an appropriate spacer technology and to come up with a suitable bond technology.

Program Execution

For executing the SLIM development, the Leibniz Universitaet Hannover (concept and magnetics design) has teamed up with the Berlin University of Technology (silicon micromachining), INESC, Lisbon, Portugal (test design), and Cambridge University (DCL coating and tribology). The program is funded by the EC within the Sixth Framework Program by Information Society technologies within the Specific Targeted Research Program (STREP) “Performance Advances in Recording through Micro Actuation” (PARMA).

[1] K. Suzuki, M. Kurita: A MEMS-Based Active Head Slider for Flying Height Control in Magnetic Recording. JSME International Journal, B 17, No. 3, pp. 453-458, 2004

[2] F. Chen, H. Xie, G. K. Fedder: A MEMS-based monolithic electrostatic microactuator for ultra-low magnetic disk head fly height control. IEEE Transaction on Magnetics Vol. 37, No. 4, pp. 1915-1918, 2001

[3] H. H. Gatzen: Micromechanical rotating device with a magnetic drive and a method for the production thereof. Patent application PZT/EO03/14319

HARD DISK DRIVE AS A LOGIC DEVICE

Vladimir L. Safonov

Mag & Bio Dynamics Inc.,
1682 Crescent Knolls Gln., Escondido, CA 92029, U.S.A.
tel. (858)776-9337, vlsafonov@magbiodyn.com

Introduction

We consider a method to perform logic operations on a hard disk drive with magnetic medium capable of superimposing the binary information. Such media consist of particles with a) different anisotropy fields and/or with b) different anisotropy axes orientations. The first is, for example, an oriented (perpendicular or patterned) medium with a distribution of anisotropy fields. The second is typical for a longitudinal medium. We can also mention AFC media, where an example of superimposition was demonstrated [1].

The elementary logic operation consists of three steps: 1) Applying a strong magnetic field, we write the first binary number A as the transitions between different average magnetization states (-*M* and +*M*, all previous information is erased). 2) Using smaller magnetic field that reverses just a part of magnetic particles, we write the second binary number B. Doing so we obtain transitions between 0 and *M*, -*M* and 0, and -*M* and *M*. 3) The reading sensor detects the peaks of magnetization variation as a result of the logic operation OR, AND, XOR or NOT. Using the results of XOR and AND operations, one can construct an adder.

Logic operations

Consider a perpendicular medium with two types of particles with the uni-axial anisotropy fields H_{K1} and H_{K2}, respectively ($H_{K1} > H_{K2}$). The absolute values of average magnetization of both types of particles are assumed to be equal to *M/2*. The binary information can be represented in the forms of "pulses" of magnetization *M* and *M/2* (relative to the -*M* and -*M/2* states). The height of pulses is *M* or *2M*. In Fig. 1a,b A=(11)(00)(11)(00) or A=**I0I0** (**I** denotes 11 and **0** denotes 00), B=(11)(00)(00)(11) or B=**I00I**.

Figure 1 illustrates the OR operation with the use of sensor that does not distinguish the height of peaks: (**I0I0**)OR(**I00I**)=**I0II**. For a sensor that detects the largest magnetization transitions (between –M and M) we have (**I0I0**)AND(**I00I**)=**I000**.

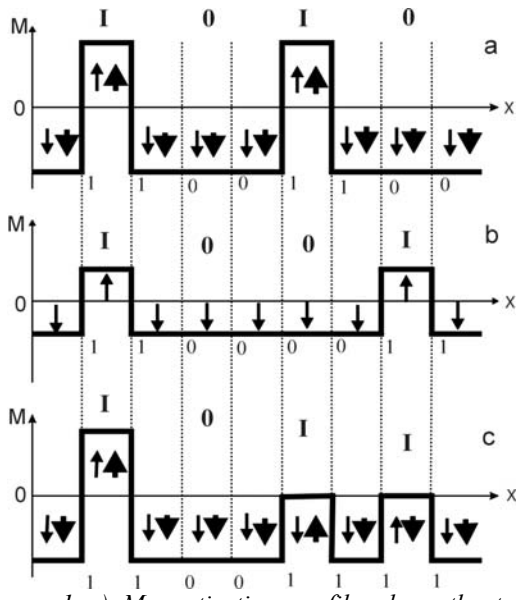

*Figure 1 a) Magnetization profile along the track written by a strong magnetic field $H_1 > H_{K1}, H_{K2}$. b) Profile for the type 2 particles written by a moderate magnetic field $H_{K2} \le H_2 < H_{K1}$. c) The resulting profile is **I0II**. The vertical dotted lines separate different bits. The ones below each profile denote transitions and zeros indicate the absence of transitions. The arrows denote the magnetizations of*

We can introduce a "negative" (**-I**) pulse. In this case the pulse is considered down relative to *M* or *M/2* states. In other words, -B is a reversed magnetization profile of B relative to horizontal axis *M=0*. It is easy to check that B-B=**0000**. In Fig. 2b we see an example: the number B=**-I-I-I-I**. Any number A being superimposed with the sequence of negative pulses gives the NOT operation. From the Fig. 2 we have: NOT(**I0I0**) = **0I0I** (the sensor does not distinguish the signs of resulting pulses).

Let us now demonstrate the XOR operation. Superimposing the first number A = **I0I0** and the second number B (in the form of –B = **-I00-I**), we obtain C = **00I-I**, or, neglecting the sign, C = **00II**. In other words, one has (A)XOR(B) = C.

Discussion

The recording time necessary for logic operations is very small and therefore the magnetic medium can consist of particles with small anisotropy field. This will reduce the energy losses and heating. The particles can also have smaller size, which is important to reduce the noise. In order to solve the problem of bit synchronization at superimposition one can increase the linear size of a pulse (e.g., by introducing extra zeros for coding: 11 become 101, and so on).

The speed of logic processor can be very high (~10^8 bit/sec or more): it is defined by the number of revolutions per second (~100 sec^{-1}) multiplied by the bit length of the track (~10^6 bit).

Hard disk drive with logic operation can be used both for independent data processing and as a supplemental tool for a conventional semiconductor processor.

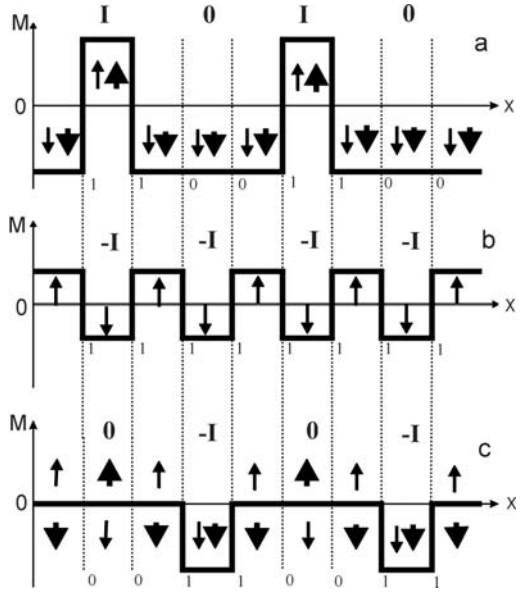

*Figure 2 a) Magnetization profile along the track written by a strong magnetic field, A = **I0I0**. b) Magnetization profile for the type 2 particles written by a moderate magnetic field, B = **-I-I-I-I**. c) The result is **0-I0-I**.*

Acknowledgements

The author wish to thank E. E. Fullerton, A. Taratorin and A. K. Khitrin for helpful discussions.

[1] E. E Fullerton et al., IEEE Trans. Magn. **39**, No. 2, p.639 (2003)

DOMAIN WALL DEPINNING OVER A SINGLE DEFECT : THE ROLE OF THERMAL ACTIVATION

M. Jean-Philippe Attané[1], Dafiné Ravelosona[2], Yves Samson[1], Alain Marty[1], Claude Chappert[2]

[1] Laboratoire Nanostructures et Magnétisme ; CEA Grenoble, 38054 Grenoble ; France
[2] CNRS / Université Paris Sud, Institut d'Electronique Fondamentale, 91405 Orsay, France
Tel.:33 – 4 38 78 35 62, Fax. : 33 – 4 38 78 51 97, yves.samson@cea.fr

Data storage [1] or logic devices [2] based on domain wall propagation have been recently proposed. These are made possible by the prospect of realiable manipulation of domain wall by a magnetic field or by spin transfer (or the combination of both) within nanometer-scale structures. Specific promises of this upcoming technology are fast operations, low power consumption and non volatility of recorded information.

Here we concentrate over the reproducibility of domain wall propagation phenomena in nanostructures combining high magnetic anisotropy and strongly pinning nanometric defects. We describe the field induced depinning process of a 5nm wide magnetic domain wall from a single bidimensional nanometric defect. A 200 nm wide wire has been prepared by e-beam lithography within thin FePt (40 nm thick) /Pt(001) films with strong perpendicular anisotropy. In such films, the defects pinning the domain walls are the microtwins, that are bidimensional strain relaxation defects that cross the whole thickness of the FePt layer (see [3] and Fig. 1(a)) and the full width of the wire. These defects provides energy potentials pinning the propagating domain wall (Fig. 1b)

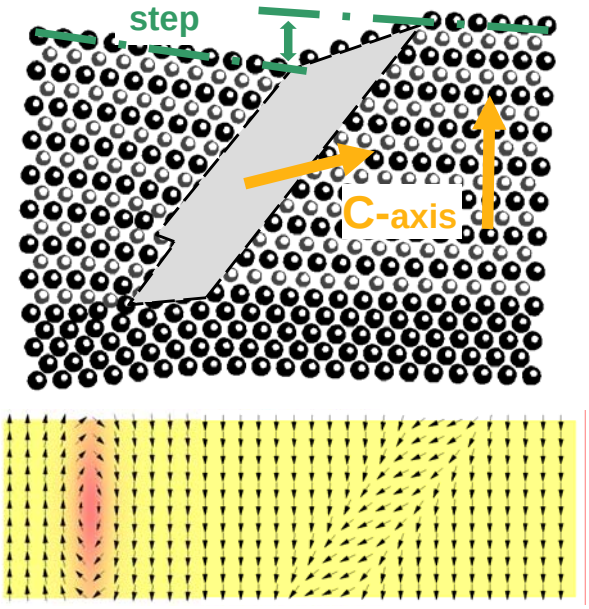

Figigure 1: (a) upper part: Cross sectionnal scheme of a microtwin within a thin FePt layer chemically ordered within the $L1_0$ phase (Fe atoms : small white balls, Pt : large black balls).
(b) Lower part: micromagnetic simulation of two domain wall. Left: "free" wall within the layer – Right: wall pinned over a microtwin comprising 20 dislocations (hence 5.4 nm wide). Calculations show that the microtwin lowers the domain wall energy and then acts as a potential well.

When applying a field step, domain nucleation occurs in a large reservoir out of the wire, and the domain wall next enters the wire and propagates within. The propagation time is measured in between two Hall crosses separated by 10 µm (Fig. 2(a)). As a result of thermally activated depinning of the domain wall from a single (dominant) defect, we observe a statistical distribution of the propagation time consistent with a Neel-Brown picture of magnetization reversal (Fig. 2(b)). By repeating the experiment over 400 times at 200 and 300 K, a detailed numerical analysis of the depinning law has been made possible. This indicates that the depinning process of the domain wall can be compared to the switch of an ideal monodomain particle over a single energy barrier (see [4], magnetisation reversal of cobalt nanoclusters). This is the first time a similar phenomenon is recorded for the propagation of a magnetic domain wall.

Recently, it has been proposed to create magneto-logic devices based on the propagation of domain wall. Such a stochastic character of domain wall depinning has to be taken into account when pushing the dimensions of spintronic devices into the nanoscale – at least in the specific conditions of low field (with respect to the pinning fields) here involved. This is quite unexpected when dealing with extended wall over strongly pinning anisotropy defects (see [5]).

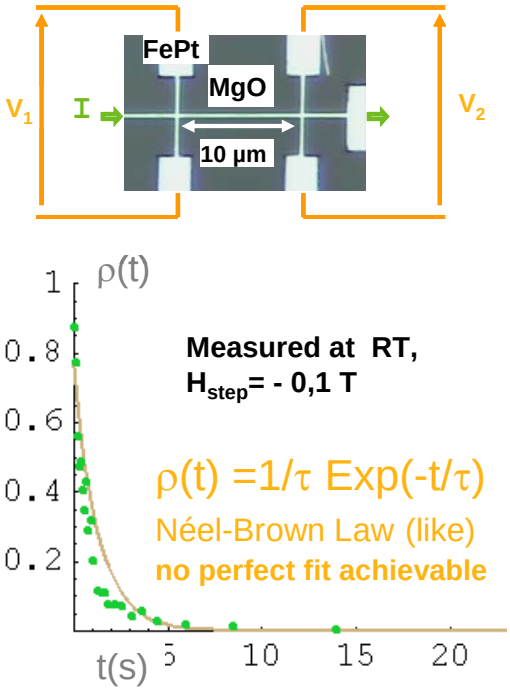

Fig. 2, upper part: image of the experimental nanostructure prepared by e-beam lithography. Lower part: probability of no-detection of the domain wall at the position of the second Hall Cross once the first one has been reversed. Discrepancies with respect to the simple written law are explained in [5].

[1] S.P. Parkin, U.S. Patent No. 6834005 (2004)
[2] D. A. Allwood et al Science 309, 1688 (2005).
[3] J.P. Attané, Y. Samson, A. Marty, J.C. Toussaint, G. Dubois, A. Mougin, J.P. Jamet, Phys. Rev. Lett. 93 (2004) 257203
[4] W. Wernsdorfer et al., Phys. Rev. Lett. 78 (1997) 1791
[5] J.P. Attané, D. Ravelosona, A. Marty, Y. Samson, C. Chappert, Phys. Rev. Lett. 96 (2006) 147204

Scanning Probe Microscopy Markup Language

T.Bolhuis, M.H. Siekman an L.Abelmann

MESA+ Reserch Institute for Nanotechnology
University of Twente, P.O.Box 217,7500 AE Enschede, The Netherlands
Tel: +31-534891041, T.Bolhuis@utwente.nl

Introduction

The lack of a standard file format for Scanning Probe Microscopy data results in a number of problems like the cumbersome quantitative comparison of data between SPM's of different brands, the short lifetime of binary data generated by the numerous non-open proprietary software and the need for costly software when analyzing data off-line or exchanging data with other researchers. These problems can be solved by adopting a standard and open data format.

Other scientific disciplines have faced the same problems and agreed on standard data formats like XRDML[2], GAML[3], ThermoML[4] and many more. A standard dedicated to SPM data does not yet exist. Because of the eminent roll SPM's are playing in the scientific world of today, a standard SPM data-format (Scanning Probe Microscopy Markup Language, SPML) is proposed in this contribution.

General requirements for a standard SPM format

In order to address the abovementioned problems a well documented, common data format is needed which should be open and free so that anyone is allowed to use it in any (commercial or non-commercial) application, able to obtain or develop dedicated tools without any fee or restraint. The format should be clearly structured, strict and easy to understand, so development of software tools would not be a difficult task on any computer-platform.
The proposed XML-based[1] SPML-format complies with these requirements. The XML-syntax is text based, hierarchical and relational structured, web-compatible and there are numerous tools and documents for software development available.

Specific requirements for a standard SPM format

SPM-data can be generated by more than one signal taken on the same grid. When saved, all data should be related to that same grid. Versatility of the data format also calls for the support of non-equidistant grid-points, multi-dimensional data and non-Cartesian coordinate systems. Spectrometric signals, retrieved at scattered positions on the grid, have to be filed in coherence with other sets of data from the same grid. Data produced by data processing should be added to the same file and the relation to the input data should be clear. The parameters as well as the retrieved signals should be associated with specific device settings. The instruments at hand will differ to a large extend, so the format for the device settings should not be predefined by the proposed data-format.

Because of the capability of XML-applications to define relations between blocks of data the proposed Scanning Probe Microscopy Markup Language (SPML) complies with all the abovementioned requirements and more.

A brief description of the structure of SPML

The basic structure of an SPML-file is depicted in fig.1. The SPML-root element contains at least the following sub-elements: Devices, Setups, Axes and DataChannels. The Devices element holds the device settings of the various instruments used. The Setups element contains references to DeviceSettings (and/or DataProcessing-operations). The Axes element holds the values and description of the parameters at which the data has been measured and thus describes the grid of the measurement points. The DataChannels element contains the

measured data and its relation to the grid (Axes). The optional note-element can contain additional information, while the Dataprocessing-element holds information on the data processing operations. The optional, but recommended, image-element contains the resulting images and thumbnail-images linked to the datasets in the DataChannels-element. Further details can be found in [5].

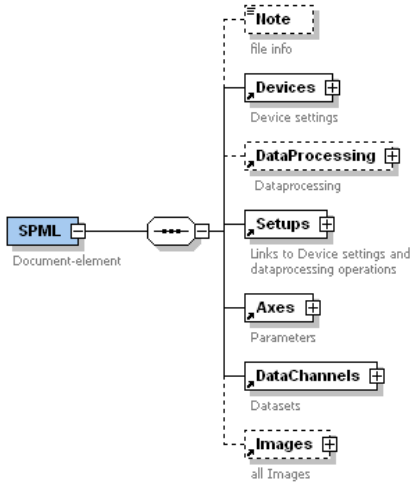

Figure 1. The basic SPML-structure.

Figure 2. Browser view on a series of SPML-files.

Results

SPML has in our and a few other SPM-labs proven to be useful and versatile. Tools for reading and writing SPML-files have been developed. SPML is a supported import and export format to Gwyddion[6], a powerful and open source SPM data visualization and analysis program. As a result Gwyddion is able to work as a converting tool from numerous SPM-data formats to SPML and open source software-modules are available for exporting to SPML.
Because SPML is based on XML and images can be embedded in the SPML-files it is easy to make an SPML-browser, by means of a stylesheet (XSL) and a simple java program (fig 2.). This way one can browse through and look into ones SPML-files by using a standard web-browser. It is also possible to produce standard report files in pdf format from SPML-files by applying XSL-files.

Conclusions

Because of the eminent roll SPM's are playing in the multidisciplinary scientific world of today, a standard SPM data-format is required. The XML-syntax has proven to be well applicable for standardized, structured, scientific data formats. The versatility and the open character of the proposed XML-based SPML-format make it suitable as a standard SPM data-format. The possibility of documenting, publishing, searching and exchanging quantitative SPM results makes SPML an appealing choice as a container for SPM-data. Full support of SPML in Gwyddion and the availability of conversion tools are the first steps to the adoption of SPML as a standard data format by prominent research institutes and leading SPM-manufacturers.

References

1. Extensible Markup Language (XML): *http://www.w3.org/XML* .
2. XRDML: *http://www.xrdml.com* .
3. Duckworth, J.,Smith, K, Kuehl, Don, *American Laboratory,* **March 2002,** p16-24.
4. Frenke, M, etal., *J. Chem. Eng. Data,* **48**, 2-13, (2003).
5. SPML: http://spml.net
6. Gwyddion: http://gwyddion.net

CORE-SHELL STRUCTURE OF FePt NANOPARTICLES SYNTHESISED BY A CHEMICAL ROUTE : A COMPARTIVE STUDY

M. Delalande[1], V. Monnier[2], P. Marcoux[2], P. Reiss[2], Yves Samson[1]

1- Laboratoire Nanostructures et Magnétisme ; CEA Grenoble, 38054 Grenoble ; France
2- Laboratoire d'Electronique Moléculaire Organique et Hybride ; CEA Grenoble, 38054 Grenoble; France Tel.:33 – 4 38 78 35 62, Fax. : 33 – 4 38 78 51 97, yves.samson@cea.fr

The requirements for ultra-high density magnetic recording have driven the development of new magnetic thin film media with smaller grains and higher coercivities. Monodisperse assemblies of high-anisotropy $L1_0$ FePt nanoparticles are considered as promising candidates for future data storage media with densities beyond 1Tbit/in². Recent developments in colloidal chemistry offer a convenient approach to monodisperse FePt nanoparticles that readily self-assemble into three-dimensional superlattices.[1]

The synthesis of FePt nanoparticles is based on the simultaneous reduction of $Pt(acac)_2$ by a diol (1,2-hexadecanediol) and decomposition of Fe(CO)5 in dioctylether at high temperature. A combination of oleic acid and oleyl amine is used to stabilise the FePt colloids. Their average diameter is controlled by the amount of stabilisers following a linear relationship between the nanoparticles' volume and the molar ratio [stabilisers]/[$Pt(acac)_2$].[2] Since the pioneering publication by Sun [1], numerous chemical synthesis paths have been explored and proposed. Most can be classified within two families: the ones using a heavy ether as a solvent, a reducing agent and organic stabilizers ("hot soap" syntheses), and the ones where the solvent (a polyol) acts as a solvent and a reducing agent.

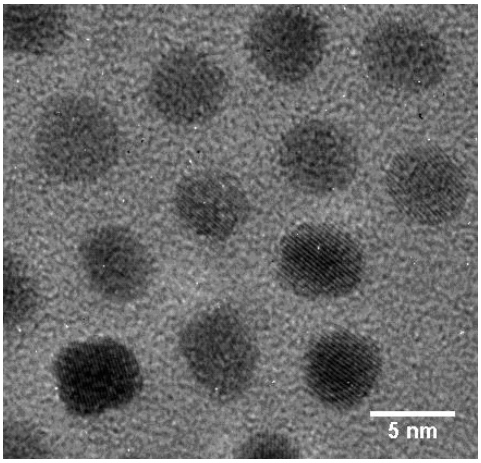

Fig. 1 : TEM image of 5 nm FePt nanoparticles (« hot soap synthesis »).

X-Ray diffraction studies demonstrate that the $Fe_{51}Pt_{49}$ nanoparticules are obtained within the chemically disordered phase, whatever the synthesis. ICP-AES and EDX reveal a stoechiometry close to $Fe_{50}Pt_{50}$. Specifically, the nanoparticles prepared through the « hot soap » syntheses exhibit a high value of the lattice parameter (with respect to the equiatomic bulk alloy). This is a first indication of a Pt-rich crystalline core. Indeed, the idea of al least one strongly Fe-enriched surface layer is confirmed by XPS measurements coupled with ionic sputtering.

Remarkably, a similar core-shell structure is not observed for the nanoparticles prepared by the "polyol" synthesis. SQUID data reveal superamagnetism at RT, an observation indicative of a chemically disordered phase. Indeed, the anisotropy values derived from ZFC-FC (Zero Field Cooled – Field Cooled) measurements are very weak (less than 10 % of the $L1_0$ phase value). Also, the magnetisation is significantly weaker than the one of the bulk alloy.

Table 1 : *Composition, structural properties for FePt nanoparticles.*

Synthesis	Mean diameter (dispersion)[c]	Overall composition (EDX)	*a* (Å) Core composition [d]
Fe^{0} Pt^{II} dioctylether[a]	3.4 nm (16 %)	$Fe_{51}Pt_{49}$	3.8845(16) Å $Fe_{32}Pt_{68}$
Fe^{II} Pt^{II} diphenylether[a]	4.2 nm (14 %)	$Fe_{60}Pt_{40}$	3.8832(17) Å $Fe_{30}Pt_{70}$
Fe^{-II} Pt^{II} dioctylether[a]	3.4 nm (15 %)	$Fe_{48}Pt_{52}$	3.8846(21) Å $Fe_{31}Pt_{69}$
Fe^{II} Pt^{II} TEG[b]	3.0 nm[e]	$Fe_{47}Pt_{53}$	3.857(6) Å $Fe_{46}Pt_{54}$

[a] "hot soap" synthesis. [b] "polyol" synthesis. [c] mean diameter from TEM images. [d] lattice parameter (chemically disordered phase) and composition from Vegard law[2]. [e] cristallites diameter from X-Ray diffraction (Scherrer).

This could be explained by the absence of ferromagnetic contribution of the Fe surface layer(s), as a result of the specific surface Fe – ligand interaction. At 300K, the magnetisation of the nanoparticles (polyol process) evolves according to the Langevin law, as expected for superamagnetic nanoparticles. Conversely, a linear dependence of M vs H is observed for the nanoparticles prepared by the "hot soap" method, suggesting that these are close to the Curie temperature at 300 K, as could be expected for a core composition close to $Fe_{30}Pt_{70}$[3] (in agreement with the proposed core-shell structure).

Whatever the solvent or Fe/Pt precursors we used, all "hot soap" synthesis led to nanoparticles with a Pt-rich core. Such a structure would result from the kinetic difference between the reduction of the Pt precursor and the availability of the Fe precursor. This difference would result from the strong interaction between the Fe and the organic stabilizers. Nevertheless, the core-shell structure does not prevent the evolution towards the chemically ordered $L1_0$ phase after UHV-annealing at 650°C. A detailed X-Ray diffraction study reveal that this evolution proceeds first by Fe-enrichment of the core of the nanoparticle (400°C), followed by chemical ordering (ending at 650°C).

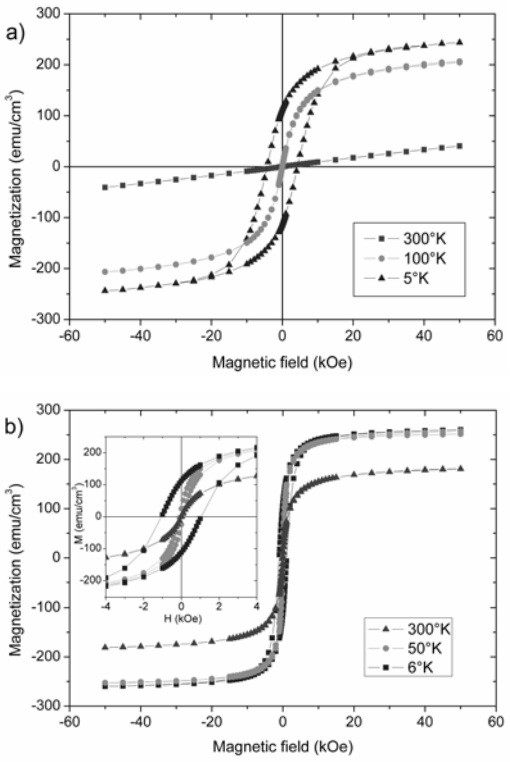

Fig. 2 : Hysteresis loops of FePt nanoparticles prepared by (a) « hot soap » (b) « polyol » processes

1) S. Sun et al., Science, 2000, **287**, 1989.
2) S. Momose et al., Jpn. J. Appl. Phys, 2005, **44**, 1147.
3) M. Delalande, J. Mater. Chem. 2007, **17**, 1579

2D CODING FOR PROBE RECORDING ON MAGNETIC PATTERNED MEDIA

J.P.J. (Hans) Groenland[1], Leon Abelmann[2]

Mesa+ Institute for Nanotechnology, TST
University of Twente, EWI, P.O. box 217, NL-7500 AE Enschede, The Netherlands
Phone +31 53 4892713[1], +31 53 4892699[2], Fax+31 53 4893343
E-mail j.p.j.groenland@utwente.nl l.abelmann@utwente.nl

Introduction

Patterned-media recording is one of the options to consider coming across the question how to guide bit densities beyond the superparamagnetic limit of conventional magnetic recording. In the two-dimensional (2D) arrangement of rows and columns of magnetized dots (islands) each dot represents one single data bit. During reading, crosstalk will manifest itself as a combination of the conventional intersymbol interference (ISI) along the rows, and the so-called intertrack interference (ITI) along the columns. The difference with continuous media is that now there is a predetermined phase relation between the tracks, which can be exploited for combatting ITI.

Our research focuses on methods for future storage devices being composed of a large number of independent, and simultaneously working probe-recording units. These units are expected not to be individually supplied with complicated electronics [1], prohibiting the application of relatively laborious coding methods like partial-response maximum likelyhood or low-density parity check (for instance [2]). In line with this requirement, we examined a relative simple method for 2D channel coding.

Magnetic recording setup and simulations

In order to analyse magnetic recording in patterned media, we used an experimental recording setup which can handle a limited number (100-1000) of dots. The recording medium is a CoNi/Pt multilayer patterned by laser interference lithography with a periodicity down to 150 nm [3]. The read-write mechanism is based on a magnetic force microscope scanning the dot pattern (x direction). Perpendicular recording (writing) is achieved by approaching the MFM tip to the recording medium in the presence of an external magnetic field in *z* direction (perpendicular to the medium surface). An MFM read signal results from the vibrating MFM tip (probe) in the stray field of the magnetized dots. Basically, positive read pulses (for instance associated with positive magnetization) will result in logical ones, negative pulses (negative magnetization) in zeros.

Figure 1 displays the simulated read signals of perpendicularly magnetized dots in a patterned medium. The waveforms are typical for both giant magnetoresistive (GMR) and magnetic-force microscope (MFM) read-head technologies, in combination with a recording medium with soft-

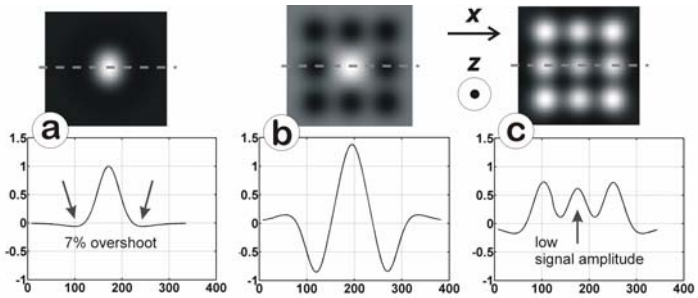

Figure 1 Three configurations of computed magnetic dots scanned by MFM probe (upper); Simulated MFM-probe read signals scanned along the dotted lines (lower). The x axes are in nanometers. (a) a single bit (b) a 'one' bit surrounded by 8 'zero' bits (c) 9 'one' bits.

magnetic underlayer (SUL). As a result of 2D ISI, the amplitude of a bit (dot) surrounded by 8 identical bits (figure 1c) is seen to be relatively low, and in view of bit-detection reliability such a bit combination can be considered to be a ”worst case” pattern

Two-dimensional coding

A simple method to avoid such worst-case patterns to occur in a patterned medium is the application of a geometric 2D channel code [4]. An example of such a code is shown in figure 2 where particular bit positions are occupied by fixed bit values (1 of 0), leaving the remaining positions for recording of user bits. This scheme stops the square nine-bit combination of figure 1c (9 ’ones’, or 9 ’zeros’) to occur. Obviously, this coding scheme results in a code rate 7/9 (or redundancy 22%). The benefit of the introduction of such a fixed bit pattern on bit detection was analysed using a computer simulation program. This program incorporates 2D ISI and offers, among other things, facilities for simulation of bit-position jitter. After computation of the read signal for a serpentine scanning trajectory (indicated in figure 2), the data bit sequence was reconstructed.

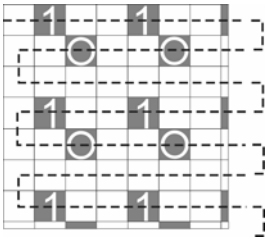

Figure 2 2D channel code with geometric constraint (fixed '1' and '0' bits

Figure 3 shows the number of detection errors in a sequence of 15876 bits as a function of the magnitude of uniformly distributed bit-position jitter. For non-coded data and low jitter levels we found the bit errors generally to occur on medium locations corresponding with the bit pattern of figure 1c, i.e. a block of nine (or more) identical bit values. Introduction of the 2D code eliminated this class of errors (figure 3). Increasing the jitter magnitude above factor 0.1 resulted in new errors at locations of bits which are surrounded by both ”one” and ”zero” bits.

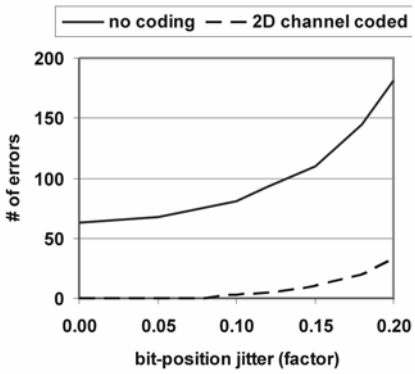

Figure 3 Impact of 2D channel code on bit- detection performance (for 16% overshoot

The code method of figure 2 does not require complicated signal processing. It can be considered as a ’brute force’ approach, because it claims redundant bit positions on the medium, which are located on fixed positions not correlated to local data content. In conclusion, a first attempt in this direction revealed that by simply preallocating bits, a considerable robustness against bit jitter could be achieved.

[1] L. Abelmann, T. Bolhuis, A. M. Hoexum, G. J. M. Krijnen, J. C. Lodder, "Large capacity probe recording using storage robots", IEE Proceedings-Science Measurement and Technology, vol. 150, pp. 218-221, 2003.
[2] J. Hu, T.M. Duman, E.M. Kurtas, F. Erden, "Coding and iterative decoding for patterned media storage systems", Electronics Letters, vol. 42, No. 16, 2 pages, 2006
[3] R. Murillo, H. A. van Wolferen, L. Abelmann, J. C. Lodder, "Fabrication of patterned magnetic nanodots by laser interference lithography", Microelectronic Engineering, vol. 78-79, pp. 260-265, 2005.
[4] J.P.J. Groenland, L. Abelmann, "Two-dimensional coding for probe recording on magnetic patterned media", IEEE Transactions on Magnetics (accepted), vol. 43, June 2007.

PERPENDICULAR EXCHANGE BIAS IN [Pd/Co]-CoO NANOSTRUCTURES

Ildico Guhr[1], Olav Hellwig[2], Christoph Brombacher[1] and Manfred Albrecht[1]

[1]University of Konstanz, Department of Physics, Fach M 621, 78457 Konstanz, Germany, phone +49-7531-88 38 85, fax: +49-7531-88 30 90, e-mail: ildico.luise.guhr@uni-konstanz.de

[2]San Jose Research Center, Hitachi Global Storage Technologies, 3403 Yerba Buena Road, San Jose, CA 95135, USA

In this presentation magnetic nanopatterns, which have been created by depositing Co/Pd multilayers onto two-dimensional arrays of self-assembled, monodisperse polystyrene nanospheres [1] will be introduced. The magnetic nanostructures formed on top of the particles are in a magnetically exchange-isolated quasi-single-domain state. Figure 1 shows a magnetic force microscope (MFM) image of a capped particle array with a diameter of 110 nm. This nanoscale system is quite distinct from the classical geometries. Here the deposited film is extended over a wide region of the sphere and thus shows substantial curvature. The film thicknesses varies and so do the intrinsic magnetic properties most notable the magneto-crystalline anisotropy [2].

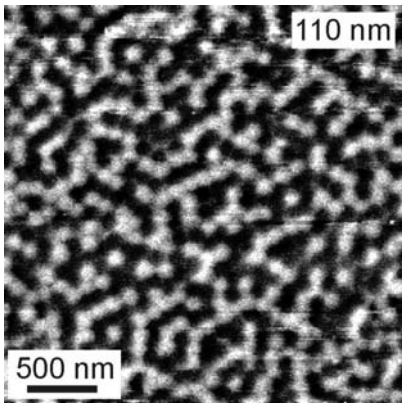

Figure 1: *Magnetic force microscope image of a magnetic cap array on top of 110 nm particles at room temperature.*

The so-formed magnetic nanopatterns were used to study the size-dependent scaling of perpendicular exchange bias in nanostructures. [Pd/Co]-CoO layers with perpendicular magnetic anisotropy were deposited onto different arrays of nanospheres with a diameter ranging from 58 to 320 nm. For comparison a continuous film was simultaneously deposited on a plain glass substrate. The samples were characterized by MFM, polar magneto-optical Kerr effect, and superconductive quantum interference device (SQUID) magnetometry measurements applying the field perpendicular to the substrate plane. All hysteresis loops were measured after cooling the samples in a field of -50 kOe.

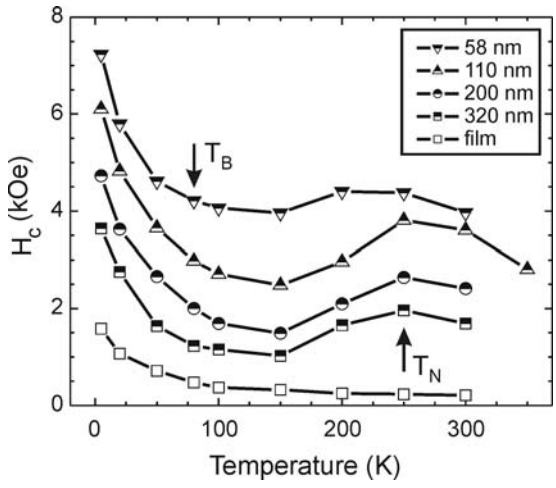

Figure 2: *Temperature dependence of the coercivity measured for various particle sizes, and for the continuous film.*

Compared to the continuous film, the biased caps show a significantly higher coercivity. This increase is more pronounced as we scale down the particle diameter. In figure 2 the temperature dependence of the coercivity H_C is presented for different particle sizes and for the continuous film. In contrast to the film, the coercivity of the nanostructure arrays is increased and exhibits a non-monotonic temperature behavior with a local maximum at about 250 K, indicating the onset of the antiferromagnetic spin order. However, a shift of the hysteresis loop occurs at

much lower temperatures of about 80 K. This blocking temperature does not show any size dependence and is similar for the nanostructures as well as for the continuous film. Additionally, the biased caps show an asymmetry of the switching field distribution (SFD) below the blocking temperature which is not observed for the continuous film. The σ-values of the switching field distribution as extracted from the hysteresis loops are given in figure 3 for the 58 nm cap array and for the continuous film for different temperatures.

The exchange bias field H_E also increases drastically with decreasing particle size and temperature. In figure 4 the dependence of the exchange bias field on the particle size is summarized for various temperatures and compared to the temperature behaviour of the continuous film. Furthermore, H_E also exhibits a strong dependence on the applied cooling field and the number of field cycles (training effect).

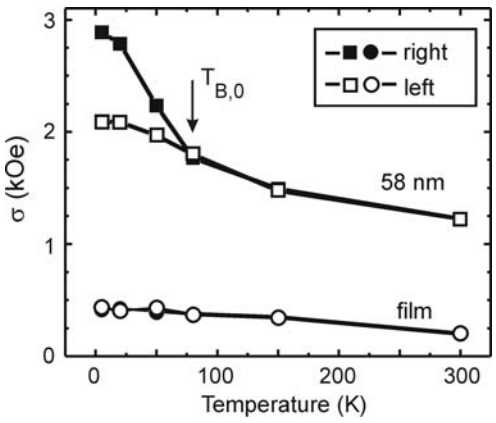

Figure 3: *σ-values of the switching field distribution for the 58 nm cap array and for the continuous film for various temperatures.*

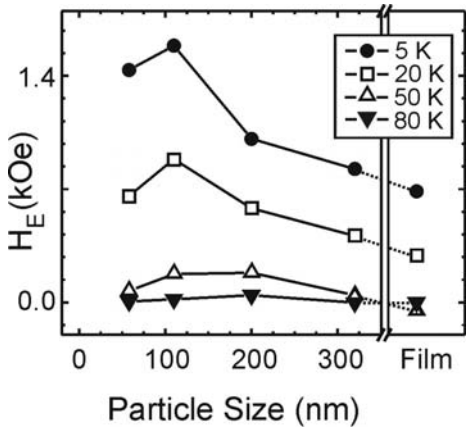

Figure 4: *Temperature dependence of the resulting exchange bias field measured for various particle sizes, and for the continuous film.*

This work was supported by the German Science Foundation (DFG) through the Emmy-Noether program at the University of Konstanz and the EU STREP Project *"MAFIN"*.

[1] M. Albrecht et al., Nature Material **4**, (2005) 203
[2] T. Ulbrich et al., Phys. Rev. Lett. **96**, (2006) 077202

IMAGE CHARGE STEPPING ACTUATOR FOR DATA STORAGE PURPOSES

A.M. Hoexum, W.W. Koelmans, T. Bolhuis, L. Abelmann and J.C. Lodder

MESA+ Research Institute for Nanotechnology, University of Twente, The Netherlands
www.uspam.nl L.Abelmann@utwente.nl

Mechanical addressing of data requires a means of positioning the read/write heads with respect to the data storage medium or vice versa. In this work, a wireless electrostatic stepping actuator is presented that can be used to complete this task in future data storage systems. The actuator is propelled by the attraction and repulsion of electrostatic charges in changing electric fields and therefore, no mechanical contact is required for its propulsion. Although the principle of propulsion has been invented by Egawa et al. [1] in the early 1990's, the use of such an actuator for data storage has not yet been considered.

The actuator consists of a moveable part called 'slider' that is placed on a set of three-phase interdigital electrodes called 'stator' (See figure 1). When a static voltage pattern is applied to the three electrodes in the stator, the charges in the poorly conducting slider redistribute to form mirror charges. To make the slider move, a dynamic voltage pattern is applied to the stator. This makes the charges in the electrodes change instantly, while the semi-permanent charges in the slider require some time to redistribute. The resulting electrostatic force has both a forward and an upward component. The latter reduces the friction of the actuator and makes it less sensitive to wear.

The design scales favorably with decreasing size. At a smaller electrode pitch, smaller voltages are required to produce electric fields of the required magnitude. In addition, this type of electrostatic actuation supports both 1D and 2D movement of the slider. The latter does increase the complexity of the stator, however.

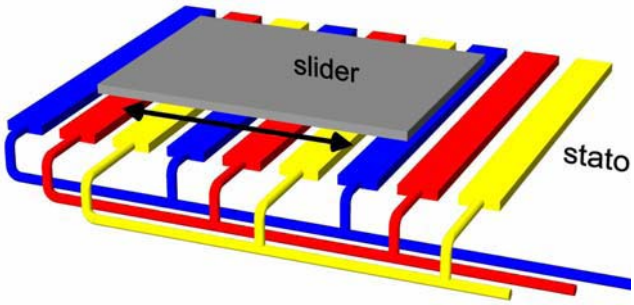

Figure 1 Slider on top of the three phase stator

Although the ICSA is suitable for many applications, two very different (future) data storage applications will be highlighted in this work. The first concerns a data storage system for archiving massive amounts of data for archiving or backup (ProTeM). In this case, the ICSA can be used to position a data storage medium of about 100 cm^2 with respect to a fixed array of read/write heads. Since the propulsion principle only requires that the slider is a poor conductor, the demands placed on the medium are considered fairly light. Since the propulsion principle only requires the slider surface resistivity to be in the 10^{13}-10^{15} Ω cm range; the demands placed on the medium are considered fairly light.

The second application involves a miniaturized version of the ICSA. In this case, the actuator is used to propel a wireless miniature data storage robot [2] (StoBot) with typical dimensions of a few hundred µm over a data storage medium. The StoBot itself is equipped with a small array of read/write probes and electronics for communication, positioning and reading and writing. In this system, it is required that the StoBot can move at speeds of several cm/s.

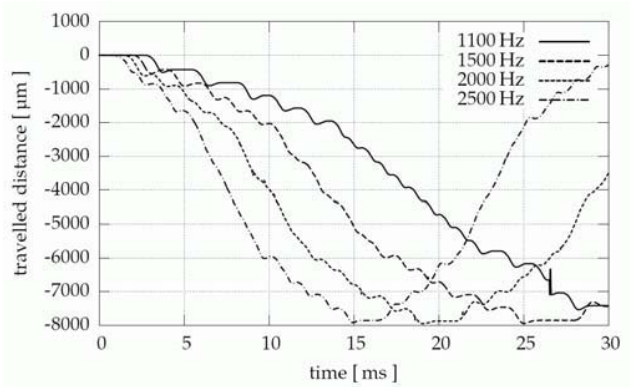

Figure 2High speed camera observation of stepping motion

Two versions of the ICSA have been developed: a macro version, measuring approximately 1 cm in size, and a micro version, with typical dimensions in the order of 200 µm. Two different stators were developed to propel the macro version. A 1D stator with an electrode pitch of 400µm and a 2D stator with an electrode pitch of 1200 µm. These stators were driven at a maximum of 774 V_{pp} for propulsion. Due to the high fields involved, sparking was observed on the 2D stator and although 2D motion was observed, no further experiments could be performed. The 1D stator was capable of driving several types of sliders (and materials). The best performing sliders were used for extensive measurements with a high-speed camera (See figure 2). The actuator proved capable of reaching speeds up to 1 m/s at 2.5 kHz driving frequency. These measurements indicated that the discrete stepping behavior of the actuator changes into continuous motion at high frequencies, which opens up the possibility to reach very high speeds.

The micro version (See figure 3) did not perform this well and no reproducible in-plane motion of these actuators has been observed. The movement of the slider was limited to a slight trembling or shaking motion. The lack of motion may well be due to problems with stiction and the mask design of the stator. Another explanation may lie in the distance of the electrode to the slider. When this distance becomes too small, the repulsive electrostatic force changes in to an attractive force, thus preventing slider motion.

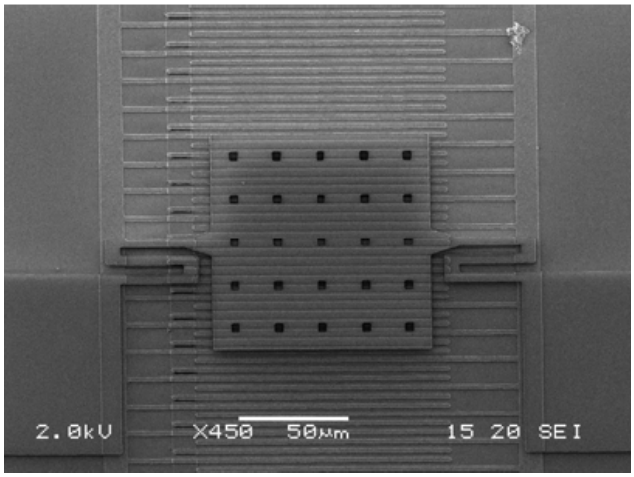

Figure 3 SEM image of the micro version of the ICSA

The use of the ICSA was considered for data storage purposes and is interesting because of its scalability and the possibility to implement electronics on a nearly featureless actuator surface. Furthermore, when correctly operated the lift reduces friction, while speed is in principle only limited by electronics when operated in vacuum. Continuous motion may be possible with good control and positioning electronics.

[1] Egawa et al. IEEE Proc. MEMS Workshop, Napa Valley, CA, USA, 166–171 (1990).
[2] L. Abelmann et al. IEE Proc.-Sci. Meas. Technol. 150, 218-221 (2003).

TRANSFER OF WIRELESS MICROACTUATORS FOR DATA STORAGE PURPOSES

A.M. Hoexum, L. Abelmann, G.J.M. Krijnen and J.C. Lodder

Transducer Science and Technology
MESA+ Research Institute, University of Twente
a.m.hoexum@utwente.nl , l.abelmann@utwente.nl
tel: +31 53 489 1014 fax: +31 53 489 3343

The context of this work involves the use of wireless microrobots for probe-based data storage, combining microactuators and read-write probes (StoBots [1]). The implementation of such a system demands that the microrobots are transferred from the wafer of origin to a substrate on which data can be stored. Parallel fabrication of actuator and substrate increases cost-efficiency and allows the use of wireless actuators, fabricated by surface micromachining, on surfaces incompatible with this kind of processing.

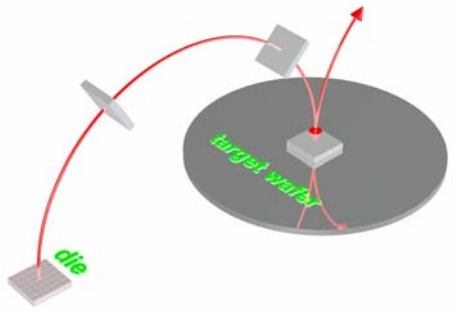

Figure 1: The concept of batch transfer. The source die is flipped over, pressed on the target wafer, a voltage is applied to the electrodes and the die retracted.

The basic concept (Fig. 1) is straightforward: actuators are fabricated upside down on the source wafer using micromachining techniques. This wafer, or only a die, is gently lowered on a surface equipped with interdigital electrodes, called target wafer. After contact, a voltage difference (AC for conductive, DC for dielectric devices) is applied to the electrodes, making the actuators clamp. The source wafer is then retracted, causing the suspension to break, thereby releasing the actuators on the target wafer. With electrostatic attraction being key element, any device that can be electrostatically clamped to the target wafer can be transferred, which makes it a universal method.

To prevent the actuators from getting crushed during transfer they are fabricated above a cavity, suspended by springs. The suspending springs have artificial weak spots, enabling actuator release at the correct point and moment (Fig. 2). The length of the spring offers control over the bending stress in the weak spot. Calculations show that the release voltage is inversely proportional to the square root of the spring length. This dependency enables selective transfer of actuators.

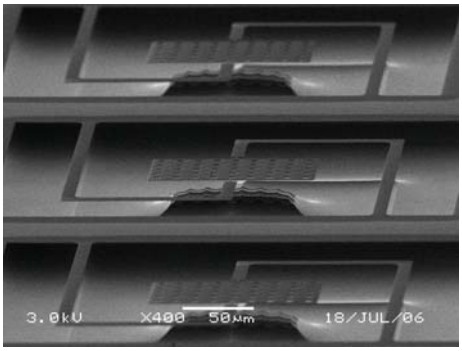

Figure 2: A part of an array of transportable actuators, above a cavity and suspended by springs. The weak point of the springs connects the spring to the actuator plate.

The method is illustrated using Image Charge Stepping Actuators (ICSA [2]), fabricated from a 1µm thick LPCVD deposited SiRN film. The actuator and suspending springs are defined within a single mask. The devices are released by isotropic dry etching of the silicon wafer at room temperature using SF6 and no forward power. The ICSA's require a set of 3-phase electrodes to function, resulting in a three-mask fabrication process to create gold electrodes with pitches ranging from 4 to 256µm. The first mask defines the bottom electrode layer, the second introduces vias and the third defines the top electrode layer. PECVD deposited SiO2 films with a thickness of 400nm are used to insulate the conducting layers.

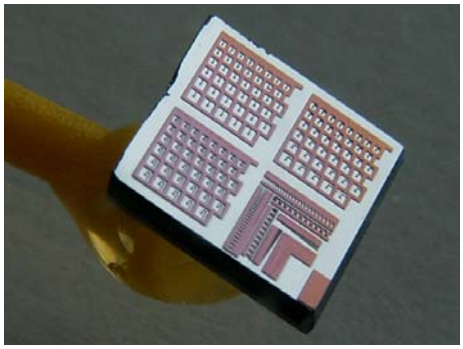

Figure 3: A die with actuators glued on to a VivaStick.

A die with actuators from the source wafer was glued onto a VivaStick (Fig. 3) and mounted on a manual probe station manipulator. The manipulator was used to establish contact between source and target in a controlled way. After application of a voltage of over 10V to the electrodes, the ICSA's with the longest springs are transferred to the target wafer. With increasing voltage, actuators with shorter springs were transferred as well, thus confirming the calculations. At 40V 46 of the 150 actuators are released. Figure 4 shows that the devices with the shortest springs remain in the die. The transfer process does not damage the actuators. Upon actuation, stepping motion was observed for several actuators. The motion was, however, not reproducible due to stiction effects.

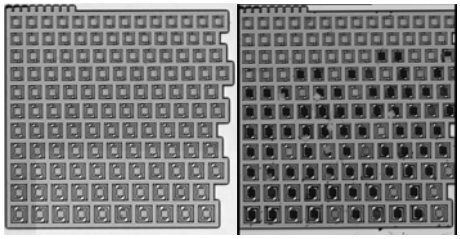

Figure 4: A die before and after release. The released actuators are those suspended by the longest springs.

A technique that allows both selective and batch transfer of microactuators from one surface to another has been developed and tested. Although the transfer method is illustrated using ICSA's, it can be used to transfer many types of wireless actuators. The successful implementation of the technique is another small step forward on the road towards a future data storage system based on wireless microrobots.

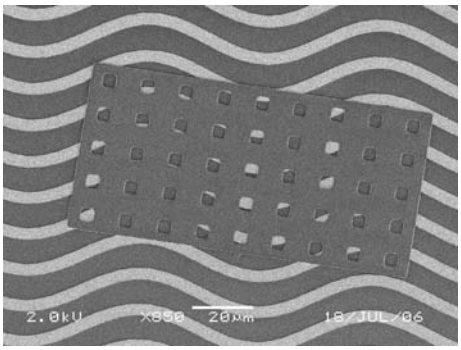

Figure 5: SEM image of an ICSA, successfully transported on to the gold electrodes. The image reveals no damage.

[1] L. Abelmann, T. Bolhuis, A.M. Hoexum, G.J.M. Krijnen and J.C. Lodder, "Large capacity probe recording using storage robots", in *IEE Proceedings - Science, Measurement and Technology*, September 2003, Vol. 150, Issue 5, pp. 218-221

[2] S. Egawa and T. Higuchi, "Multi-layered electrostatic film actuator", in *Proceedings IEEE Micro Electro Mechanical Systems Workshop, Napa Valley, CA, USA*, February 1990, pp. 166-171

Exploring the Data-Layout Design Space of MEMS-Based Storage Systems

M.G. Khatib, B.J. van der Zwaag, H.W. van Dijk, G.J.M Smit, and P.H. Hartel

Department of Computer Science University of Twente
P.O. Box 217 Enschede, the Netherlands
{m.g.khatib | b.j.vanderzwaag | h.w.vandijk | g.j.m.smit | p.hartel}@utwente.nl

Introduction

Storage devices based on MEMS (Micro-Electro-Mechanical Systems) are expedient as secondary storage for future (mobile) computer systems. Designing a MEMS-based storage system however is a non-trivial task because of its large design space. As shown in Figure 1, the design parameters span different levels: the physical, the layout, and the system level. Typical design targets of any storage system include data throughput, service time, effective capacity, power consumption, and data error rate. In this paper we show how the striping policy parameter influences the capacity and service time.

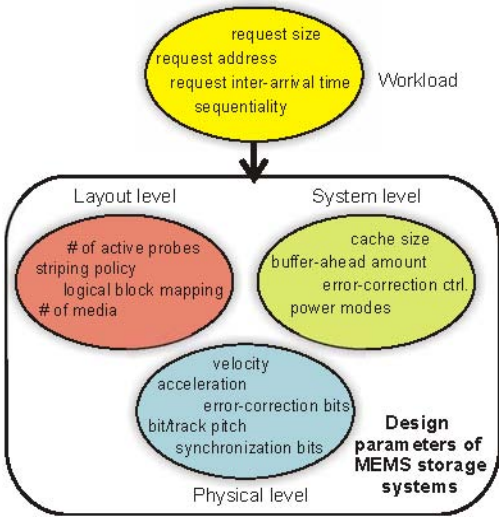

Figure 1: Design space of MEMS-based storage systems

Case Study

In a MEMS-based storage system, many (i.e., 100s or 1000s) read/write heads, so-called probes, operate concurrently. Due to this parallelism, MEMS-based storage systems face a particular design challenge: how should a data block be partitioned across the active probes, called the *striping policy*? In this work, we show how the striping policy impacts the timing performance and the effective capacity of MEMS-based storage systems in opposing ways. The former is reflected in the bandwidth efficiency, whereas the latter is reflected in the format efficiency of the storage system.

Let *m* be the *striping policy* of a MEMS-based storage system, then the maximum number of data blocks the system can access simultaneously equals *m*. A fixed length data block thus is striped over a maximum of *m* sub-blocks.

Definition 1: Format efficiency is the ratio between the net (logical) capacity and the raw (physical) capacity.

Definition 2: Bandwidth efficiency is the ratio between the actual and optimal service times of requests.

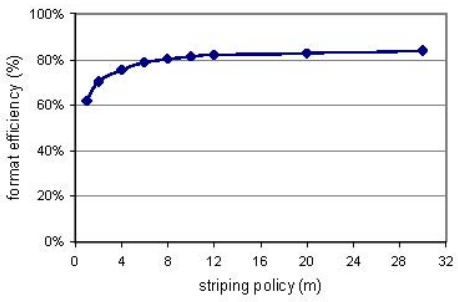

Figure 2: the format efficiency for several values of m.

Two Design Targets

I. Format Efficiency – The physical capacity of MEMS-based storage is reduced due to the need to store system data, which include the servo, synchronization, and error-correction data. For the dependable functioning of the system, system data must be deployed on a sub-block level, which decreases the raw

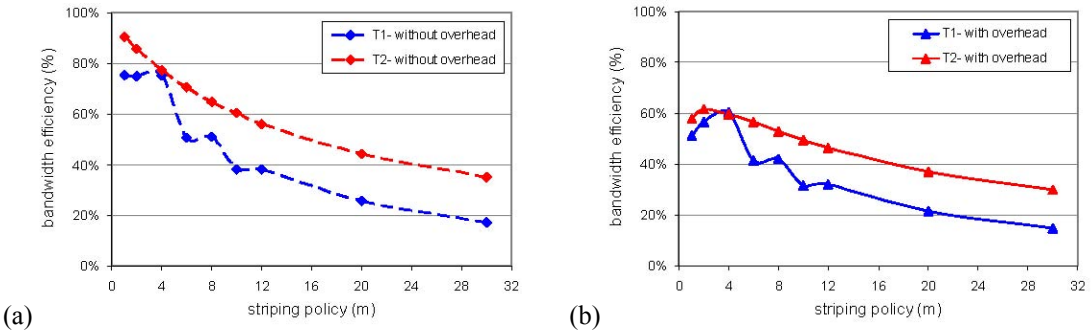

Figure 3: the bandwidth efficiency (a) excluding and (b) including the format overhead for several values of m.

capacity. Deploying a large *m* mitigates this loss since the number of sub-blocks per block decreases. Figure 2 depicts the format efficiency for various values of *m*. The efficiency improves by 15% when deploying *m*=4 relative to *m*=1.

II. Bandwidth Efficiency – The service time increases when the request size and address are not aligned on an *m*-boundary. This is because not all probes are used, causing additional seeks and transfers. Striping with a small *m* mitigates such imperfection; setting *m*=1 factors it out entirely. However a small *m* increases the actual service time because of the reduced format efficiency. Figure 3a shows that the bandwidth efficiency for two different workload traces (T1, T2) decays as *m* increases, not accounting for the loss due to the format overhead. Including the format overhead, as shown in Figure 3b, causes an additional drop, which is most sincere for *m*=1 (compare the bandwidth efficiency among *m*=1, 2, and 4 for T1 with and without the format overhead).

A Design Trade-off

As shown in Figure 4 large *m* can be deployed to allow for high format efficiency, where the bandwidth efficiency is sacrificed. In contrast, the best values of *m* from performance perspective cause loss in the format efficiency. A trade-off between the two design targets is thus necessary. Moreover the trade-off depends on the temporal and spatial characteristics of the actual workload trace. As an example, *m*=4 and *m*=2 both satisfy a design constraint of a 3:1 bandwidth efficiency to format efficiency ratio for the T1 and T2 respectively.

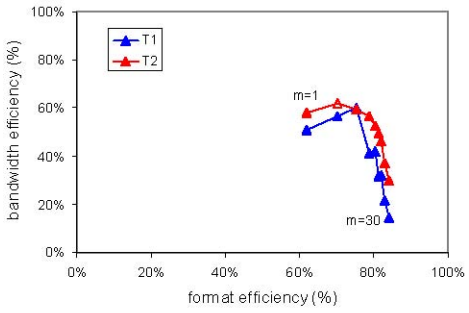

Figure 4: the design space for bandwidth efficiency vs. format efficiency, given a range of m.

The interested reader is referred to [1] for an in-depth discussion of our work.

[1] M.G. Khatib, B.J. van der Zwaag, F.C. van Viegen, and G.J.M. Smit: **Striping Policy as A Design Parameter of MEMS-based Storage Systems**. *Proceedings of the 2nd International Workshop on Software Support for Portable Storage (IWSSPS 2006)*, pages 25–32, Seoul, Korea, October 2006.

FIELD EMISSION TO CONTROL TIP-SAMPLE DISTANCE IN PROBE RECORDING

A.J. le Fèbre, L.A.A. Bouwman, L. Abelmann and J.C. Lodder

MESA+ Institute for Nanotechnology, P.O. Box 217, 7500 AE Enschede, Netherlands
Email: a.j.lefebre@utwente.nl Tel: +31 (0)53 4894673 Fax: +31 (0)53 4893343

For high density probe recording on a patterned magnetic medium, a constant tip-sample distance on the order of several nanometers is needed to be able to sense the small magnetic stray fields [1]. In this work, we present a new concept for high resolution proximity sensing based on field emission and provide more insight in field emitter materials, vacuum conditions and electronics needed for stable operation of field emission distance control. This technique can be implemented in a probe recording storage system by using thousands of field emission tips that are individually positioned at several nanometers above the magnetic recording medium.

For characterization we used highly doped (<0.01 Ohm·cm) single crystal silicon AFM probes as field emitters, with various coating materials (Mo, W) to enhance the field emission properties. A UHV AFM microscope scanner was used to approach individual probes to a silicon wafer sample coated with ~100 nm TiW. To improve the stability of the field emission current the system was operated at $5 \cdot 10^{-10}$ mbar. I/V curves (figure 1a) and Fowler-Nordheim plots (figure 1b) were measured for increasing gaps and fitted to obtain the emission area and field enhancement factors using a dedicated fitting procedure from [2].

By keeping the field emission current constant using position feedback, it can be used to control the tip-sample distance [3]. Displacements were measured as function of voltage by controlling the tip position to maintain a constant current of 3 nA (figure 2). Above 25V, the displacement becomes linear with 3.8 nm/V. The non-linearity for lower voltages is caused by a varying electric field enhancement due to the small gap regime, which can be modeled using a factor *k* to describe the tip sharpness.

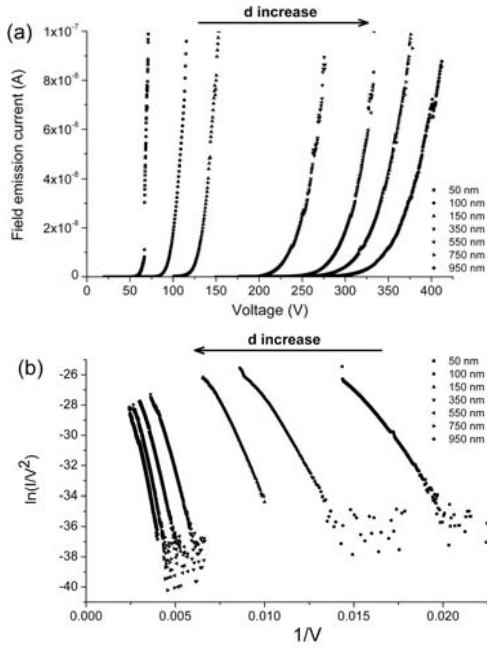

Figure 1.Distance dependence of field emission in (a) I/V characteristics and (b) corresponding Fowler-Nordheim plots, measured for gaps from 50 nm to 950 nm between standard AFM probe and TiW sample.

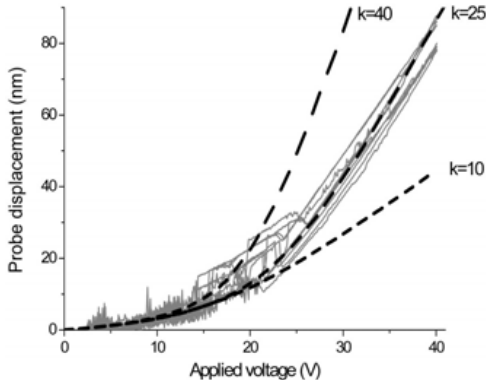

Figure 2. Displacement as function of applied voltage using position feedback (constant field

Fluctuations are caused by instabilities in the field emission current, which was improved by using a conductive diamond coating (figure 3a), or by using a carbon nanotube mounted at the tip end (figure 3b).

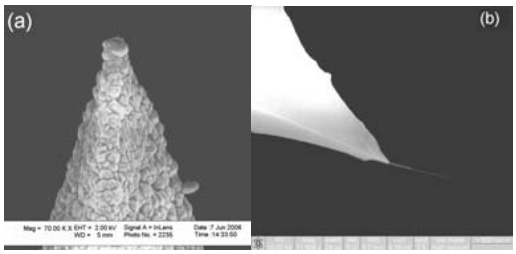

Figure 3. Field emission probe tips with (a) ~100 nm diamond coating, and (b) carbon nanotube, radius ~5 nm.

Next to controlling the tip-sample distance, from the field emission current also the cantilever resonance was obtained (figure 4). A piezo actuator was used to bring the cantilever in resonance. The resonance curve was obtained from the field emission current using a high-bandwidth current amplifier and spectrum analyzer. Measured peak is at 162 kHz with a quality factor of ~8000, corresponding well to the expected values. Since shifts in this frequency can ultimately be used to sense magnetic stray fields, the field emission current detection method can result in an integrated method for reading data in magnetic probe recording.

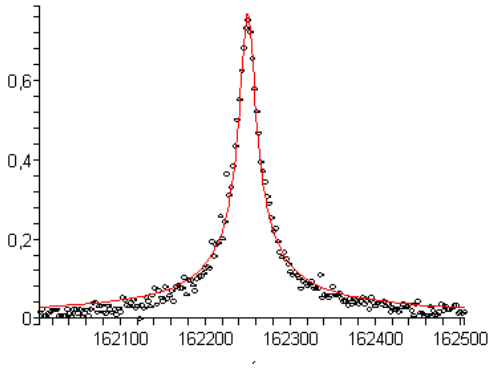

Figure 4. Cantilever resonance curve obtained by field emission current detection.

To test the field emission control method for scanning on a patterned medium, a non-magnetic sample with nanodots was prepared by laser interference lithography (LIL) [4]. Figure 5 shows 1x1 µm scans using 0.5, 5.0 V and 50.0 V bias voltage respectively at 0.3 nA current setpoint. Increasing the bias voltage results in a loss of resolution, caused by the increase in tip-sample distance.

The measurements confirm that field emission can be applied to control the tip-sample spacing, with sufficient resolution and current stability for probe recording applications.

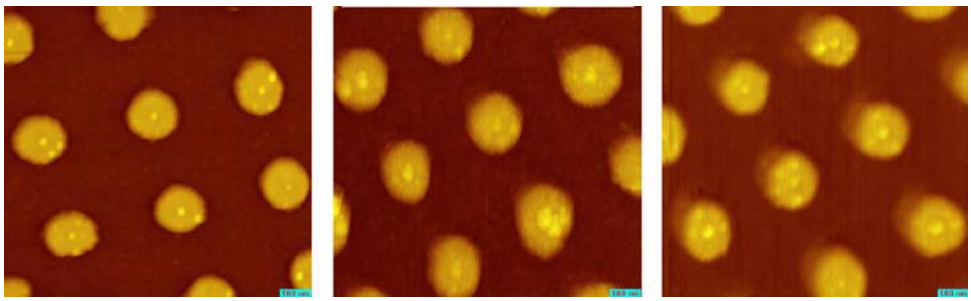

Figure 5. Image scans of LIL sample using field emission at 0.5V(left), 5V(mid) and50V(right).

Acknowledgements

This work is part of the STW program ‘Micro Scanning Probe Array Memory’. The authors thank M. Siekman and T. Bolhuis for technical assistance and R. Luttge for sample preparation.

[1] A.J. le Febre et al, ICNT2006 conference, Basel. Accepted in Journal of Physics: Conference Series (JPCS).
[2] R.G. Forbes, Ultramicroscopy 79, 11, (1999).
[3] R. Young et al, Rev. Sci. Instrum. 43, 999, (1972).
[4] R. Luttge, this conference

Heating and cooling dynamics in thermally assisted MRAM

C. Papusoi[1], R.C. Sousa[1*], I.L. Prejbeanu[2], J.P. Nozieres[2], K. Mackay[2], B. Dieny[1]

[1] *Spintec URA 2512 CEA/CNRS, 17 r. des Martyrs, Bat. 10-05, 38 054 Grenoble, France*
[2] *Crocus Technology, 4 Robert Schuman, Grenoble, France*
[*] *Corresponding author, email: ricardo.sousa@cea.fr*

Introduction

In thermally assisted MRAM, the storage layer is pinned by exchange coupling using a low blocking temperature antiferromagnet (T_b <150°C). Heating above T_b allows writing of low aspect ratio bit elements with a magnetic field along a single axis. The total time required for the write cycle is determined by the heating and cooling process occurring in the tunnel junction. This work investigates the tunnel junction heating and cooling dynamics for micron and sub-micron size junctions to be used in a thermally assisted MRAM.

Heating and cooling dynamics

The time evolution of the heating process was obtained from experimental measurements performed on MTJs with the following layer stack Ta 50 / PtMn64 20 / CoFe20 2.5 / Ru 0.8 / CoFeB20 3.0 / Al 0.5 + Oxidation / CoFeB20 1.5 / NiFe 3 / IrMn 5 / Ta 5 / Al 20 / Ta 120nm, lithographically patterned into circular pillars of 0.35µm diameter.

The junction was submitted to the simultaneous action of a step applied field H_{appl}=800 Oe and a voltage step pulse, of amplitude V. The duration of the applied field is much larger (6 ms) than that of the voltage pulse (2 - 100 ns), allowing the freezing of the antiferromagnet with a well defined orientation of the free layer. After the suppression of H_{appl}, the MR curve is measured and the exchange bias H_{exch} between the free layer and its pinning antiferromagnet, is determined. This procedure is repeated for a reverse orientation of the applied field H_{appl}=-800 Oe in order to establish, based on the change of sign of H_{exch}, whether the free layer has switched or not in the direction of the applied field. This is equivalent to saying that the heating temperature caused by the application of the voltage pulse becomes higher than the blocking temperature T_b of the antiferromagnet. The corresponding amplitude of the voltage pulse is denoted by V_{SW} (switching) and the corresponding power by P_{SW} (Fig.1). Both of them are dependent on the voltage pulse width, as suggested by Fig.1. The maximum writing frequency is determined by the time required for the junction to cool down after the application of a heating pulse. We have investigated the cooling process *via* the application of a two-pulse sequence. The first pulse, denoted by (1), having a constant amplitude and 7 ns width, is used for heating the junction while the second pulse, denoted by (2), having 3 ns width and variable amplitude and time delay δ with respect to the first pulse, is used to probe the temperature variation created by (1). The amplitude of the first pulse was chosen equal to V_{SW} for a pulse of width equal to the sum of widths of (1) and (2), i.e. 10 ns. For each delay of pulse (2), δ, its amplitude is progressively increased until it reaches the switching value. For δ =0 ns, the V_{SW} value of (2) is equal to V_{SW} for a pulse having 10 ns width, denoted by V_{ini}. When δ is increased, the V_{SW} of (2) progressively increases, reaching a saturation value equal to the V_{SW} of an isolated voltage pulse of 3 ns width, denoted by V_{fin}. This value is reached when δ is large enough for the heat due to (1) to be completely dissipated by the instant when (2) is applied. The normalized values of V_{SW} for pulse (2), $(V_{fin}-V_{SW})/(V_{fin}-V_{ini})$, are plotted as a function of δ in Fig.2. This dependence was fitted by a double exponential $y = y_{01}*\exp(-\delta/\tau_1) + y_{02}*\exp(-\delta/\tau_2)$, where y_{01}=0.7, τ_1=1 ns correspond to the cooling rate of the junction, and y_{02}=0.4, τ_2=11 ns correspond to the cooling rate of the leads.

These results show that by operating the TAM-RAM in the adiabatic regime (i.e. by minimizing the heating of the leads), the time constant of heating and cooling can be of only a few nanoseconds.

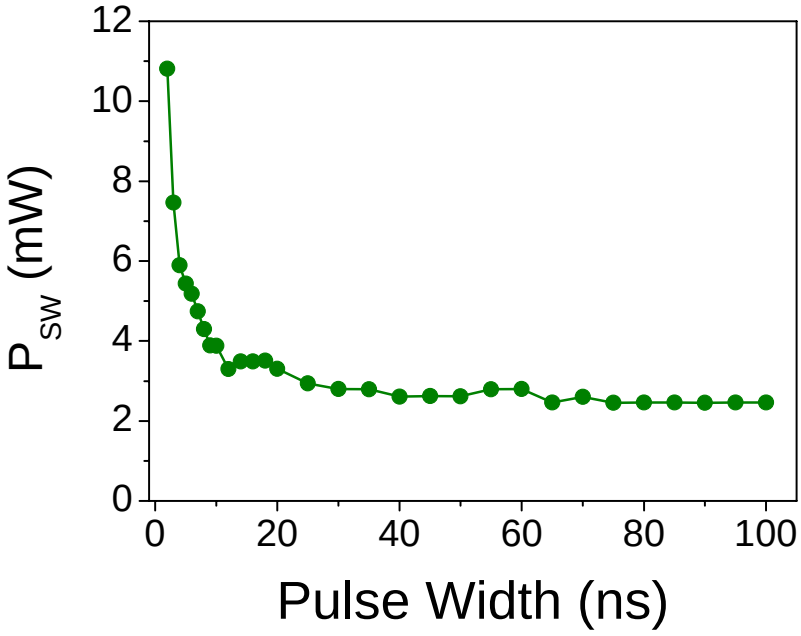

FIG.1 : Minimum power required to write as a function of the heating pulse width.

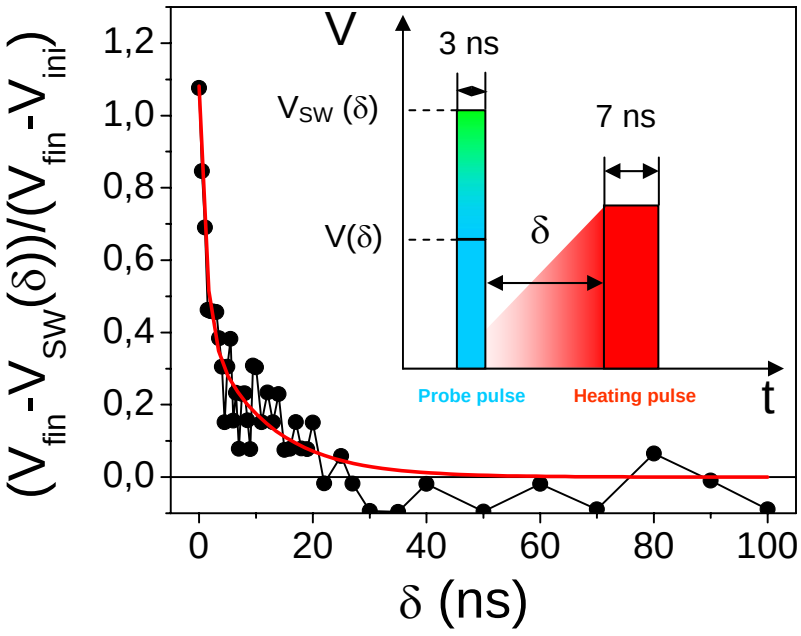

FIG.2 : experimental determination of the cooling rate of TAM-RAM memory cell using two successive heating pulses.

Reliability For Probe Storage

Tom Parnell[1], David Wright[2], Oleg Zaboronski[1]

[1]: Arithmatica Ltd and Department of Mathematics, University of Warwick. [2]: Department of Computer Science, Exeter University. Contact: Tom Parnell, Arithmatica Ltd, Haseley Business Centre, Warwick, CV35 7LS, e-mail: tom.parnell@arithmatica.com, Phone: +44 (0) 01926 484025, Fax: +44 (0) 870 922 3589

Introduction

The ProTem project aims to create a probe storage system with the following specifications:

	Lifetime	***Latency***	***Energy use***	***Data rate***	***Cost/GB***	***Capacity***	***Architecture***
Archive	50 years	1000 ms	Low	100 MB/s	Low	10-20 TB	1 actuator, large area
Backup	10 years	500 ms	Low	500 MB/s	Medium	10-20 TB	4-8 actuators, large area

A non-redundant arrray of probes

Suppose that the average life time of a single probe is $\lambda^{-1}=100$ years. Assuming that probes fail with a constant rate, it can be shown that the probability that a probe does not fail during the first 10 years of operation is close to 1. However in order to achieve the throughput of 128 MB/s required by archival applications, an array of 1024 probes reading and writing in parallel is required (each probe provides 1 MB/s). If no redundancy is introduced, a single probe failure will lead to an read/write error. Under these assumptions the probability of an array of N probes not failing for T years is:

$$P_T(N)=e^{-\lambda NT}$$

For $T=10$ years and $N=1024$, this probability is essentially zero. It can, in fact, be shown from the above expression that the mean lifetime of an array of 1024 probes is just over one month.

Traditional Coding (Write-redundancy)

Traditional coding solutions to this problem would involve adding parity bits and thus sacrificing capacity. Given that the position of errors are known we can construct a 'perfect' linear block code with N - m information bits and m parity bits which can correct up to m errors in known positions. The probability of non-failure in the interval $[0,T]$ for a write-redundant array of size N is:

$$P_T^{wr}(N)=\sum_{k=0}^{m}\binom{N}{k}(1-e^{-\lambda T})^k e^{-\lambda T(N-k)}$$

Using this expression it can be shown that for backup applications a reliable probe storage system can be built (using write-redundancy) if we are willing to sacrifice 10 percent of storage capcity. For archival applications however, 43 percent of storage capacity is needed for a reliable probe storage system using write-redundancy. These

results cannot be improved as they saturate the Shannon limit for a noiseless erasure channel, which can be stated as follows: given the probability of probe failure *p*, then the minimal share of redundancy *R* required for error free operation of an array of probes is also *p*.

Read-redundancy

An alternative solution is suggested which assumes that the probes are organized into an array of N_r rows and N_c columns, and that the array moves in steps of N_c/k where $k>1$ is an integer dividing N_c. For the example $k=2$: in order for a read error to occur at least one pair of probes belonging to the same row and separated by precisely $N_c/2$ spaces needs to fail. The probability that this pair does not fail up to time *T* is as follows:

$$P_T(2)=1-(1-e^{-\lambda T})^2=2e^{-\lambda T}-e^{-2\lambda T}$$

Given that probes fail independently of one another, it can be shown that the probability the array not failing in the interval *[0,T]* is:

$$P_T^{rr}(N_r N_c)=P_T(2)^{N_r N_c/2}$$

It can be shown that for an array of size *N=1024*, this scheme (*k=2*) gives us an increase in survival probability of 20 orders of magnitude over the non-redundant array but even for a backup application the probability of failure is still 10^{-2}.

Read/write-redundancy

If we combine both of the above techniques we can construct an array with the following non-failure probability (in the interval *[0,T]*):

$$P_T^{rw}(N)=\sum_{k=0}^{m}\binom{N/2}{k}(1-P_T(2))^k P_T(2)^{N/2-k}$$

It can be shown that using this read/write-redundancy scheme, an array can be built with a survival probabiltiy after 50 years of 0.99 with only 18 percent of storage capacity wasted on parity bits (see Figure 1).

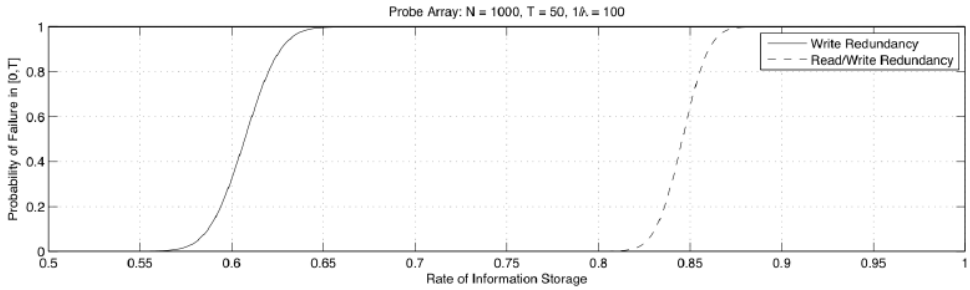

Figure 1 : Comparing the read/write-redundancy scheme against the write-redundancy scheme

Wear and friction of silicon nitride surfaces of an electrostatic MEMS actuator for µSPAM

M. Patrascu[1,A] , S. Stramigioli[1], G. Krijnen[2] and M. de Boer[2]

[1] EL-CE – EW, Universiteit Twente, 7500AE Enschede, The Netherlands

[A] Current affiliation
IMEC-NL / Holst CentreHigh Tech Campus 48, 5656AE Eindhoven, The Netherlands
tel: +31 40 277 4092, fax: +31 40 274 6400, Mihai.Patrascu@imec-nl.nl

[2] TST – EWI, Universiteit Twente, 7500AE Enschede, The Netherlands

Introduction

µSPAM is one of the probe storage projects active in Europe, having as target to investigate the feasibility of a novel probe recording-based storage system. In the past, we have looked at various performance-related properties of a stepper motor for reading and writing data [1, 2].

Wear and friction experiments

In this summary, we report on wear and friction of contact components of a MEMS-based stepper motor (Fig.1). Actuation is being accomplished by electrostatically attracting the legs and the plate towards the walking surface. Fig.2 shows how to obtain one step to the right (~50nm). Larger displacements follow from repeating the sequence. The accent lies on the coefficient of stiction between the walking surface and a number of torus-shaped bumps underneath the mobile legs (Fig.3). These bumps reduce the effective leg contact area and thus undesired stiction effects once the leg is free to move sideways. Using adjustable vertical forces, we look at slipping to determine the friction forces between the silicon-nitride interfaces and thus the stiction coefficient.

The stiction coefficient $\mu_{stiction}$ is derived experimentally by electrostatically applying a vertical force F_{vert} that fixes the leg to the surface in combination with a horizontal force F_{hor} from the spring structure (Fig.4). Slightly decreasing F_{vert} makes the structure slip until the stiction force equals F_{hor}. This procedure yields $\mu_{stiction}$ as a function of the vertical force (Fig.5). $\mu_{stiction}$ is not constant but a function of the applied force, because the effective contact area increases with higher F_{vert}.

From lifetime experiments it resulted that the micro motor can perform more than $4{,}25.10^9$ steps without performance decrease, an unprecedented value for MEMS stepper actuators. Deep traces of adhesive wear have lead to the final failure, a short circuit (Fig.6). This suggests using a thicker Si_RN layer to increase life time and coatings to reduce adhesive wear.

Acknowledgments

The µSPAM project is funded by STW (TES.5178). Edin Sarajlic is acknowledged for designing, fabricating and testing the first shuffle motors. This presentation is supported by IMEC-NL/Holst Centre.

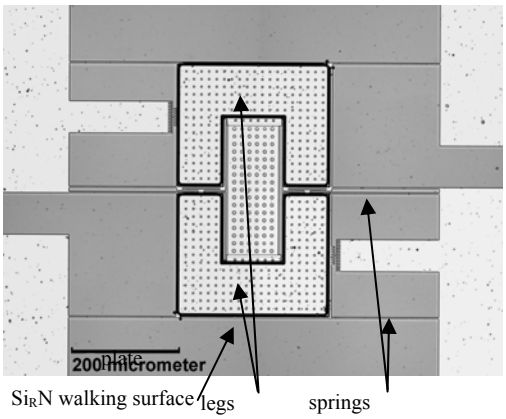

Figure 1. Top photograph of the µWalker.

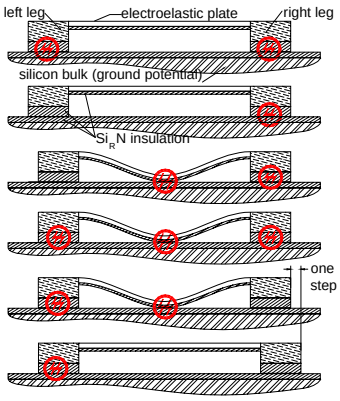

Figure 2. Actuation principle for obtaining one step to the right, side view.

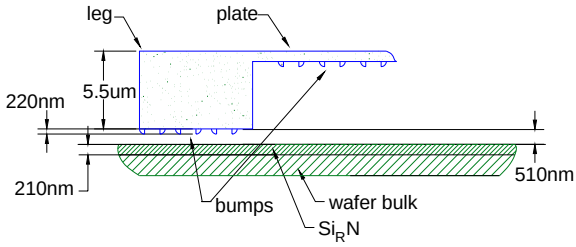

Figure 3. Interesting dimensions of the contacts at one leg.

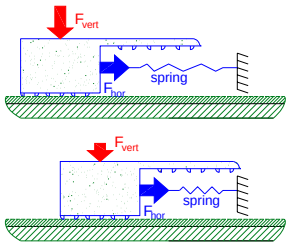

Figure 4. Forces for obtaining the coefficient of stiction.

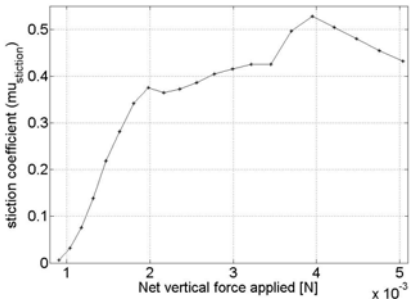

Figure 5. Derived coefficient of stiction as a function of the vertical force.

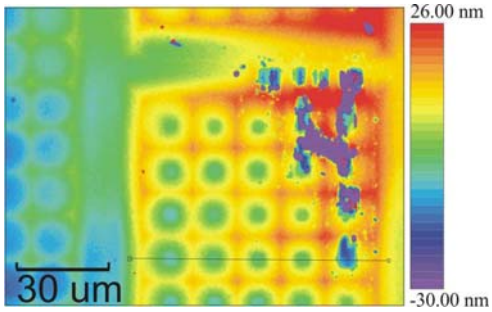

Figure 6. Wear patterns of the flat layer under one of the legs.

[1] M. Patrascu: *Characterization, modeling and control of the µWalker – a micro actuator for data storage.* PhD Thesis, University of Twente, The Netherlands, 2006. ISBN: 90-365-2398-2.
[2] N.E. Ligerink, M. Patrascu, P.C. Breedveld and S. Stramigioli: *An energy-based electrostatic beam model for MEMS applications*. Sensors and Actuators A: Physical, 121(2):500-507, June 2005.

MAGNETIC PROBE RECORDING WITH A MAGNETIC FORCE MICROSCOPE

M.H. Siekman, L.Abelmann and J.C. Lodder

TST, MESA+ Institute for Nanotechnology,
University of Twente PoBox 217, 7500 AE Enschede, The Netherlands
phone+31(0)53 4892749 FAX+31(0)53 4893343 e-mail m.h.siekman@utwente.nl

Introduction

In this paper we present an MFM, which is mounted in between the pole shoes of conventional electromagnet with a maximum field of 1350 kA/m (1.7 T). This MFM has been used to image and write into a perpendicular patterned medium consisting of CoNi/Pt multilayered dots with a spacing of 346 nm and a size of 140 nm.

Magnetic Force Microscope in field and in vacuum

Our microscope design (Figure 1) was derived from the high field, UHV microscope of Hug et al [1]. The instrument is mounted in a glass tube that is evacuated to 10^{-7} mbar. This increases the Q-factor of the cantilever significantly and therefore, the sensitivity. The MFM has to be able to rotate inside the field and the pole shoe distance of the conventional magnet is 6 cm. Given these constraints , an MFM was designed which has a maximum dimension of 4 cm. The instrument is constructed using non-magnetic materials such as titanium and sapphire. The sample coarse approach is obtained by a piezo shuffle motor. Scanning is achieved by a tube scanner with a scanrange of 15 µm. The cantilever is driven on its resonance frequency. To detect the defection of the cantilever a fiber interferometer is used (figure 2 left). The cantilever is brought in resonance and the phase shift is measured with a lock-in amplifier. In this microscope it is possible to excite the cantilever either by using a piezo placed under the cantilever or by applying a alternating voltage between the cantilever and the glass fiber. The advantage of the second method is that the forces are only applied to the cantilever beam. To excite the cantilever using the piezo much more energy is needed to get the same oscillation amplitude. This is not desirable since, the piezo also vibrates the complete microscope structure, which causes resonances in different parts of the microscope. This can distort the measurements as can be seen in figure 2 right.

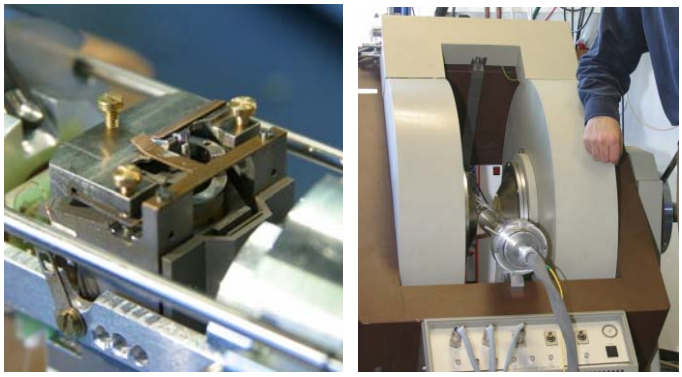

Figure 1 Vacuum, in-field Magnetic Force Microscope Left: close-up of microscope, right:vacuum tube and magnet.

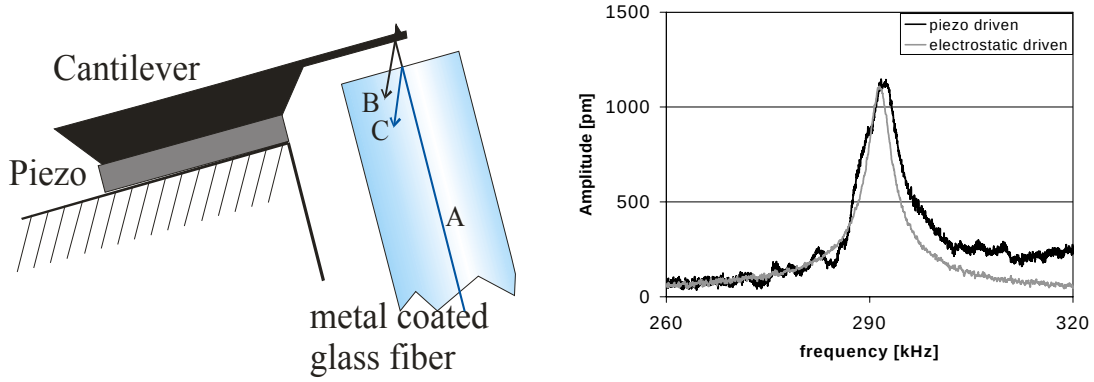

Figure 2 left:interferometer. Right: resonance frequency of cantilever excited by piezo or electrostatically

Recording experiments

Recording experiments of magnetic probe writing and reading has been demonstrated [3]. Using the electromagnet, the sample is saturated completely into one direction first. Subsequently the field is applied in the opposite direction, at a value just below the switching field of the individual dots. This field is sufficient however to reverse the magnetization of the tip. Than the tip is brought in contact with the medium, and by selecting a very limited scan range, 16 bits are reversed by the combination of the background field and the field of the tip (figure3, left). As can be seen in the figure, some bits outside the scan area were reversed so the background field was too large. On the other hand not all addressed bits were reversed either. Apparently the switching field distribution of the medium is still too large and improvements need to be made. Still we could demonstrate erasure, by applying the opposite experiment using a smaller scan area which only addressed 6 bits (figure 3, right). These experiments demonstrate that field-only writing on patterned media is possible if the switching field distribution is improved.

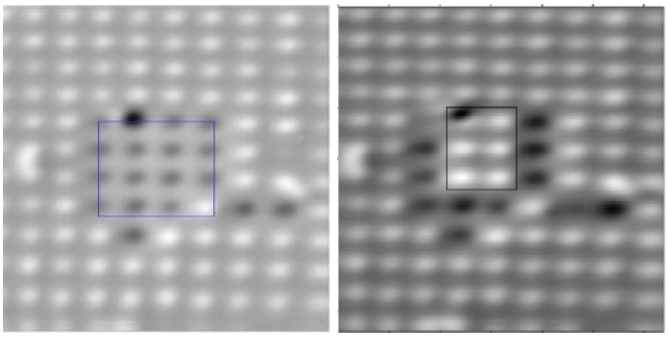

Figure 3 Write experiment on CoNi/Pt pattern medium of 300 nm periodicity. Left: area of 16 bits written. Right: Area of 6 bits rewritten.

Reference

[1] H.J.Hug et al, "A low temperature ultrahigh vacuum magnetic force microscope" Review of Sci. Instr. (1999).
[2] M.H.Siekman et al,"High Field Magnetic Force Microscopy of CoNi/Pt Patterned Media" PMRC 2004
[3] M.H.Siekman et al,"Magnetic probe recording on patterned media" IMST 2006

Determination of the Absolute Heat capacity in MAGNETIC tunnel junction nanopillars

R.C. Sousa[1*], C. Papusoi[1], F. Delille, I.L. Prejbeanu[2], J.P. Nozieres[2], K. Mackay[2], O. Redon[3], A. Astier[3], B. Dieny[1]

[1] *Spintec URA 2512 CEA/CNRS, 17 r. des Martyrs, Bat. 10-05, 38 054 Grenoble, France*
[2] *Crocus Technology, 4 Robert Schuman, Grenoble, France*
[3] *LETI/DIHS/LIMN, CEA, 17 r. des Martyrs, 38 054 Grenoble, France*
[*] *Corresponding author, email:ricardo.sousa@cea.fr*

Introduction

Current induced heating is an important aspect to take into account in lot of magnetic devices spanning from magnetoresistive read-heads of computer disk drives to magnetic memory elements. In Thermally Assisted Magnetic Random Access Memories (TAM-RAM), each memory element consists of a magnetic tunnel junction (MTJ) with an exchange biased storage layer (CoFe/IrMn). The write selectivity is achieved by combining a very short heating of the memory cell produced by a pulse of current through the junction, with the application of a pulse of magnetic field. In order to switch the magnetization of the storage layer, the tunnel junction must be heated at a temperature at least equal to the blocking temperature of the exchange biased storage layer. In this study, we investigated the minimum amplitude of the current required to write the memory element as a function of current pulse width in the range 300ps up to several ms. For very short pulse width (below 7ns), the energy produced in the immediate vicinity of the tunnel barrier, does not have enough time to diffuse towards the leads (adiabatic regime). In this regime, the energy dissipated by the current is entirely converted in heating of the MTJ. This regime allows a direct experimental determination of the absolute value of the specific heat of the MTJ nano-pillar. After a preliminary rough estimate of this specific heat, finite element numerical simulations of the heat transport were performed to calculate the temporal variation of the profile of temperature across the MTJ stack. These simulations confirmed a striking result already obtained from the rough estimate: the specific heat of the MTJ pillars is 5 to 10 times smaller than what could be expected by simply adding the specific heat of the individual layers, assuming bulk values of specific heat for each layer in the investigated range of temperature. Theoretical investigations are under way to understand the physical origin of this drastic reduction. We emphasize that these studies of dynamic heating in TAM-RAM provide a unique way to access to the absolute value of specific heat in nanopillars. In contrast, most microcalorimetric experiments only measure relative variations of specific heat.

Heating regimes

In our previous work, the tunnel junction heating dynamics was investigated in sub-micron size junctions used in TAM-RAM. The results showed two distinct regimes: a first one, at times scales below ~7ns, in which the heating occurs only in the tunnel junction, and a second one in which the heat diffuses towards the contact electrodes with a much longer time constant, increasing the tunnel junction base temperature.

The general form of the heat equation is $cd\frac{\partial T}{\partial t} = -div\vec{j}_Q + Q$ where d is the density of the material, c its specific heat capacity per unit mass (*cd* being the specific heat capacity per unit volume in J/m^3/K), $\vec{j}_Q$ (in W/m²) is the heat flow given by $\vec{j}_Q = -k\vec{\nabla}T$, k the heat conductivity (W/K/m) and Q is the energy being dissipated in the system by the current ($Q=R.A(V).j^2$, where j is the current density through the stack and $R.A(V)$ is the bias dependent resistance area product of the MTJ). For very short time after the current is turned on (t<~7ns), before

heat diffusion starts to occur, the temperature increase is essentially proportional to the energy: $\Delta T \approx \frac{Q\Delta t}{cd}$. Knowing the heating power and the corresponding temperature increase at very short times ($DT=T_{blocking}-T_{standby}$), it is possible to directly derive the heat capacity of the tunnel stack.

The tunnel junction structure under study was Ta 50 / PtMn64 20 / CoFe20 2.5 / Ru 0.8 / CoFeB20 3.0 / Al 0.5 + Oxidation / CoFeB20 1.5 / NiFe 3 / IrMn 5 / Ta 5 / Al 20 / Ta 120nm and devices were lithographically patterned to 0.35µm diameter circular pillars. Fig. 1 shows the energy density necessary to heat the CoFe/IrMn storage layer above its blocking temperature as function of the pulse width. Two different device geometries are represented, with the junction centred at the intersection of two connecting leads, type "LDPP" or shifted with respect to one of the leads type "LDPL". The lead geometry only plays a role for pulses longer than 10ns. At shorter times (adiabatic regime), the values are geometry independent. As the pulse width becomes shorter and shorter, the minimum energy value required to write approaches a constant lower limit value from which the heat capacity can be derived. This requires also an exact determination of the temperature increase needed to unpin the storage layer which must take into account the evolution of the blocking temperature as a function of measuring time. Indeed, the depinning of the storage layer as the system is heated up is itself a thermally activated process which therefore depends on the duration of the heating pulse. We took into account this dependence and modelled it according to the model proposed in Ref.1. This allowed the determination of the blocking temperature and the heat capacity which was found 5 to 10 times lower than expected from bulk values.

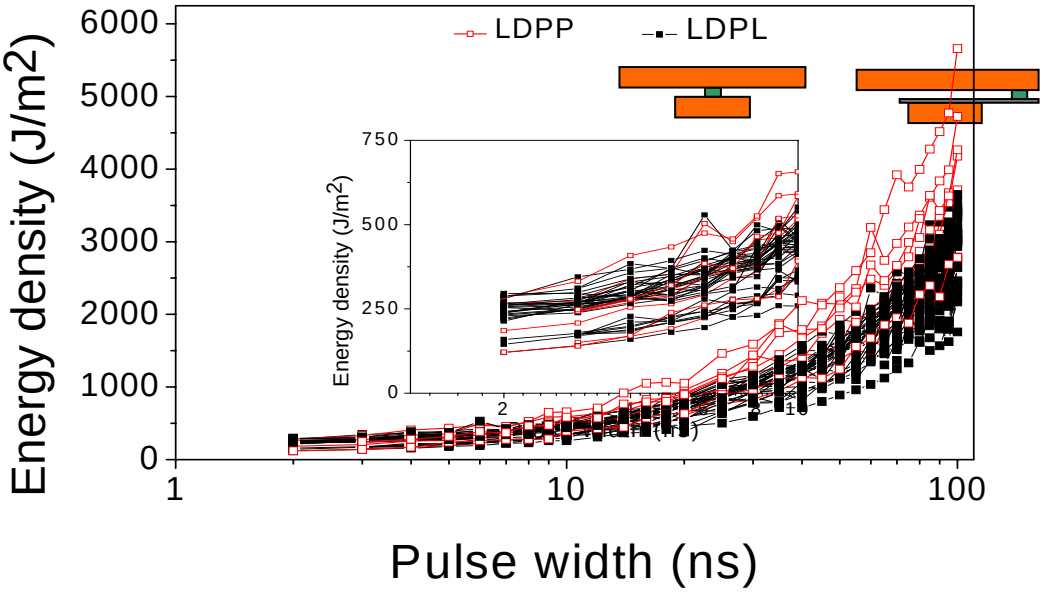

Fig.1 Energy required to heat the CoFeB/NiFe/IrMn storage layer at its blocking temperature as a function of the pulse width. Inset: same data plotted in the range below 10ns.

Acknowledgement:
This work has been partly supported by the European research program IST project NEXT (IST-2001-37334)

References:
[1] C.Papusoi, Al.Stancu, J.L.Dormann, J.Magn.Magn.Mater. 174, 236 (1997)

FORMATION OF MAGNETIC PATTERNS USING SPHERICAL NANOPARTICLES

F. Springer[1], L. Baraban[1], D. Makarov[1], I. L. Guhr[1], J. Gobrecht[2], J. Boneberg[1], P. Leiderer[1], M. Albrecht[1]

Email of the corresponding author: felix.springer@uni-konstanz.de
Department of Physics, University of Konstanz, D-78457 Konstanz, Germany
Laboratory for Micro- and Nanotechnology, Paul Scherre Institute, CH-5232 Villingen

Introduction

Perfectly ordered magnetic nanopatterns are assumed to be the ideal future magnetic recording media. The fabrication of nanopatterns on a large scale using lithographical techniques is expensive and time consuming. In contrast to that, self assembly processes are more suitable for large-scale device fabrication at low cost. Patterns that were formed by self assembly can either be used as a mask or can directly build the desired nanostructure. However, achieving key requirements like control of the magnetic anisotropy orientation along with magnetic domain isolation is hard. Here we present an approach to the formation of suitable magnetic patterns using nanoparticles. A two dimensional topographic pattern is formed by the self assembly of spherical polystyrene or silicon oxide particles. Coating the hexagonal particle array with Co/Pd or Co/Pt multilayers results in exchange isolated nanostructures with a uniform magnetic anisotropy orientation. Similar arrays of particles can also be used to form nanoindentations by imprinting a soft mold. The resulting troughs are coated with Co/Pd multilayers. The magnetic structures formed in the indentations can be exchange isolated from their neighbors, depending on their specific shape.

Experiment

Densely packed two-dimensional arrays of monodisperse polystyrene particles on glass substrates are formed via self-assembling upon slow evaporation of a solvent under ambient conditions. Hexagonal order is demonstrated for spherical particles with diameters ranging from 720nm down to 50nm. The following deposition of Co/Pd multilayers results in spherically shaped nanostructures referred to as magnetic caps in the following. The samples were characterized by atomic and magnetic force microscopy (AFM and MFM) as wells as by supplemental magneto optical Kerr effect (MOKE) measurements. Figure 1 shows a MFM image of 110nm particles with Co/Pd multilayers in the demagnetized state. The uniform dark and bright contrast on one particle indicates the formation of a single domain state with the magnetization pointing perpendicular to the substrate surface. The observation of single caps with bright contrast surrounded by caps with a magnetization in the antiparallel state suggests that the particles are exchange isolated. The exchange isolation is contributed to the small contact area between each particle and his six neighbors and the spherical shape of the surface. Geometrical considerations that lead to the suppression of the ferromagnetism in the outer parts of the caps are illustrated in figure 2. An analogous approach to the fabrication of exchange isolated magnetic nanopatterns is using spherical indentations followed by Co/Pd film deposition. Arrays of particles in the range from 130nm to 420nm were covered by a liquid prepolymer

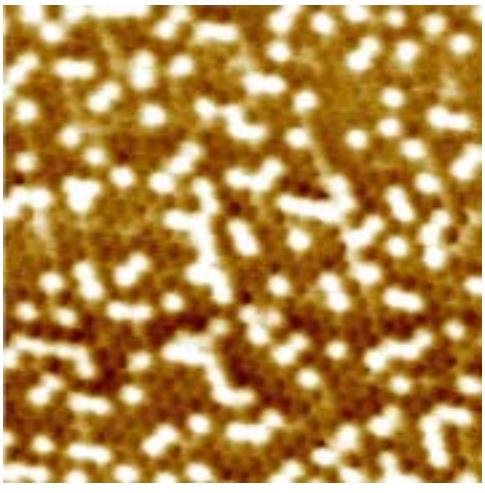

Figure 1: MFM image of self assembled 100nm particle array after deposition of Pd(50Å)[Co(4Å)/Pd (7Å)]$_9$Pd(13Å) in the demagnetized state.

and a curing agent as illustrated in figure 3. Samples with different indentation depths *D* were investigated by AFM and MFM. Those studies revealed that the exchange coupling depends on the ratio of indentation diameter *D* to width *W*. Exchange isolation of the formed magnetic nanostructures was only observed for $0.2<D/W\leq0.5$. In figure 4, two MFM images for D/W values of 0.3 and 0.09 are shown for example.

The presented low cost imprint process might be more suitable for application than the magnetic patterns formed directly on the particle array.

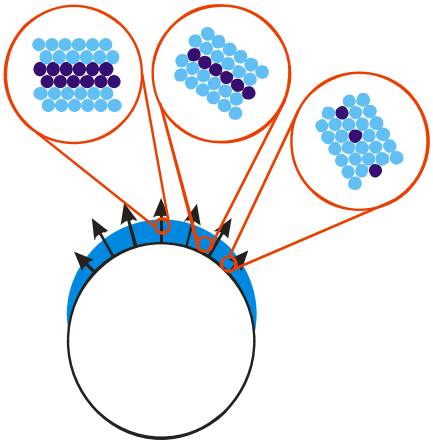

Figure 2: The spherical surface leads to the for-mation of an ordered Co/Pd multilayer system in the center of the sphere. The diluted film system in the outer parts of the sphere is non magnetic.

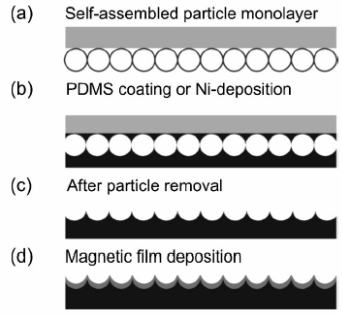

Figure 3: Schematic of the various steps for fabricating magnetic arrays of spherical nano indentations

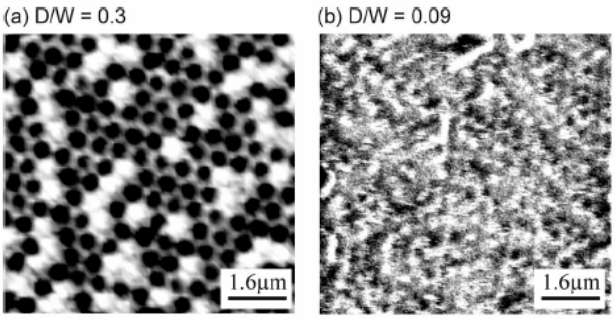

Figure 4: (a) MFM image of an array with D/W=0.3 fabricated by employing 410 nm particles. (b) MFM image of a magnetically exchange coupled array with D/W=0.09.

[1] M. Albrecht, G. Hu, I. L. Guhr, T. C. Ulbrich, J. Boneberg, P. Leiderer and G. Schatz, Nature Materials 4, 203-206, (2005).
[2] D. Makarov, L. Baraban, I. L. Guhr, J. Boneberg, H. Schift, J. Gobrecht, G. Schatz, P. Leiderer, M. Albrecht, Appl. Phys. Lett. 90, 093117 (2007).

MAGNETIC PATTERNING BY FOCUSED ION BEAM IRRADIATION

S. Tibus[1], D. Makarov[1], C.T. Rettner[2], T. Thomson[3], B.D. Terris[3], and M. Albrecht[1]

[1]University of Konstanz, Department of Physics, D-78457 Konstanz, Germany
stefan.tibus@uni-konstanz.de

[2]IBM Almaden Research Center, 650 Harry Road, San Jose, CA 95120, USA

[3]Hitachi San Jose Research Center, 650 Harry Road, San Jose, CA 95120, USA

Introduction

The ability to magnetically pattern continuous thin films has a number of applications [1]. The use of focused ion beam (FIB) irradiation opens new possibilities for magnetic pattern creation by tailoring the magnetic properties of a magnetic medium [2, 3]. This technique is potentially useful in the creation of servo patterns for the purposes of high density magnetic recording, as presented recently [4].

Here, we report on the magnetic domain configurations and the reversal behavior of strip patterns including an interpretation of the results by micromagnetic simulations.

Experimental details

Nanometer-scale magnetic strip structures were made by patterning a Co/Pt multilayer medium using a focused 30 keV Ga beam. Strips of 80 nm width were exposed, separated by 170 nm wide unexposed areas. The atomic force microscope (AFM) image (Fig. 1a) shows a small topographic contrast (0.9 nm) caused by the sputtering effect of the ion beam.

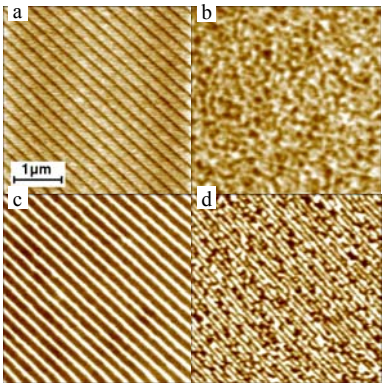

Figure 1: AFM/MFM images

After ac-demagnetization the magnetic force microscope (MFM) image (Fig. 1b) reveals magnetic domains in the size range of about 100 to 200 nm. The underlying strip pattern is not reflected in the domain configuration. This situation changes when the sample is saturated in a perpendicular field and then imaged in zero field (remanence). A well-defined strip domain pattern is observed (Fig. 1c). The exposed and unexposed segments create a pattern of modulated magnetic properties, wherein the exposed regions are magnetically softer than the unexposed regions. Thus, the irradiated segments have reversed their magnetization direction due to the demagnetization fields of the adjacent unexposed medium.

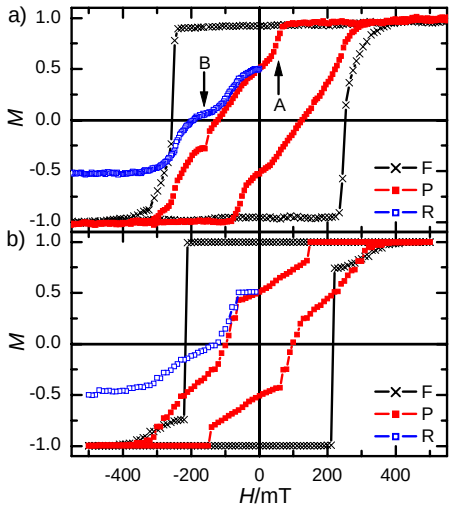

Figure 2: a) Experimental and b) simulated M-H-loop

The corresponding M-H loop and remanence curve were measured by polar magneto-optic Kerr effect (Fig. 2a). The M-H loop reveals a well pronounced step (arrow A) in magnetization at about 60 mT, indicating the reversal of the soft, irradiated strips. At remanence a reduced magnetization is observed consistent with the MFM image. For reverse field values between -100 mT and -200 mT (arrow B) an additional stable domain configuration appears in remanence. This domain configuration was imaged by MFM after applying a reverse field of -160 mT revealing an additional strip pattern (Fig. 1d).

Micromagnetic simulations

In order to get a better understanding of the reversal behavior and the underlying spin structure of the stable domain configurations, micromagnetic simulations were performed using the freely available micromagnetic simulation package MAGPAR [5].
A reasonable correspondence between the simulation results and the experimental data was obtained using reduced values of 2/3 for the saturation magnetization and 1/8 for the anisotropy of the exposed strips. The simulated M-H loop and the remanence curve (Fig. 2b) reproduce the experimentally observed features (Fig. 2a). To follow the reversal process in more detail, the equilibrium spin configuration was extracted at various external field strengths from the simulations (Fig. 3). Coming from positive saturation to remanence the change in magnetization is dominated by the reversal of the magnetically soft exposed strips, starting at around +140 mT. At remanence, the moments of the irradiated strips are pointing mainly in the opposite direction with respect to the surrounding hard magnetic material. The driving force is a competition between the magnetostatic interaction and the exchange interaction between the hard and soft strips. When applying negative fields, the reversal is mainly due to domain wall motion in the hard magnetic strip material. The domain configuration in remanence as a function of applied reverse field reveals, at -150 mT, a second stable domain configuration. Here, the hard strip splits, approximately, into a central domain pointing antiparallel to its outer parts while the soft parts of the exposed strips reveal mainly an in-plane orientation of the magnetization pointing along the strip. This configuration again minimizes the magnetostatic energy and is in qualitative agreement with the measured MFM image shown in Fig. 1d.

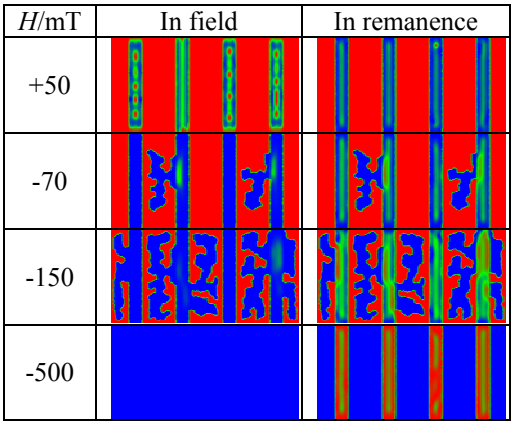

Figure 3: Simulated domain configurations

Summary

FIB irradiation was used to create strip patterns with modulated magnetic properties in a perpendicular Co/Pt film. Micromagnetic simulations were used to understand the nature of the magnetic domain configuration and their reversal in these periodic strip systems. The strip patterns reveal an antiparallel alignment of neighboring irradiated and unirradiated strips where the coupling strength can be tuned simply by varying the pattern period and/or exposure dose. The formation of such laterally coupled strips is determined by the competition between the magnetostatic interaction and the exchange interaction.

Acknowledgements

Financial support by the Deutsche Forschungsgemeinschaft through the Emmy-Noether program is gratefully acknowledged. The authors would like to thank Thomas Schrefl (University of Sheffield, GB) for fruitful discussions.

[1] A. Moser, K. Takano, D.T. Margulies, M. Albrecht, Y. Sonobe, Y. Ikeda, S. Sun, and E.E. Fullerton, *J. Phys. D: Appl. Phys.* **35**, R157 (2002).
[2] C. Chappert, H. Bernas, J. Ferré, V. Kottler, J.-P. Jamet, Y. Chen, E. Cambril, T. Devolder, F. Rousseaux, V. Mathet, and H. Launois, *Science* **280**, 1919 (1998).
[3] J. Faßbender, L. Bischoff, R. Mattheis, and P. Fischer, *J. Appl. Phys.* **99**, 08G301 (2006).
[4] M. Albrecht, C.T. Rettner, M.E. Best, and B.D. Terris, *Appl. Phys. Lett.* **83**, 4363 (2003).
[5] W. Scholz, J. Fidler, T. Schrefl, D. Suess, R. Dittrich, H. Forster, and V. Tsiantos, *Comp. Mat. Sci.* ***28****, 366 (2003)*

TUNING PROBE-STORAGE PARAMETERS FOR QUALITY OF SERVICE

Berend Jan van der Zwaag, Mohammed G. Khatib, Gerard J.M. Smit, Pieter H. Hartel

Department of Computer Science – University of Twente
P.O.Box 217, 7500 AE Enschede, The Netherlands
T: +31 53 489 4655, F: +31 53 489 4590, E: b.j.vanderzwaag@utwente.nl

Introduction

This paper studies the influence that different striping policies for probe-based storage have on the Quality of Service (QoS). The QoS components that we study are power efficiency, effective storage capacity, and effective bandwidth. We investigate their interdependencies as well as their dependency on a given workload using trace-driven simulations. The results will help us to design efficient file systems for probe-based storage.

Effective capacity and effective bandwidth

Our system consists of 7680 probes, each one accessing 4096 tracks of 8192 bits. At any time only a subset of probes is active in parallel, and we can choose how many of those probes are used to read a 512-byte sector, i.e., logical data blocks are striped over a subset of the available active probes. We identify different striping policies by the number of blocks that can be accessed in parallel; e.g., *striping policy 256* allows 256 different blocks to be simultaneously read and *striping policy 1* just one at a time, which is, in that case, striped over all available probes. The portion of a block that is accessed by a single probe is called a *subblock*.

For reliability reasons, low-level error coding (ECC) is deployed on the subblock in such a way that for large subblocks the relative ECC overhead is smaller than for small subblocks: in our experiments the number of ECC bits per subblock ranges from 4 for small subblocks (16 data bits) to 265 for large subblocks (4096 data bits). For a given physical storage capacity this means that striping policies that use smaller subblocks have to dedicate a larger number of physical bits to ECC, resulting in lower effective storage capacity (fig. 1).

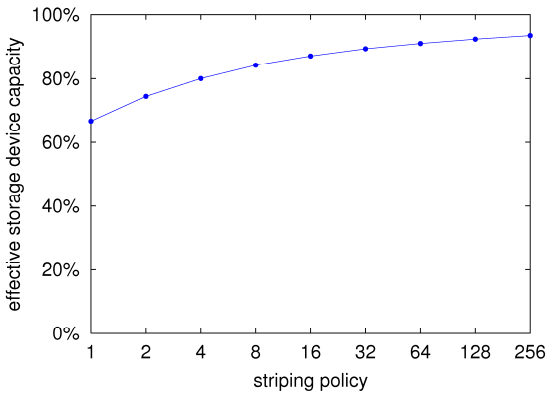

Fig. 1 Effective capacity vs. striping policy.

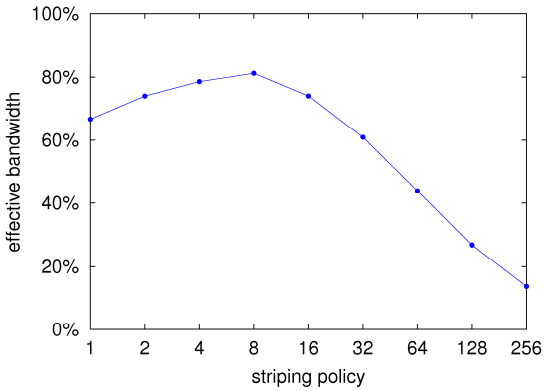

Fig. 2 Effective bandwidth vs. striping policy.

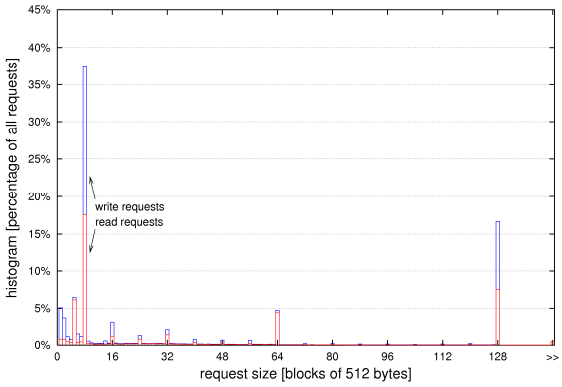

Fig. 3 Histogram of request sizes.

The high parallelism of higher striping policies allows higher bandwidth (because of less overhead), but this can only be used effectively if there are enough data blocks to be accessed in parallel. Our simulations use a recent disk trace consisting of over 3 million requests. Its workload is that of a typical notebook user [2]. For this trace, the effective bandwidth as a function of the striping policy is shown in fig. 2. The maximum reached at striping policy 8 can be explained if we look at the distribution of request sizes in the trace (fig. 3): most requests contain 8 blocks, which can be accessed in parallel using striping policy 8. The loss in bandwidth for lower striping policies is due to the larger number of ECC bits that have to be transferred, and for higher striping policies it is due to the larger number of probes that are unused when there are not enough blocks to be accessed in parallel. As the optimum for effective capacity is at striping policy 256 (fig. 1), a trade-off is necessary (fig. 4).

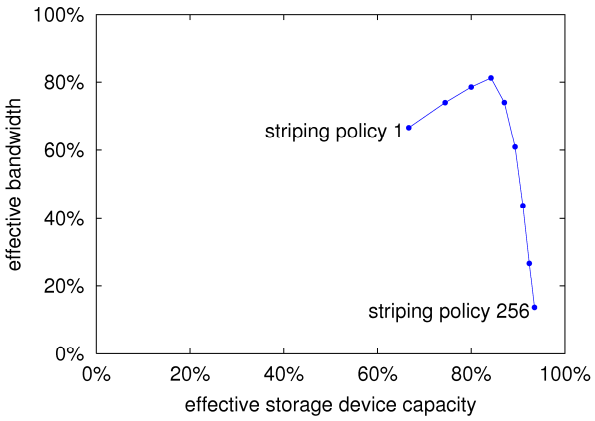

Fig. 4 Trade-off: bandwidth vs. capacity.

Power efficiency

The above results assume a fixed number of 256 simultaneously active probes out of a total of 7680 (e.g., due to a limited power budget). Now, if instead a certain minimum bandwidth is required – say 75% of the theoretical maximum (no-overhead) bandwidth for 256 active probes – we can determine the minimum number of active probes required to achieve this bandwidth for different striping policies. Fig. 5 shows this as the power efficiency relative to the power required for the theoretical optimum. The trade-off with effective capacity is shown in fig. 6.

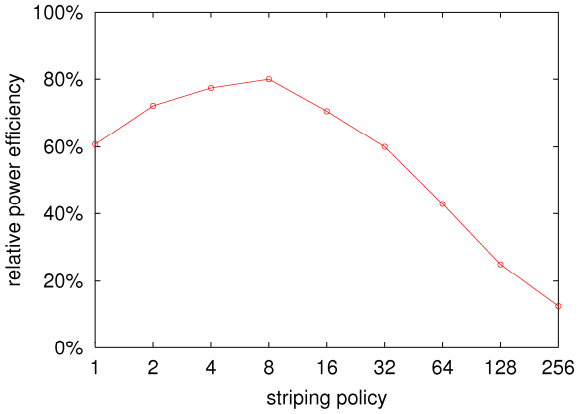

Fig. 5 Power efficiency as a function of striping policy.

Conclusions

Our study shows that tradeoffs between the studied QoS components are necessary. Bandwidth and power efficiency are workload dependent, whereas capacity is independent of the request size distribution. We have to take this into consideration when we design an efficient file system for probe-based storage systems.

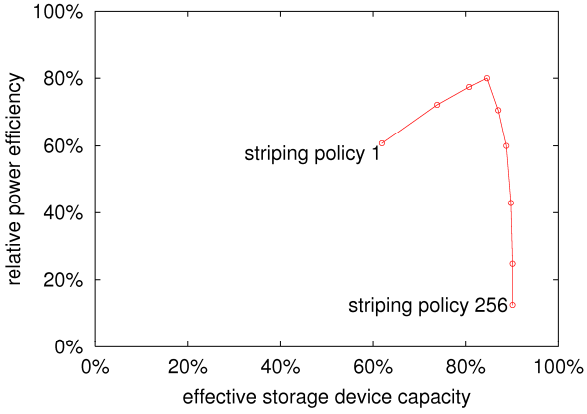

Fig. 6 Trade-off: effective capacity vs. power efficiency.

[1] M.G. Khatib, B.J. van der Zwaag, F.C. van Viegen, and G.J.M. Smit, "Striping policy as a design parameter for MEMS-based storage systems," *Proceedings of IWSSPS*, Seoul, Korea, October 2006, pp. 25-32.

[2] L.P. Chang and T.W. Kuo, "Efficient management for large-scale flash-memory storage systems with resource conservation," *ACM Tr. on Storage*, 1(4):381-418, 2005.